Study on plasma etching of GaN at high temperatures for damageless fabrication of next-generation power devices

Zecheng LIU

Content

Content i

Chapter 1: Introduction 1

1.1 Advantages of gallium nitride (GaN) for power devices 1
1.2 Fabrication of GaN power devices using plasma etching 4
1.2.1 Lateral GaN power devices 4
1.2.2 Vertical GaN power devices 8
1.3 Degradations in device performances after plasma etching 10
1.4 Requirements of plasma etching of GaN in a gate recess process 12
1.5 Plasma-induced damage (PID) in GaN-related materials 14
1.6 High-temperature Cl_2 plasma etching of GaN 16
1.7 Scope of this study 19
1.8 References 21

Chapter 2: Plasma diagnostic and film analyses 25

2.1 Overview 25
2.2 Optical emission spectroscopy (OES) 26
2.3 X-ray photoelectron spectroscopy (XPS) 28
2.3.1 Principle 28
2.3.2 Calculation for chemical composition 29
2.3.3 Depth profiling by angle-resolved XPS 31
2.4 Atomic force microscopy (AFM) 33
2.5 Scanning electron microscopy (SEM) 36
2.6 Photoluminescence (PL) 38
2.6.1 Principle 38
2.6.2 PL spectrum of GaN 41
2.6.3 Penetration depth 42
2.6.4 Photoluminescence peak position: Energy levels 44
2.7 References 45

Chapter 3: Suppression of damage formation on GaN by the control of stage temperature 47

3.1 Introduction 47
3.2 Experimental details 48
3.3 Results and discussion 51
3.3.1 Characterization of PID in the Cl_2 high-temperature etching of GaN 51
3.3.2 Separation of the effects of ions, radicals and photons on PID 57
3.4 Conclusions 60

3.5 References 61

Chapter 4: Optimization of plasma conditions for GaN etching in terms of both plasma-induced damage and surface morphology 63

4.1 Introduction 63
4.2 Experimental details 64
4.3 Results and discussion 65
4.3.1 Dependence of etch time on damage formation 65
4.3.2 Dependence of incident ion energy on damage formation 69
4.3.3 Optimization of the etching process 72
4.4 Conclusions 77
4.5 References 78

Chapter 5: Thermally enhanced formation of photon-induced damage on GaN 80

5.1 Introduction 80
5.2 Experimental details 81
5.2.1 Sample preparations 81
5.2.2 Measurements and calibrations of emission spectra with different optical windows 81
5.2.3 Approaches of damage diagnoses 82
5.3 Results and discussion 86
5.3.1 Photon-induced PL degradation at early process at 500 ºC 86
5.3.2 Photon-induced degradation in the surface stoichiometry 89
5.3.3 Wavelength dependence of damage formation induced by the photon irradiation 93
5.4 Conclusions 100
5.5 References 101

Chapter 6: GaN surface roughness reduction with photon irradiation during etching by chlorine radicals 103

6.1 Introduction 103
6.2 Experimental details 104
6.3 Results and discussion 106
6.4 Conclusions 119
6.5 References 120

Chapter 7: Conclusions 122

7.1 Present work 122

7.2 Perspectives in the future 125

Acknowledgements 128

Award 132

International Research Project 132

Journal publications 133

International conferences 134

Chapter 1: Introduction

1.1 Advantages of gallium nitride (GaN) for power devices

The modern industry and a large amount of applications are rapidly developed due to the progressing semiconductor technology. Traditionally, Si became the focus of the modern electronics and Si based transistors have been widely studied in a large variety of applications. In recent decades, advanced technologies using semiconductors that have wide band gap energies like GaN-related materials are maturing, which provide enough performance benefits in specialized fields.

GaN has been focused on optoelectronics and high power/frequency applications because of its remarkable physical properties, as shown in Fig. 1.1.[1,2)] Compared with the band gap energy of Si (1.22 eV) and GaAs (1.43 eV), GaN and 4H-SiC provide much higher band gap energies of 3.39 and 3.26 eV, respectively. As a result, a larger breakdown electric field could be easily achieved in wide band gap semiconductors of 4H-SiC and GaN, resulting in higher breakdown voltages for power devices. Hence, the device can be manufactured much thinner at the same breakdown voltage with higher doping levels than that of Si and GaAs. On the other hand, high saturated electron drift velocities of GaN and 4H-SiC directly improve the capability in the high frequency switching. Typically, the saturated electron drift velocities of GaN and 4H-SiC are more than twice that of Si and GaAs (~1×10^7 cm/s). In addition, the charges in the depletion region of a diode can be removed faster as a result of the higher saturated electron drift velocity. Therefore, the reverse recovery times of GaN and 4H-SiC diodes are shorter and reverse recovery currents are smaller.

Figure 1.2 shows the theoretical comparison of on-resistance (R_{on}) of lateral field effect transistors (LFETs) fabricated by Si, Diamond, 4H-SiC, and GaN.[3)] Compared with other semiconductors like Si, GaAs, and even SiC, GaN based high electron mobility transistor

(HEMT) has a potential to provide a most promising electrical property with a rather low R_{on} less than 0.1 $m\Omega \cdot cm^2$ in a wide high voltage range from 100 V to 3 kV.

SiC was widely considered as a replacement of Si to provide a high performance of power device before the year of 2000. However, a transistor using the AlGaN/GaN heterostructure achieved a breakdown voltage of 1.2 kV and a specific R_{on} of 2 $m\Omega \cdot cm^2$.[4] As a result, GaN attracted many attentions as a more preferable candidate than SiC in the manufacture of next-generation power devices.

In recent decades, GaN power devices have been rapidly studied and their performances were highly improved. A vertical structure of GaN has been highly expected for its high potential (e.g., a high breakdown voltage, a tiny chip dimension, and a facile wiring),[3] but the development of the vertical GaN power devices is tardier than that using the lateral structures because of the issue for GaN substrate quality. Recently, a lateral GaN power device was successfully manufactured with promising high performances (e.g., a high blocking voltage and a low R_{on}), which were extremely more preferable than those of Si power devices.[5] Therefore, GaN is highly expected as a candidate of next-generation power devices.

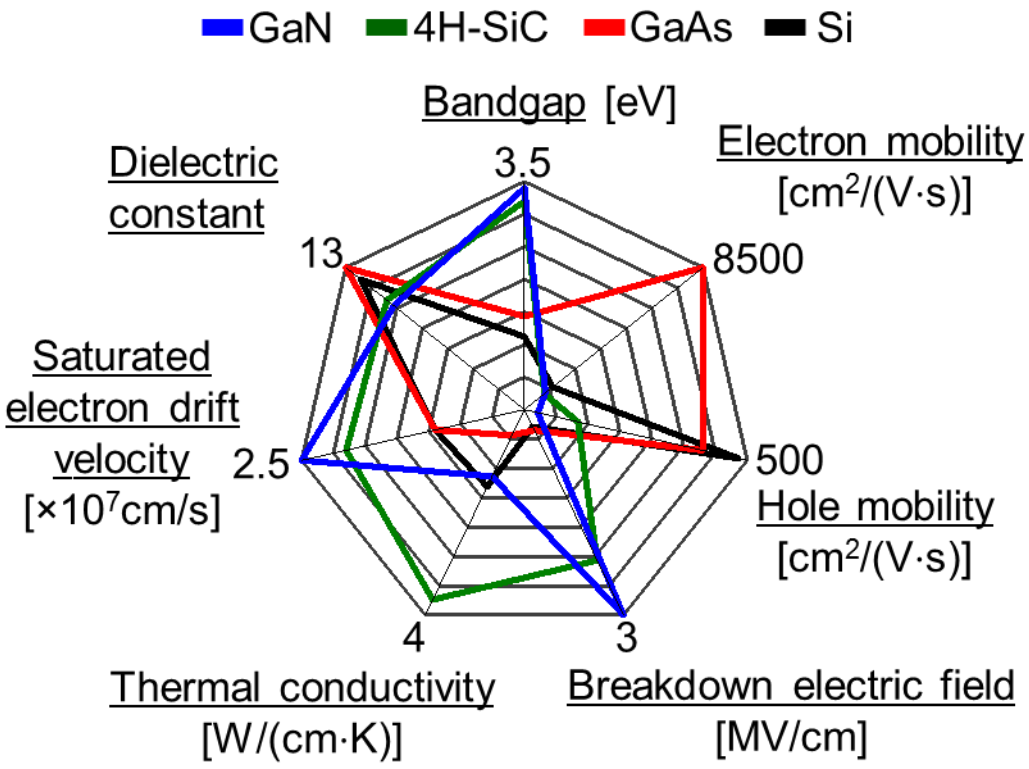

Fig. 1.1 Comparison of physical properties of semiconductor materials.[1,2)]

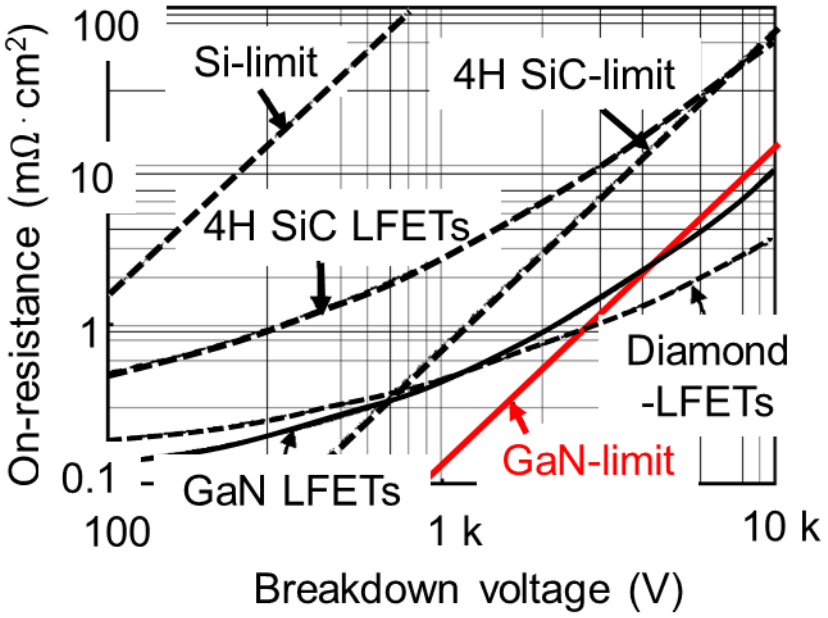

Fig. 1.2 Theoretical comparison of R_{on} of LFETs.[3)]

1.2 Fabrication of GaN power devices using plasma etching

1.2.1 Lateral GaN power devices

The popularity of lateral GaN power devices is that the gate–drain distance (L_{GD}) could be enlarged to improve the breakdown voltage while a promising low R_{on} is obtained as the unique property of GaN. The typical illustration of a lateral structure in GaN power device is depicted in Fig. 1.3, where two-dimensional electron gas (2DEG) is formed at the interface between AlGaN and GaN. Notably, the electron mobility is impressively improved from approximately 200 to 1700 $cm^2/(V \cdot s)$.[6] Because of the potentially high density of 2DEG, a low R_{on} is highly expected and a high breakdown voltage can be simultaneously achieved. Previously, P. Srivastava *et al.* reported a heterojunction FET using GaN-related materials that grown on Si substrates, which achieved a high breakdown voltage of 2.2 kV.[7]

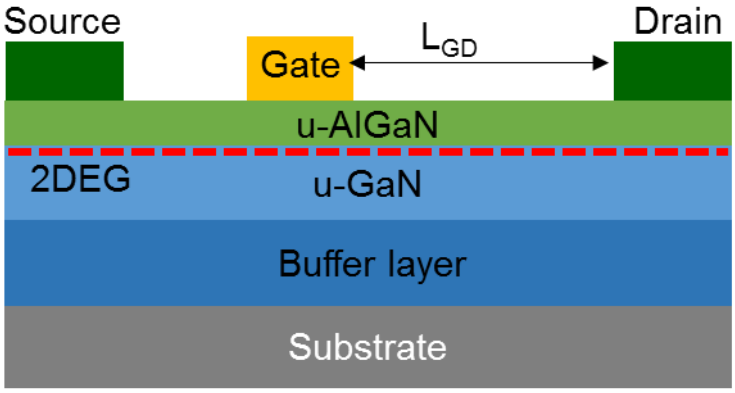

Fig. 1.3 The typical illustration of a lateral structure in GaN power device.[9]

However, the achievement of normally-off operation in GaN power devices is difficult due to the high-density 2DEG at the AlGaN/GaN interface.[8] A metal-oxides-semiconductor (MOS) channel is usually used in power devices fabricated on Si or SiC, which obtained normally-off operation.[9] Typically, a threshold voltage higher than 3 V formed by an inversion gate is demanded to avoid errors in gate signal induced by noises.[9] However, an inversion layer is hard

to be formed in GaN, and several approaches have been proposed to achieve normally-off operation, as shown in Fig. 1.4.

Figure 1.4 (a) involves a recessed-gate structure.[10] A depth of approximately 14 nm of the AlGaN layer that has a total depth of 20 nm is required to be etched beneath the gate, which successfully reduced the 2DEG density in the etched region.[11] Here, wet etching method using hot alkali solutions has been proven to be inefficient because of the chemical stabilities of GaN-related materials.[12] Instead, the plasma etching provides a relatively higher etch rate, an anisotropic etch profile, a smooth side wall, and a clean bottom surface.[12,13] Even though this recessed-gate structure succeeds in a positive shift for the threshold voltage, a complete depletion of the 2DEG is still required to achieve a sufficiently high threshold voltage. To solve this, the etching of the gate-recess is demanded to penetrate gate electric field of the GaN layer, in which the 2DEG completely disappears.[14] As a result, normally-off operation was successfully realized. However, the disadvantages are a high R_{on}, a difficult management in the threshold voltage, and plasma-induced damage during the plasma etching of GaN, contributing to another issue called current collapse. Another issue is the uniformity in the recess-etching depth, which directly affects the uniformity in the threshold voltage.

Figure 1.4 (b) shows fluoride-based plasma treatment in the gate region of the AlGaN layer.[15] The 2DEG density is successfully depleted as a result of the negatively charged F ions. Hence, the normally-off operation is achieved. However, the channel mobility deteriorates when F ions are accelerated into the GaN layer as a result of the degraded carrier mobility by plasma-induced damage.

Figure 1.4 (c) proposes a unique gate structure using p-GaN.[16] An extended depletion layer is formed in the p–n junction and thereby depletes the 2DEG, leading to a successful normally-off operation. However, a large gate leakage current can easily occur when the bias voltage in gate region is higher than the built-in potential of the p–n junction, indicating a

limitation for the threshold voltage. For the manufacture of the gate structure, how to selectively etch the p-GaN layer is critical. Consequently, a precise management of plasma etching and a reduction of plasma-induced damage on the etched region is highly demanded.

Figure 1.4 (d) depicts a p-InGaN cap structure.[17] Compared with a p-GaN gate stucture, an InGaN cap layer is expected to induce more large negative charges at the interface between the AlGaN and InGaN cap by piezoelectric polarization as a result of the larger lattice constant of InGaN than that of GaN. On the other hand, because the temperature in the growth of InGaN is lower than that of GaN, p-InGaN can be easier activated, and the effect of Mg doping can be reduced. Hence, a precise control of the selective etching of p-InGaN and a reduction of plasma-induced damage on the etched region is highly required to promote the device performance.

Consequently, the plasma etching is highly efficient in the fabrication of lateral GaN power devices with normally-off operations. Unfortunately, plasma-induced damage degrades device performances, failing to achieve the high potential of GaN in high power devices. Namely, a damageless plasma etching of GaN is required for fabrication of next-generation power devices.

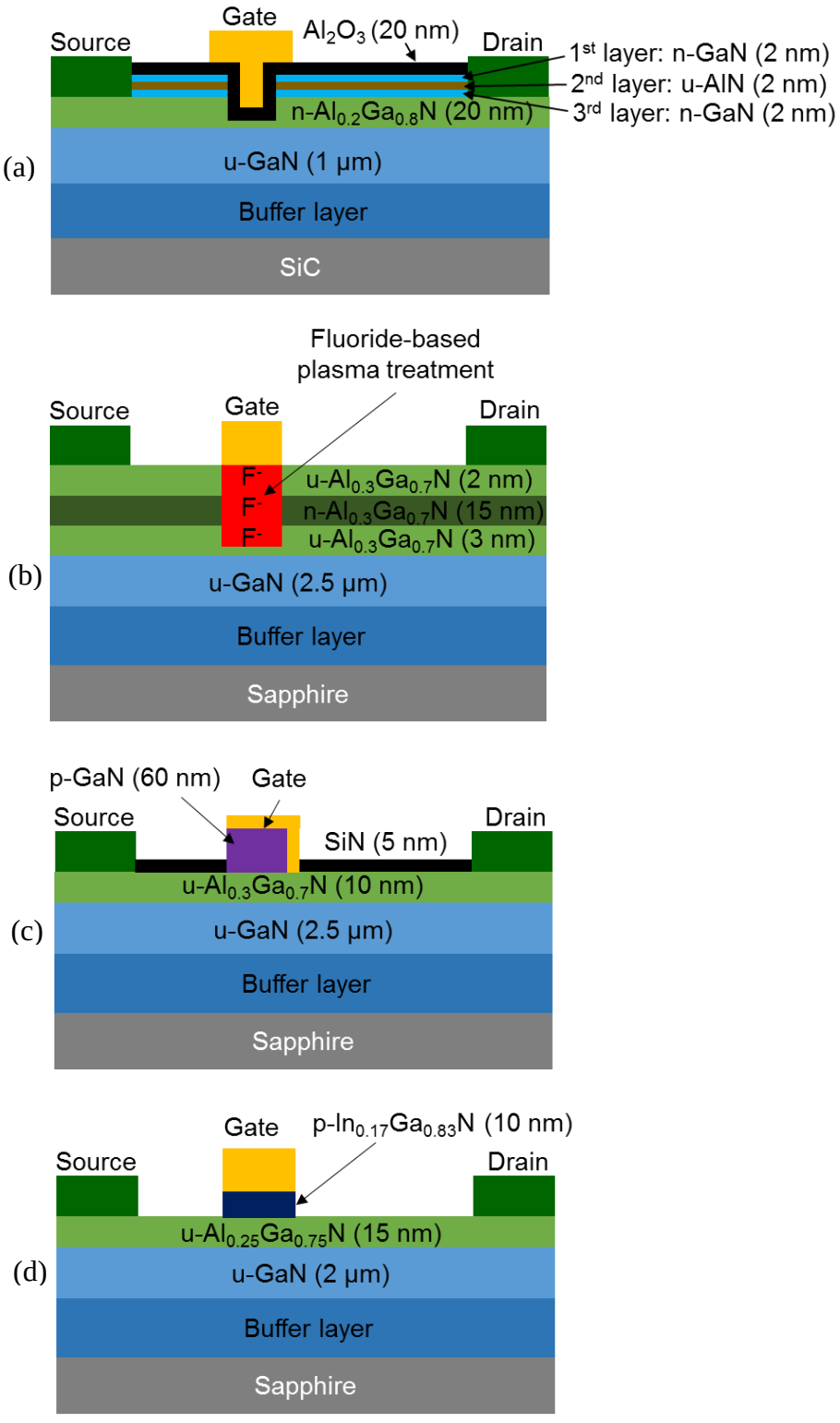

Fig. 1.4 Approaches of normally-off operations. (a) Recess gate structure.[10)] (b) Fluoride-based plasma treated gate structure.[15)] (c) p-GaN gate structure.[16)] (d) p-InGaN cap strucute.[17)]

1.2.2 Vertical GaN power devices

Recently, a promising approach employing a current aperture vertical electron transistor (CAVET) structure is highly expected to realize bulk breakdown limitations in GaN power devices.

Figure 1.5 shows an illustration of the CAVET structure, where the source and the drain regions are isolated using an insulating GaN. Indeed, it is also considered as a kind of a double-diffused metal-oxide semiconductor (DMOS) structure.[18,19] Moreover, this source region contains a confined aperture, which is full of conductive materials. To be similar with the lateral structure, a 2DEG is formed in the interface between AlGaN and GaN and comprises the source region. Here, the author notes that an n-GaN consists the drain region. Namely, the electrons firstly drift from the source regions, then travel across the aperture, and are gathered at the drain regions finally. The advantage of the CAVET structure is that because the pinched off region lies beneath the gate area, the accumulation of charges hardly occur at the edges of the gate region and thereby the side effect of the high electric fields near the edges is suppressed. Consequently, the CAVET structure is considered to be a promising option for vertical GaN power devices in terms of high bias voltages from source to drain and mitigated DC-RF dispersion.[20]

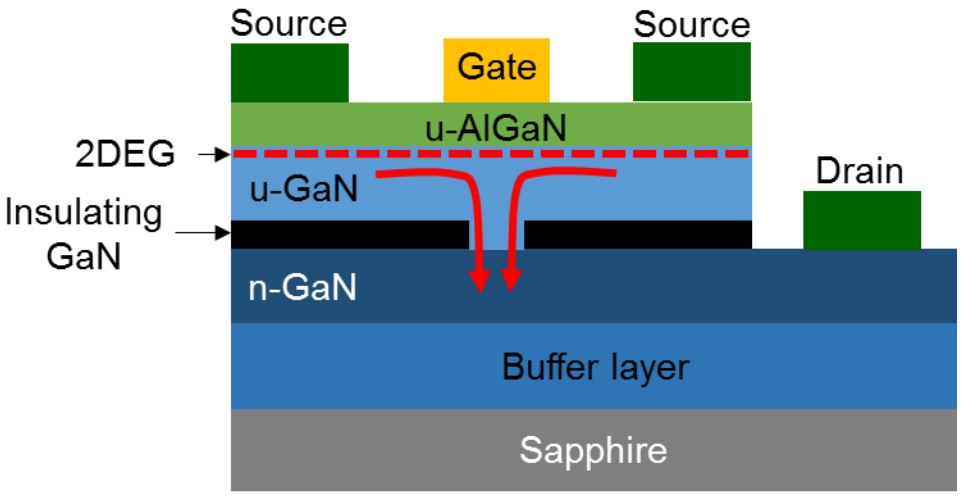

Fig. 1.5 Schematic diagram of GaN-based CAVET structure.[20]

In the fabrication of this CAVET structure, the plasma etching should be applied to fabricate the patterning of the device mesa and channel apertures. Ben-Yaacov *et al.* reported the process flow as follows.[20] An insulating Mg-doped GaN of 0.4 μm-thick on a Si-doped GaN with a 2 μm-thick were firstly grown using metal organic chemical vapor deposition (MOCVD) on sapphire substrates. Next, Cl_2 plasma was used to etch channel apertures through the insulating GaN layer. Then a regrowth of 170-250 nm of undoped GaN was performed on this insulating GaN layer. After that, a 25 nm of AlGaN cap was grown on this undoped GaN layer. Finally, the Cl_2 plasma etching was utilized to fabricate the patterning of the device mesa followed by the deposition of drain, source, and gate metals.[20]

Obviously, the etch depth is much larger for vertical GaN power devices than that of lateral ones. Therefore, a precise control of the etch profile of GaN has been recently studied.[21] Moreover, as the regrowth process of unintentionally doped GaN would be performed on the etched channel apertures, the plasma-induced damage was considered to potentially degrade the crystal quality of the regrown layer.[22] In addition, plasma-induced damage is considered to deteriorate Ohmic contacts, leading to the increased resistance after plasma etching.[23]

As a result, the plasma etching is an effective method in the fabrication of vertical GaN power devices to achieve bulk breakdown limitations of GaN power devices. Unfortunately, plasma-induced damage potentially degrades device performances and thereby a damageless plasma etching is highly demanded.

1.3 Degradations in device performances after plasma etching

Despite benefits of GaN properties, the plasma etching induces damages in the fabrication of lateral GaN power devices and result in degradations in device performances such as a current collapse phenomenon and a high leakage current.

The high voltage application for the lateral AlGaN/GaN HEMT is difficult to be achieved due to a critical issue called current collapse, referring to a reduced drain current when the high voltage is switched on and off. This phenomenon is usually a result of negative charges potentially formed in the AlGaN/GaN interfaces and on the device surfaces.[24-26] Typically, in the fabrication of a recess gate structure, plasma-induced damage forms a large number of point defects which can trap negative charges.

Figure 1.6 shows the current collapse in a lateral AlGaN/GaN HEMT resulted from electron trapping during on/off switching. The current flows normally after the formation of the channel in the first on state of the GaN device. Then, some electrons remain trapped in the channel when the device is turned off, behaving as trapped electrons. Finally, these trapped electrons would obstruct the smooth current flow. As a result, R_{on} increases when the device keeps on switching on and off, which degrades the efficiency such as heating up the device and finally destroy the device.

On the other hand, a high reverse-bias gate leakage current of lateral AlGaN/GaN HEMT was reported after plasma etching.[27] Particularly, leakage currents not only interfere device reliability but also degrade noise performance and power efficiency. Indeed, the mechanism of leakage currents still has remained unsolved totally and trap-assisted tunneling is considered as one of the possible reasons. Indeed, plasma etching could potentially introduce a high density of defect donors near GaN or AlGaN surfaces, leading to a reduction of the Schottky barrier width. Then, electrons could travel though the barrier under a high reverse bias by the thermionic field emission or the field emission tunneling transport.[28]

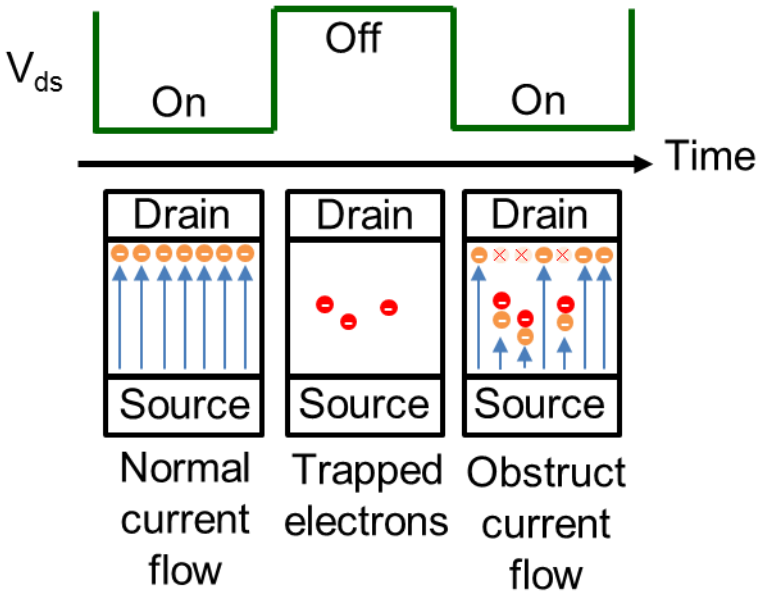

Fig. 1.6 GaN electron trapping during on/off switching leading to current collapse.

1.4 Requirements of plasma etching of GaN in a gate recess process

In this study, the author mainly focused on damageless fabrication of GaN for a shallow etching in a gate recess structure.

Figure 1.7 shows an example for a recessed-gate normally-off AlGaN/GaN MOS-HEMT.[14] A depth of approximately 7 nm of GaN is expected to be precisely and smoothly etched off without damage formation.

As a result, a gate recess process for the high-performance HEMT requires following characteristics of plasma etching:

- Very low speed etching
- Precise depth control
- Smooth bottom surface
- Damageless

The etching depth is time-controlled and strongly depends on the experimental conditions and the semiconductor surface before the plasma etching. Hence, for the shallow etching such as 7 nm, very slow etch rates are required to achieve the high-accuracy.

A smooth surface and a reduced damage formation are important because of their significant influences on drain current dispersion and gate leakage current.[2] Typically, the drain current dispersion effect is related with surface traps in AlGaN/GaN HEMTs that act as hole traps during drain current transients.[29] Hence, proper dielectric materials and suitable plasma pretreatments have been widely studied to passivate these surface traps, which lead to a remove of trap states and thereby avoid trapped charges.[30] Here, the author notes that the plasma pretreatments should be precisely controlled. Figure 1.8 shows experimental results of N_2 plasma pretreatment before the deposition of SiN as a passivation layer in AlGaN/GaN HEMTs.[30] Apparently, the sample treated by the N_2 plasma at the low power of 60 W successfully promoted the gate lag ratio (GLR) compared with the untreated one, indicating a

better high-frequency performance. However, the sample treated by N_2 plasma at high powers of 150 and 210 W showed degraded GLR properties, suggesting that the N_2 plasma at high powers resulted in the formation of surface traps on the AlGaN surface, which should be attributed to plasma-induced damage and roughened surface by strong ion bombardment effects. Namely, a flat surface and damageless are highly demanded in the plasma etching of GaN to prevent the drain current dispersion effect.

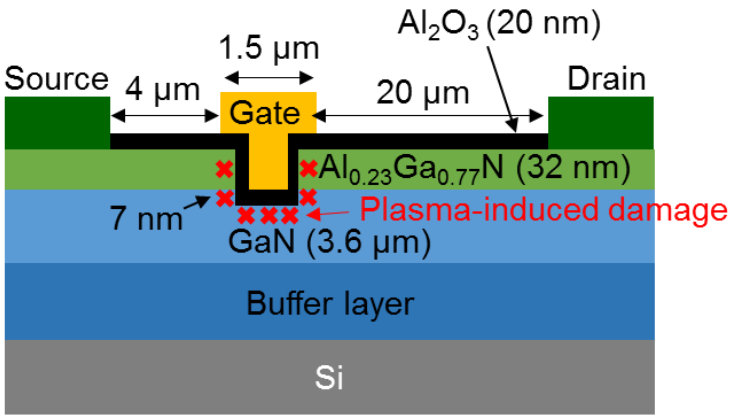

Fig. 1.7 Recessed-gate normally-off AlGaN/GaN MOS-HEMT.[14)]

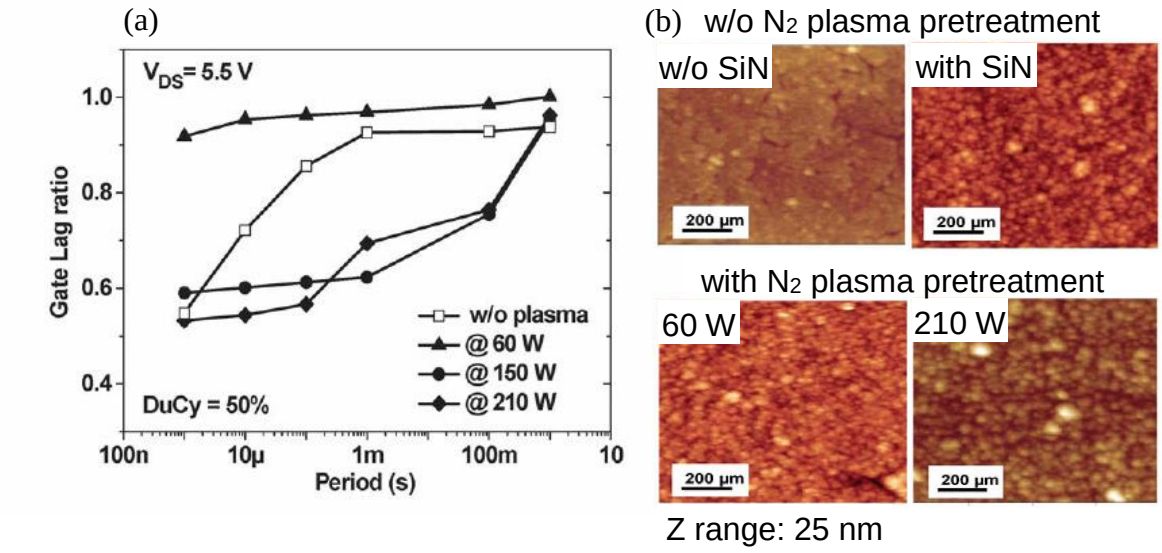

Fig. 1.8 (a) The dependence of gate pulse periods on the gate lag ratio for AlGaN/GaN samples without N_2 plasma pretreatment and with N_2 plasma pretreatment at 60, 150, and 210 W. (b) Surface morphology of AlGaN/GaN samples without SiN, with SiN, with N_2 plasma pretreatment at 60, and with N_2 plasma pretreatment at 210 W.[30)]

1.5 Plasma-induced damage (PID) in GaN-related materials

Since plasma contains various reactive species such as ions, radicals, and photons, the degradative effect of each species on the characteristics needs to be clarified.

Ion bombardment in plasma etching have been widely considered as physical damage, behaving as a lattice disorder in the GaN film. Lai *et al.* reported that N atoms were preferentially removed by the sputtering of energetic ions and thereby a Ga-rich surface was formed.[31] Hashizume *et al.* reported that the nitrogen-vacancy-related state near the conduction-band edge was introduced to the GaN surface in the H_2 plasma.[32] Aoki *et al.* reported that a high density of Ga-vacancy was observed in p-GaN films in CH_2Cl_2/Cl_2 plasmas.[33]

Radiations in ultraviolet (UV) / vacuum ultraviolet (VUV) regions degrade the GaN films, where the scissions of chemical bonding are formed by photon with a higher energy than that of the GaN band gap (3.4 eV). Minami *et al.* reported that the photoluminescence (PL) properties of GaN/InGaN single quantum well (SQW) deteriorated under the irradiation of ultraviolet (UV) from $Cl_2/SiCl_4/Ar$ plasmas with photon energies higher than the InGaN band gap energy (3.1 eV).[34] Kawakami *et al.* reported a synergistic effect of particle irradiation and UV from Ar plasmas. UV irradiation with a wavelength corresponding to the GaN band gap energy promoted the Ar^+-ion-induced roughening of the GaN surface.[35] Tamura *et al.* reported damage-free neutral beam etching without UV photon irradiation, in which PID was suppressed and both PL and Hall properties of GaN based HEMTs were promoted.[36]

On the other hand, the formation of a nonstoichiometric surface is a critical issue in conventional Cl_2-based plasma etching at room temperature (RT) owing to the preferential vaporization of the byproducts of nitrogen chlorides (NCl_3) and N_2 other than gallium chlorides (GaCl and $GaCl_3$) at relatively low vapor pressures, as shown in Fig. 1.9. Chen *et al.* reported this preferential removal of N atoms on the GaN surface, in which the N/Ga ratio decreased

from 84% of the as-cleaned sample to 38% after Cl_2 plasma etching at RT.[37] As a result, the non-stoichiometry degraded the PL properties of the GaN film. Consequently, to improve the GaN stoichiometry, the vaporization of gallium species is suggested to be enhanced by increasing the stage temperature of the etching process.

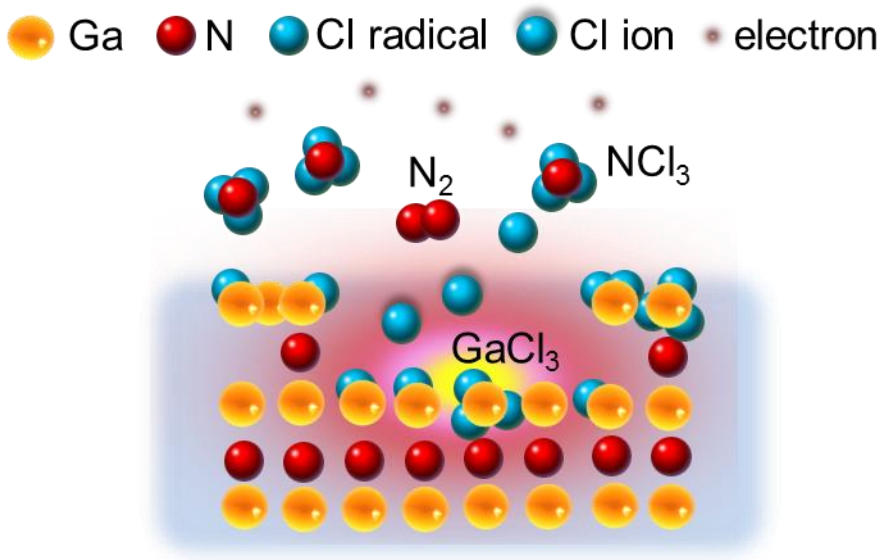

Fig. 1.9 Conventional Cl_2 plasma at RT.

1.6 High-temperature Cl_2 plasma etching of GaN

The principle of the high-temperature etching of GaN in Cl_2 plasma is proposed with two expectations:

- The vaporization of gallium chlorides (e.g., GaCl and $GaCl_3$) is enhanced with higher temperature, as shown in Fig. 1.10,[38-41] which leads to an equal remove of Ga and N atoms during plasma etching. Hence, a stoichiometric GaN surface can be fabricated, as illustrated in Fig. 1.11.
- The high-temperature results in an atomic ordering, which facilitates the recombination of the dissociated Ga and N atoms on the ion-sputtered surface at higher temperatures.

Here, the author notes that $GaCl_3$ is the main species of gallium chlorides at a temperature ranging from 100 to 500 ^oC, because other potential byproducts like $GaCl_2$ and GaCl are reported to decompose according to the following equilibrium reactions:[41,42]

$Ga_2Cl_4(g) \rightarrow GaCl(g) + GaCl_3(g)$, $Ga_2Cl_4(g) \rightarrow 1/2Ga_2Cl_2(g) + 1/2Ga_2Cl_6(g)$, and $GaCl(g)$ decomposes into Ga(l) and $GaCl_3(g)$.

However, when the temperature is higher than 500 ^oC, GaCl should also be regarded as one of the etch products because the disproportionation reaction will be suppressed.[41]

The effects of thermal annealing on plasma-damaged GaN was previously studied to recover or improve properties optically and electrically.[43-47] Cao *et al.* showed that plasma-induced deteriorations in current-voltage (IV) properties on Schottky diodes fabricated with the plasma-treated GaN were recovered by thermal annealing at temperatures between 550 and 750 ^oC after etching.[46]

Shul *et al.* previously reported that the CH_4 plasma etching of GaN, InN, and AlN at a high temperature of 170 ^oC increased etch rates, which was considered as the result of an increased vaporization of the volatile etch products.[47]

Kometani *et al.* firstly reported a damageless GaN surface etched by Ar and N_2 plasmas, where the stage temperatures was elevated to 600 °C.[48] When the Ar plasma etching was performed at 600 °C, Ga–N bonds were dissociated by the Ar^+ ion bombardment that nitrogen atoms were preferentially removed. Hence, the surface roughness of the GaN surface increased because of the aggregated gallium atoms. On the other hand, for N_2 plasmas at high temperatures, the stoichiometry of the GaN surface was much more preferable than that of Ar plasma with a higher N/Ga ratio. In addition, a smoother surface was observed. Therefore, the aggregation of metallic Ga roughened the GaN surface during ion-enhanced etching of GaN at high stage temperatures.

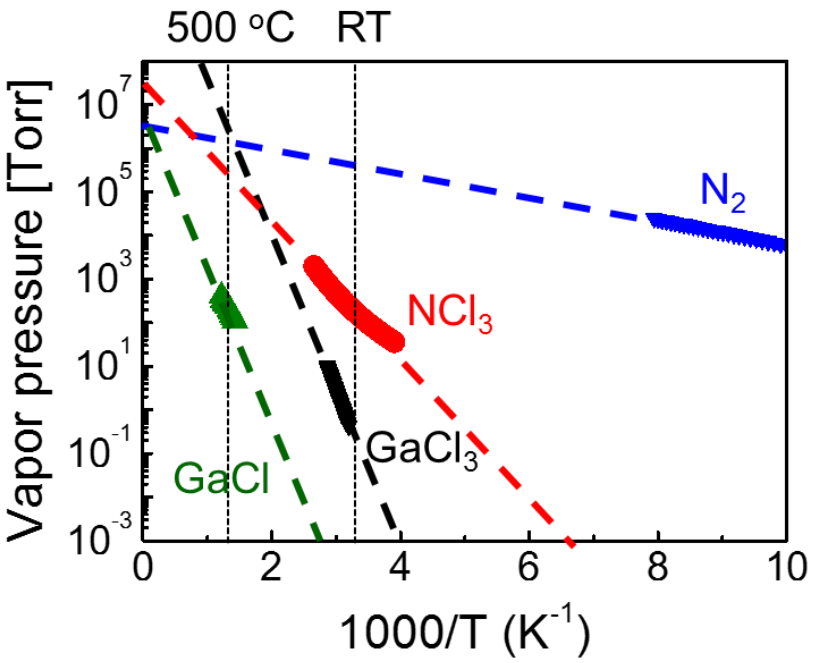

Fig. 1.10 Vapor pressures of etch products in Cl_2 plasma etching of GaN with temperatures.[38-41]

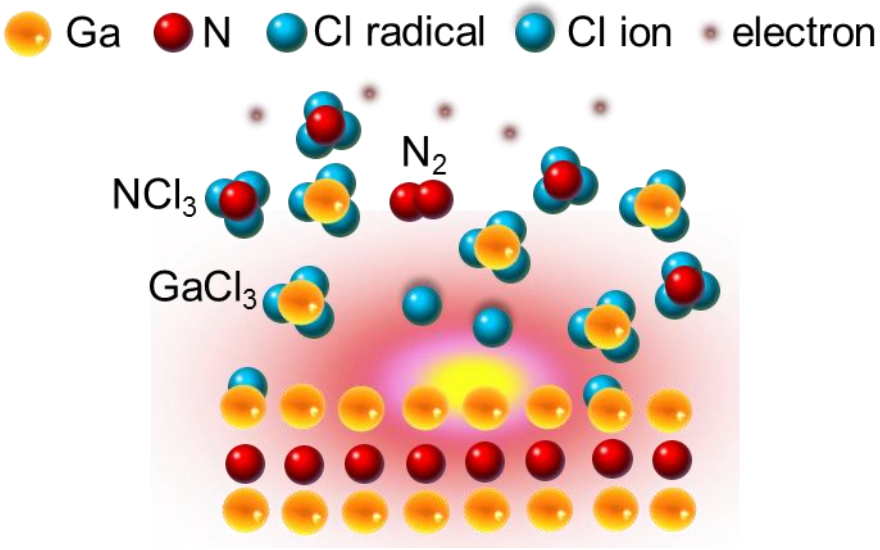

Fig. 1.11 Cl_2 plasma etching of GaN at high temperatures.

1.7 Scope of this study

This study represents an investigation to understand the principles of the high-temperature Cl_2 plasma etching of GaN on suppression of damage formation, which describes the detailed mechanisms of individual contributions of ion, photon and radical on both PID and surface morphology.

In chapter 2, the principals of plasma diagnostic and film analyses are stated. Optical emission spectroscopy (OES) is utilized to diagnose plasma. X-ray photoelectron spectroscopy (XPS) is applied to calculate the surface stoichiometry. Atomic force spectroscopy (AFM) is performed to observe the surface morphology. Scanning electron microscopy (SEM) is used to observe the etch profiles and estimate the etch depths. PL is used to investigate the optical properties of GaN films.

In chapter 3, the author states that PID during plasma-etching processes was successfully suppressed by the application of Cl_2 plasma etching at an optimal temperature of 400 ^oC, based on results of evaluations of PL, stoichiometric composition, and surface roughness. The effects of ions, photons, and radicals on damage formation were separated from the effects of plasma using the pallet for plasma evaluation (PAPE) method. The PID was induced primarily by energetic ion bombardments at temperatures lower than 400 ^oC and decreased with increasing temperature. Irradiations by photons and radicals were enhanced to form the PID and to develop surface roughness at temperatures higher than 400 ^oC.

In chapter 4, further discussions of ion-induced damage occurred at 400 ^oC is described for the minimization of PID in plasma etching for the precise and smooth removal of a depth of approximately 7 nm of GaN films, which is important for damageless fabrication of gate-recess GaN-based normally-off power electronic devices. The author systematically studied the PL properties and surface morphologies of GaN films exposed to Cl_2 plasma at 400 ^oC, focusing on their dependences of etch time and ion energy. It is noticeable that PL degradation saturated

at etch times of more than 2 min, while surface roughness increased continuously with etch time. Variations of surface roughness were negligible when bias voltage varied. PID was successfully suppressed by reducing bias voltage, leading to the decrease in incident ion energy on the surface, and thus the near-band-edge emission (NBE) intensity as the PL properties were increased to 98.8% of the initial value in the optimally plasma etching condition for a remove of 6.8 nm of GaN films.

In chapter 5, a further study about photon-dominated damage formation in Cl_2 plasma etching of GaN at 500 ^oC is presented. Deep UV photons emitted from Cl_2 plasmas become a critical cause of degradation in both PL properties and surface stoichiometry as PID in the GaN films after the high-temperature Cl_2 plasma etching. As depended on the stage temperatures above 500^oC, the thermally enhanced formation of photon-induced damage, originated from Cl_2 in Cl_2 plasma emissions at wavelengths around 258 and 306 nm, was observed on the GaN surface with a depth of approximately 3.2 nm. The degradation of the PL properties occurred at an early period of the photon irradiation and then photon-induced damage reached a constant value.

In chapter 6, the author focused on the critical issue in a deep etch of GaN films using the high-temperature Cl_2 plasma etching of GaN, where the severely roughened surface morphology was caused by Cl radicals. Compared with Cl radical exposure at 600 ^oC, simultaneous irradiations of photon and radical successfully prevented the large etch pit formation and the increase of surface roughness. The author notes that Cl_2 plasma emissions in VUV region and UV region at 258 and 306 nm lead to the photodissociation of both Ga and N chlorides and thereby the suppression of chemical reactions in the roughening of a GaN surface was achieved.

Finally, the experimental results in this research were concluded and future perspectives were stated in chapter 7.

1.8 References

1) K. Shenai, R. S. Scott, and B. J. Baliga, IEEE Trans. Electron Devices **36,** 1811 (1989).

2) S. Tirelli, Dr. Thesis, Department of Information Technology and Electrical Engineering, ETH Zurich, Zurich (2014).

3) W. Saito, I. Omura, T. Ogura, and H. Ohashi, Solid-State Electron. **48,** 1555 (2004).

4) N. Q. Zhang, B. Moran, S. P. DenBaars, U. K. Mishra, X. W. Wang, and T. P. Ma, Phys. Status Solidi A **188,** 213 (2001).

5) Z. Diel, Compd. Semicond. **19** [2], 35 (2013).

6) E. Frayssinet, P. Leclaire, J. Mohdad, S. Latrach, S. Chenot, M. Nemoz, B. Damilano, and Y. Cordier, Phys. Status Solidi A (2016) in press.

7) P. Srivastava, J. Das, D. Visalli, M. Van Hove, P. E. Malinowski, D. Marcon, S. Lenci, K. Geens, K. Cheng, M. Leys, S. Decoutere, R. P. Mertens, and G. Borghs, IEEE Electron Device Lett. **32,** 30 (2011).

8) K. Nishizono, M. Okada, M. Kamei, D. Kikuta, K. Tominaga, Y. Ohno, and J. P. Ao, Appl. Phys. Lett. **84,** 3996 (2004).

9) T. Kachi, Jpn. J. Appl. Phys. **53,** 100210 (2014).

10) M. Kanamura, T. Ohki, T. Kikkawa, K. Imanishi, T. Imada, A. Yamada, and N. Hara, IEEE Electron Device Lett. **31,** 189 (2010).

11) J. P. Ibbetson, P. T. Fini, K. D. Ness, S. P. DenBaars, J. P. Speck, and U. K. Mishra, Appl. Phys. Lett. **77,** 250 (2000).

12) M. E. Lin, Z. F. Fan, Z. Ma, L. H. Allen, and H. Morkoç, Appl. Phys. Lett. **64**, 887 (1994).

13) C. B. Vartuli, S. J. Pearton, C. R. Abernathy, R. J. Shul, A. J. Howard, S. P. Kilcoyne, J. E. Parmeter, and M. Hagerott-Crawford, J. Vac. Sci. Technol. A **14,** 1011 (1996).

14) J. J. Freedsman, T. Egawa, Y. Yamaoka, Y. Yano, A. Ubukata, T. Tabuchi, and K. Matsumoto, Appl. Phys. Express **7,** 041003 (2014).

15) Y. Cai, Y. Zhou, K. M. Lau, and K. J. Chen, IEEE Trans. Electron Devices **53,** 2207 (2006).

16) T. Sugiyama, H. Amano, D. Iida, M. Iwaya, S. Kamiyama, and I. Akasaki, Jpn. J. Appl. Phys. **50,** 01AD03 (2011).

17) M. Shimizu, G. Piao, M. Inada, S. Yagi, Y. Yano, and N. Akutsu, Jpn. J. Appl. Phys. **47,** 2817 (2008).

18) J. B. Casady, A. K. Agarwal, L. B. Rowland, W. F. Valek, and C. D. Brandt, *55th Annual Device Research Conference Digest*, p. 32 (1997).

19) B. Metzger, Compd Semicond. **8,** 33 (2002).

20) I. Ben-Yaacov, Y.-K. Seck, U. K. Mishra, and S. P. DenBaars, J. Appl. Phys. **95,** 2073 (2004).

21) M. Kodama, M. Sugimoto, E. Hayashi, N. Soejima, O. Ishiguro, M. Kanechika, K. Itoh, H. Ueda, T. Uesugi, and T. Kachi, Appl. Phys. Express **1,** 021104 (2008).

22) T. Kachi, IEICE Technical Report, ED2008-147 (2008).

23) K.-M. Chang, C.-C. Cheng, and J.-Y. Chu, J. Electronchem. Soc. **149,** G367 (2002).

24) R. Vetury, N. Q. Zhang, S. Keller, and U. K. Mishra, IEEE Trans. Electron Devices **48,** 560 (2001).

25) A. F. Anwar, S. S. Islam, and R. T. Webster, Appl. Phys. Lett. **84,** 1970 (2004).

26) K. Horio, K. Yonemoto, H. Takayanagi, and H. Nakano, J. Appl. Phys. **98,** 124502 (2005).

27) H. J. Nam, H. G. Choi, M.-W. Ha, H. J. Song, C. H. Roh, J. H. Lee, C.-K. Hahn, and J. H. Park, J. Korean Phys. Soc. **59,** 439 (2011).

28) T. Hashizume, J. Kotani, and H. Hasegawa, Appl. Phys. Lett. **84,** 4884 (2004).

29) G. Meneghesso, G. Verzellesi, R. Pierobon, F. Rampazzo, A. Chini, U. K. Mishra, C. Canali, and E. Zanoni, IEEE Trans. Electron Devices **51,** 1554 (2004).

30) M.-F. Romero, A. Jiménez, F. G.-P. Flores, S. Martín-Horcajo, F. Calle, IEEE Trans. Electron Devices **59,** 374 (2012).

31) Y. H. Lai, C. T. Yeh, J. M. Hwang, H. L. Hwang, C. T. Chen, and W. H. Hung, J. Phys.

Chem. B **105,** 10029 (2001).

32) T. Hashizume and R. Nakasaki, Appl. Phys. Lett. **80,** 4564 (2002).

33) T. Aoki, H. Wakayama, N. Kaneda, T. Mishima, K. Nomoto, and K. Shiojima, Jpn. J. Appl. Phys. **52,** 11NH03 (2013).

34) M. Minami, S. Tomiya, K. Ishikawa, R. Matsumoto, S. Chen, M. Fukasawa, F. Uesawa, M. Sekine, M. Hori, and T. Tatsumi, Jpn. J. Appl. Phys. **50,** 08JE03 (2011).

35) R. Kawakami, T. Inaoka, K. Tominaga, A. Kuwahara, and T. Mukai, Jpn. J. Appl. Phys. **47,** 6863 (2008).

36) Y. Tamura, J. Ohta, H. Fujioka, and S. Samukawa, Ext. Abstr. 2012 Int. Conf. Solid State Devices and Materials, 2012, p.925.

37) S. Chen, Y. Lu, R. Kometani, K. Ishikawa, H. Kondo, Y. Tokuda, M. Sekine and M. Hori, AIP Advances **2,** 022149 (2012).

38) B. Brunetti, V. Piacente, and P. Scardala, J. Chem. Eng. Data **55,** 98 (2010).

39) G. T. Armstrong, J. Res. Natl. Bur. Stand. **53,** 263 (1954).

40) T. F. O'Brien, T. V. Bommaraju, and F. Hine: in *Handbook of Chlor-Alkali Technology Volume I: Fundamentals* (Springer, New York, U. S. A., 2005) p. 921.

41) C. Bernard, C. Chatillon, A. Ait-Hou, R. Hillel, Y. Monteil, and J. Bouix, J. Chem. Thermodynamics **20,** 129 (1988).

42) B. Brunetti, J. Chem. Eng. Data **55,** 2455 (2010).

43) D. G. Kent, K. P. Lee, A. P. Zhang, B. Luo, M. E. Overberg, C. R. Abernathy, K. D. Mackenzie, S. J. Pearton, and Y. Nakagawa, Solid-State Electron. **45,** 1837 (2001).

44) S. Nakamura, T. Mukai, M. Senoh, and N. Iwasa, Jpn. J. Appl. Phys. **31,** L139 (1992).

45) Q. Fan, S. Chevtchenko, X. Ni, S. J. Cho, F. Yun, and H. Morkoc¸, J. Vac. Sci. Technol. B **24,** 1197 (2006).

46) X. A. Cao, H. Cho, S. J. Pearton, G. T. Dang, A. P. Zhang, F. Ren, R. J. Shul, L. Zhang, R.

Hickman, and J. M. Van Hove, Appl. Phys. Lett. **75,** 232 (1999).

47) R. J. Shul, S. P. Kilcoyne, M. H. Crawford, J. E. Parmeter, C. B. Vartuli, C. R. Abernathy, and S. J. Pearton, Appl. Phys. Lett. **66,** 1761 (1995).

48) R. Kometani, K. Ishikawa, K. Takeda, H. Kondo, M. Sekine, and M. Hori, Appl. Phys. Express **6,** 056201 (2013).

Chapter 2: Plasma diagnostic and film analyses

2.1 Overview

The introductions of the principals of both plasma diagnostic and film analyses are the focus in this chapter. Optical emission spectroscopy (OES) was applied to diagnose plasma status and identify active species in the plasmas. X-ray photoelectron spectroscopy (XPS) was carried out for both compositional and chemical information on the GaN surface after plasma etching. Atomic force spectroscopy (AFM) was utilized to observe the morphology of etched GaN surfaces. Scan electronic spectroscopy (SEM) was applied to observe the cross sectional image of etch profiles and measure the etch depths. PL was performed to analyze the optical properties of GaN films, which could diagnose bulk PID after plasma etching.

2.2 Optical emission spectroscopy (OES)

To diagnose plasma chemistries, the author focused on active species in plasmas of atomic and molecular radicals. Typically, various spectroscopic analyses such as laser and absorption spectroscopy, interferometry, and OES are utilized.[1)] In this study, the author applied OES because it could directly detect active species. Moreover, OES promises advantages that plasmas are hardly affected during the measurement, and the setup for the whole apparent would not be expensive as the absence of lasers.

The observation of measured OES of plasmas is widely performed through identical optical emissions of each active species that are formed by a variety of complicated processes such as electron impact, electron dissociation, and photon absorption. Indeed, the dominant process of the excitation of the ground state of a species is attributed to electron impact that occurs in plasmas frequently, as shown in Fig. 2.1. Hence, this process is formulated in (2.2.0):

$$e + Y \rightarrow e + Y^* \tag{2.2.0}$$

where Y is the species of the ground state and the superscript $*$ the excited state of the species in plasmas. On the other hand, Fig. 2.1 also shows a de-excitation of the active species Y^* that emits a photon with the energy equal to the difference between the excited and the ground state, as formulated in (2.2.1):

$$Y^* \rightarrow Y + h\nu \tag{2.2.1}$$

where h is the Planck constant and ν the frequency of a photon. Here, the optical emission intensity I_Y results from the transition process from the excited to the ground state, as formulated in (2.2.2):

$$I_Y \propto n_Y n_e \int v(\varepsilon) f_e(\varepsilon) \sigma_Y(\varepsilon) d\varepsilon = n_Y n_e k_{eY} \tag{2.2.2}$$

where n_Y is the concentration of species Y, n_e the electron density of the plasmas, $v(\varepsilon)$ the electron velocity of an electron energy ε, $f_e(\varepsilon)$ the electron energy distribution function of an electron energy ε, $\sigma_Y(\varepsilon)$ the collisional cross-section of an electron energy ε, and k_{eY} a

coefficient of the excitation rate. Obviously, when n_e and k_{eY} are maintained, I_Y should be in direct proportion to n_Y. In fact, some external parameters like pressure and power in plasmas easily affect n_e and k_{eY}. As a result, OES is frequently used to monitor plasma chemistries.[2-6)]

Generally, the utilization of a spectrometer is essential in the measurement of OES. Typically, there are two experimental setups for the spectrometer, one is a monochromator equipped with a photomultiplier tube (PMT) and the other is a multi-channel spectrometer equipped with a charged coupled device (CCD) array. For a monochromator system, an incident light travels through the exit slit and its intensity is measured by PMT. For a multi-channel spectrometer system, the intensity of an incident light is directly measured by CCD array. Apparently, the multi-channel spectrometer is capable to simultaneously detect a wide wavelength range. However, the dimension of the pixel of CCD array limits its resolution.

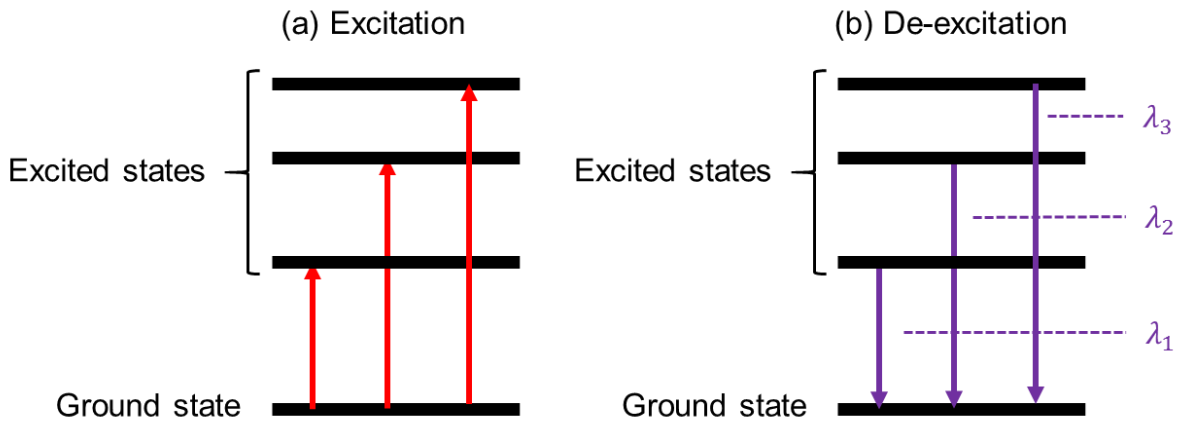

Fig. 2.1 Schematic illustrations of the principles of OES:

(a) Excitation and (b) De-excitation.

2.3 X-ray photoelectron spectroscopy (XPS)

2.3.1 Principle

In recent decades, XPS has become one of the most powerful techniques in the surface analysis. For the surface characterization, photoelectrons are excited by X-ray radiations and then escape from the material into the vacuum.[7] Here, the electrons of some element in the measured material are featured by their binding energies. Moreover, the compositional information can be acquired from the energy spectrum that is surveyed by a spectrometer. The binding energies and the energy of X-ray radiations can be used to obtain the kinetic energy of the electrons, which is formulated in (2.3.0):

$$E_k = h\nu - E_B - \phi \tag{2.3.0}$$

where E_k is the kinetic energy, $h\nu$ the energy of the X-ray photon, E_B the binding energy of an electron, and ϕ a constant, representing the work function of the spectrometer.

Apparently, E_B must be weaker than $h\nu$. The electrons can potentially escape from the valence band or from core levels. The author notes that electrons in core levels are primarily studied in XPS measurement. Moreover, the elemental analysis is enabled by the measurement for the identical kinetic energies of photoelectrons of a certain element.

Generally, the relatively low escape depth of the elastically scattered electrons with a range from 0.5 to 2 nm determines the surface sensitivity.[8] Moreover, all elements besides H and He can be detected through identical peak positions of binding energies. On the other hand, chemical information of the interest element, depending on its chemical bonding of the material, can be easily acquired through the characteristic chemical shifts of binding energies.

2.3.2 Calculation for chemical composition

The number of detected photoelectrons is easily calculated because it is in direct proportion to the intensity of the photoelectron spectrum. However, to determine the concentration quantification of a certain element in the material, not only the intensity of the photoelectron spectrum but also other parameters like the photoionization cross-section need to be taken into account. Hence, the basic calculation for chemical composition of a certain element A is formulated in (2.3.1):

$$I_{iA} = n_A K \sigma_{iA} \lambda_{iA} T_{iA} \tag{2.3.1}$$

where I_{iA} is the total photoelectron intensity of the core level i of element A, n_A the atomic concentration of element A, K the instrumental factor including terms of angular acceptance, total transmission of the spectrometer, and X-ray flux, σ_{iA} the photoionization cross-section, λ_{iA} the electron escape depth, and T_{iA} the transmission coefficient of the electrons through the sample surface.

The proper method to subtract the background of the photoelectron spectrum of a certain element is quite critical. Typically, an easy linear approach or a physically determined function has been widely studied. In this dissertation, the author utilized a mostly used method called Shirley for the background subtraction, which enables the integrated calculation of a background under the photoelectron peaks.

Usually, the author defines a unique term called sensitivity factor S_{iA} of the core level i of a certain element A in (2.3.2), which allows the simplest calculation for the chemical concentration n_A that is formulated in (2.3.3):

$$S_{iA} = \sigma_{iA} \lambda_{iA} \tag{2.3.2}$$

$$n_A = \frac{I_{iA}/S_{iA}}{\sum_X I_X/S_X} \tag{2.3.3}$$

where I_{iA} is the integrated intensity of the photoelectron spectrum of the core level i of the element A, I_X the integrated intensity of the photoelectron spectrum of another element X, and S_X its relative sensitivity factor.

The author notes that this simple strategy for the calculation of chemical concentration using sensitivity factors can achieve a high accuracy with a reasonable error of 10%.[8] Generally, the sensitivity factors can be acquired from a certain element or a standard sample measured under equivalent conditions in a first approximation. However, errors would become significantly for the inhomogeneous sample, suggesting that the energy dependence of photoelectron escape depth should also be considered to evaluate the chemical composition. In this study, the author estimated chemical compositions using sensitivity factors of Ga *3d*, N *1s* and O *1s* from literature values determined in the bulk GaN because of small differences of photoelectron escape depths between GaN and Ga_2O_3.[9]

2.3.3 Depth profiling by angle-resolved XPS

Besides the calculation of atomic composition, depth profiling categorized into destructive and nondestructive methods can be analyzed by XPS.

Ion sputtering is a destructive depth profiling technique using noble gases like Ar, Xe, and Kr with a medium energy range between 1 and 5 keV.[8)] Then, the surface of the measured material is eroded by ion sputtering with an erosion rate ranging from 1 to 10 nm/min.[8)] Hence, after several intervals of the sputtering depth, depth profiling can be acquired through sequential measurements of atomic intensities. However, ion sputtering is capable to cause bond-breaking and structural changes, leading to the limitation of the chemical information from depth profiling.

On the other hand, angle-resolved XPS (ARXPS) is the most used nondestructive depth profiling technique. Its resolution is generally limited to the first few nanometers of the surface region because of the limited escape depth of electrons used in this technique. Here, the author firstly defines an effective information depth d that contains approximately 95% of the photoelectron signals and strongly depends on the take-off angle θ of the surface normal to the photoelectron detector, as formulated in (2.3.4):

$$d = 3\lambda cos\theta \tag{2.3.4}$$

where λ is the inelastic mean free path (IMFP), which strongly depends on both electron energy and material. Namely, the XPS sampling depth can be determined.

Generally, ARXPS can be utilized to measure the thickness of a certain layer quantitatively. Here, the author describes an example of the thickness calculation using a two layer material A and B, as shown in Fig. 2.2. The author notes that the thickness of layer B (D > 5 λ) is larger than that of layer A (d < 3 λ). The photoelectron intensity of I_A is then integrated from 0 to d and formulated in (2.3.5):

$$I_A = I_A^{\infty}(1 - e^{-\frac{d}{\lambda_{A,A}cos\theta}}) \tag{2.3.5}$$

where I_A^∞ is the photoelectron intensity from the bulk A and $\lambda_{A,A}$ is the IMFP of photoelectrons from layer A travelling through layer A. The photoelectron intensity of I_B is then attenuated by travelling through layer A and thereby formulated in (2.3.6):

$$I_B = I_B^\infty e^{-\frac{d}{\lambda_{B,A}cos\theta}} \tag{2.3.6}$$

where I_B^∞ is the photoelectron signal from layer B arriving at the $B-\mathrm{A}$ interface and $\lambda_{B,A}$ is the attenuation length of the emitted electrons from layer B passing through layer A.

Apparently, with the increase of θ, I_A increases but I_B decreases. Then, by simplifying $\lambda_{A,A} = \lambda_{B,A} = \lambda$, the ratio of I_A and I_B can be determined in (2.3.7):

$$\frac{I_A}{I_B} = \frac{I_A^\infty}{I_B^\infty}(e^{\frac{d}{\lambda cos\theta}} - 1) \tag{2.3.7}$$

Therefore, the thickness d of layer A is described in (2.3.8):

$$d = \lambda cos\theta \ln(\frac{I_B^\infty}{I_A^\infty} \times \frac{I_A}{I_B} + 1) \tag{2.3.8}$$

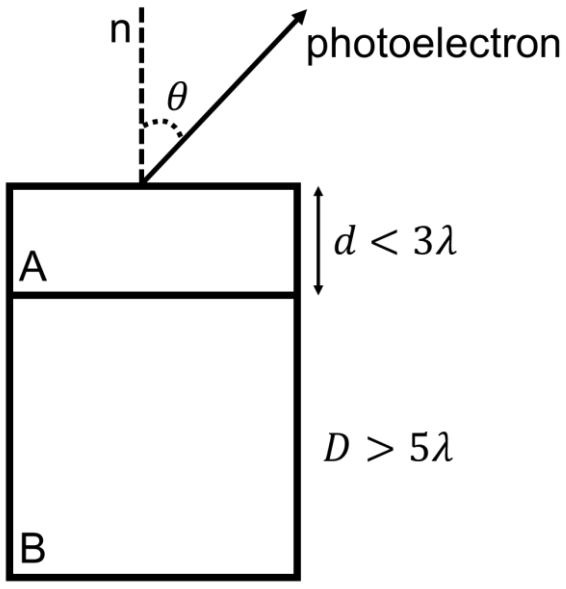

Fig. 2.2 Relation of take-off angle and sample surface.

2.4 Atomic force microscopy (AFM)

AFM promises a high-resolution three-dimensional surface morphology of a certain material, which enables imaging, measuring and manipulating at a nano-scale.[10] In this dissertation, AFM is mostly used to observe the surface morphology of the GaN films, allowing the author to analyze the intrinsic threading dislocations on GaN before and after plasma etching. As a result, the author can extensively understand the mechanism of the surface reactions and achieve in the optimization of the low damage plasma etching of GaN.

Figure 2.3(a) shows an example of the surface morphology for a fully coalesced GaN film with a dimension of 10 × 10 μm^2.[10] Typically, the high quality GaN film was grown by the metal-organic chemical vapor deposition (MOCVD) method on the sapphire substrate. Moreover, the surface morphology of this sample characteristically showed a long and uniform crystallographic step and the altitude of terrace was measured to approximately 0.3 nm. On the other hand, the surface morphology of an un-coalesced GaN film with a dimension of 20 × 20 μm^2 was shown in Fig. 2.3(b), where obvious black pits were easily observed in this poor-quality GaN film.[10]

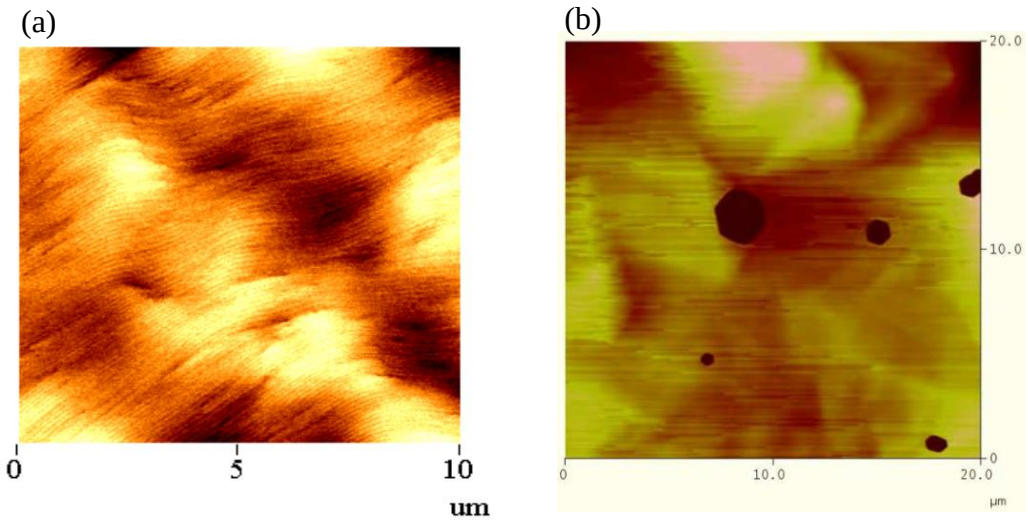

Fig. 2.3 AFM images for (a) high quality, fully coalesced GaN films and (b) for un-coalesced GaN films.[10]

Next, the typical experimental apparatus for AFM is introduced, as shown in Fig. 2.4(a). Generally, a sharp and tiny tip made of Si_3N_4 or Si with an order of a few nanometers is mounted at the end of a cantilever that is the most important part of AFM, as shown in Fig. 2.4(b). To successfully observe a surface morphology, the distance between the tip and the sample surface needs to be close enough so that interatomic forces (e.g., van der Waals, chemical bonding electrostatic, magnetic, and mechanical contact forces) can affect the tip atoms. Therefore, different dominant interatomic forces are expected to depend on the distance between the tip and the sample surface, as shown in Fig. 2.5.[11] Taking van der Waals forces as an example, they are considered to be predominant in the interactions for the surface-tip distance larger than 1 nm, which can result in a deflection of the cantilever. Particularly, a laser spot reflected from the cantilever surface can measure the deflection and then photodiodes are sequentially used to detect these laser signals, as shown in Fig. 2.4(a).

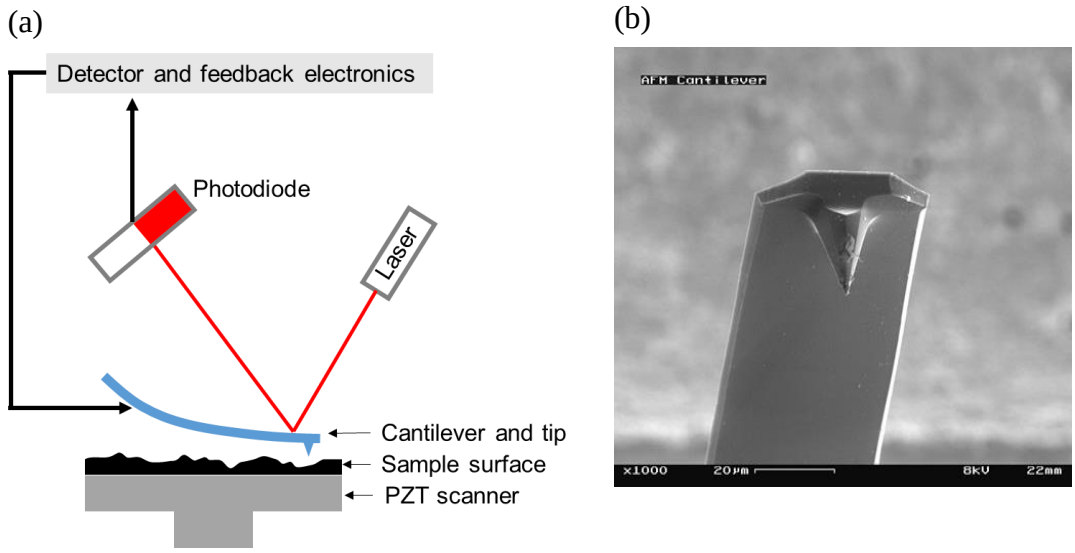

Fig. 2.4 (a) Schematic scheme of AFM setup. (b) SEM image of an AFM cantilever and tip.[11]

The operation of AFM can be divided in two primary modes, contact and non-contact modes.[12] For contact mode, the cantilever is straightly towed across the sample surface and thereby the surface profiles are recorded according to the deflection of the cantilever. The author notes that the deflection of the cantilever is maintained using a feedback loop to adjust the z position of a scanner and therefore the analysis of the sample morphology is possible. On the other hand, for the non-contact mode, the tapping mode is one of the representative that is used in this dissertation because of its damageless for the sample surface during the measurement. Typically, the cantilever is peripherally oscillated according to its primitive resonance frequency. Hence, the magnitude of the oscillation would gradually decrease when the tip approaches the sample surface as a result of the interatomic forces performed on the cantilever. In addition, not only the oscillation phase but also the resonance frequency are controllable by varying the surface-tip interaction forces. Namely, the relative variations of peripheral oscillation compared with the reference one allows the author to obtain effective information about the characteristic sample surface.

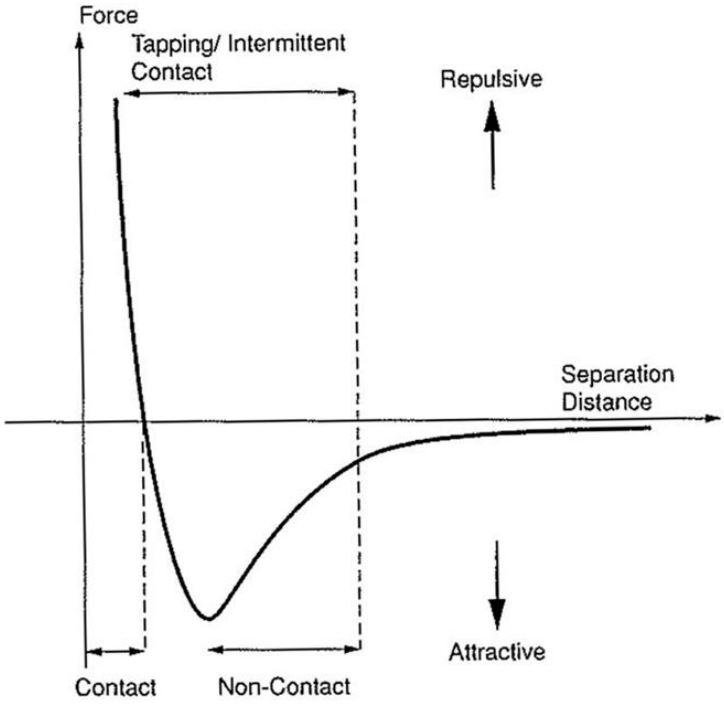

Fig. 2.5 Schematic of interatomic forces as a function of surface-tip distance.[11]

2.5 Scanning electron microscopy (SEM)

SEM is an extremely powerful method that enables nanometer-scale images for both a sample surface and a cross-sectional view.[13,14] Figure 2.6 depicts a simple scheme of a SEM setup that contains an electron gun, condenser lenses, scan coils, objective lenses, and a detector of secondary electrons. A vacuum column is used to guarantee a high vacuum in the measurement. Here, the resolution of SEM is determined based on the De Broglie equation,[15] as formulated in (2.5.1):

$$\lambda_e = \frac{h}{mv} = \frac{h}{\sqrt{2qmV}} = \frac{1.22}{\sqrt{V}}\ (nm) \tag{2.5.1}$$

where h is the Planck constant, λ_e the wavelength of electrons, m the mass of an electron, v the electron velocity, q the elementary charge, and V the accelerating voltage (kV). Apparently, when V is increased to 10 kV, λ_e can be reduced to a remarkable extent of approximately 0.012 nm, which is rather smaller than that of the visible light with a wavelength range from 350 to 770 nm. Namely, SEM allows a rather higher resolution compared with the optical microscope.

The electrons are firstly ejected from the electron gun in random directions and their energies are particularly ranging from 1 to 30 keV. Then, these electrons, travelling through condenser lenses, are emitted as an electron-beam. Next, this electron-beam is deflected by scan coils within a rectangular area, and the observation spot of interest is aimed and focused using the objective lenses before the beam arrived at the sample.

Generally, collecting secondary electrons with energies below 50 eV that are commonly formed beneath the sample surface for a few nanometers is the fundamental imaging method. The author notes that the detected signals are usually smaller for the flat samples than those of rough ones when they are placed normal to the electron-beam. On the other hand, the range of magnification used in SEM is commonly from 10 to 2×10^5 times, resulting in a resolution ranging from 4 to 10 nm.[13]

Indeed, not only can SEM provide a further higher two dimensional resolution than that of the common optical microscope but also enable a much wider observation in the vertical direction, allowing the author to focus a variety of objectives. In addition, SEM promises a relatively simple preparation for the conductive samples. However, as SEM measurements are performed in vacuum, the preparation for insulating samples like SiO_2 is difficult because of a critical issue called excessive charge built-up. To solve it, a thin conductive layer such as C or Au is suggested to be deposited onto the sample surface, which is quite effective but also cause damages on samples.

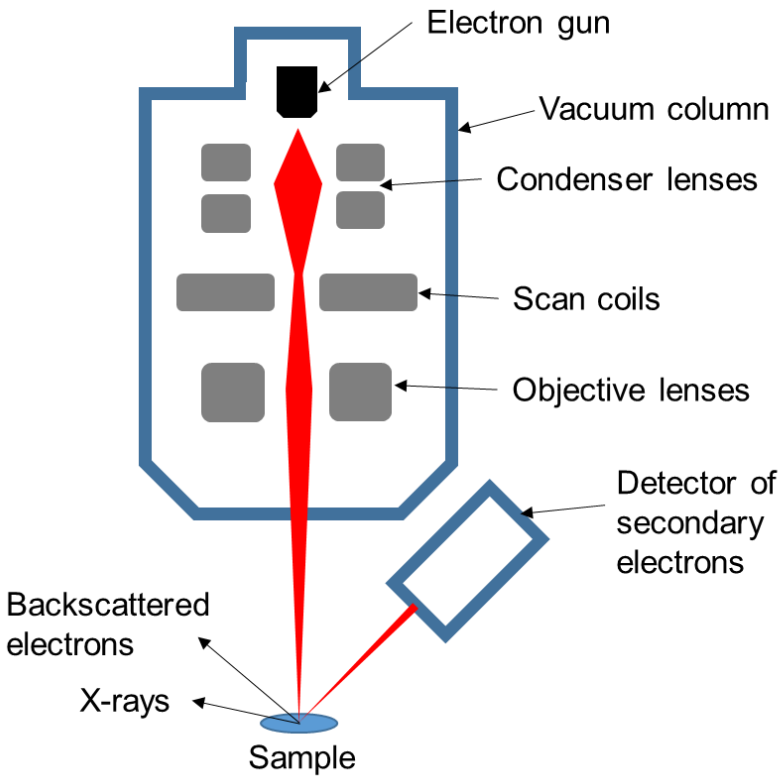

Fig. 2.6 Schematic scheme of SEM setup.

2.6 Photoluminescence (PL)

2.6.1 Principle

PL is widely used in analysis of surface and interfaces. In this dissertation, PL is used to diagnose plasma-induced damage of GaN. Generally, a light that is spontaneously emitted from a certain sample under the optical excitation can be used in the interpretation of PL.[16] The detailed mechanisms are described as follows. When the optical excitation like a laser light with a sufficient energy is injected into a material, the absorption of photons would occur and thereby electronic excitations are generated. Next, the relaxation of these excitations would finally occur, letting the electrons return to the ground state. Here, PL is the emitted light if radiative relaxation arises. As a result, the author can achieve the information about the transition energies and thereby determine electronic energy levels according to the PL spectrum.[16] The author notes that the PL measurement is damageless for samples because of its gentle manipulation and little environmental control.

Typically, PL is a powerful instrument to analyze surfaces of a material because it is usually derived from the surface. A variety of discrete electronic states that lie near surfaces and interfaces can be probed in detail by PL because of its distinct sensitivity. By analyzing the dependence of the excitation intensity on the PL spectrum, both the density of interface states and the energy distribution can be determined. The author also notes that PL intensities can be affected by the surface adsorbates. Moreover, the depth profile of the long-lived trap states can be ascertained using thermal activation that the temperature dependence of PL is performed. Particularly, for nonradiative traps that vary the time-resolved PL signals of radiative transitions are predominant in the transient PL signal of a certain material with a low carrier density.[16]

Figure 2.7 shows a typical schematic diagram of a PL measuring system. An optical excitation is generated from a laser with a typical energy that verges on the bandgap of a certain

material, and then penetrates this material with a penetration depth determined by the absorption coefficient. Usually, the sample preparation is not complicated because no electrical excitation or detection is concerned in the PL analysis, which enables an evaluation for the unpromising conductive materials that contact or junction technology has not been well developed. Particularly, PL is remarkably attractive for analyzing a prompt transient behavior of a certain material because it promises a fast and straightforward measurement of the PL spectrum.

Regarding the temperature commonly used in the PL analysis, RT is sufficient for a variety of purposes although PL is characteristically temperature-dependent. In some cases, an extremely low temperature using liquid helium is demanded to obtain the highest resolution. Moreover, PL is less sensitive about material thickness, surface roughness, and beam alignment compared with other optical tools (e.g., reflection and absorption).[16)]

Apparently, PL has become so popular because it is very simple to measure optical properties and probe the primary electronic characteristics. However, there is a fundamental requirement that the material under the optical excitation should emit light, indicating that indirect bandgap semiconductors have intrinsically poor PL efficiency. Moreover, the author notes that nonradiative centers are predominantly in the relaxation of excitations, and this phenomenon will be enhanced for a surface of poor quality.[16)] As a result, PL analysis can be applied to analyze the mechanisms about not only nonradiative but also radiative recombinations. The author emphasizes that PL analysis is difficult to straightforwardly characterize the nonradiative traps, but their specificities in the PL measurements.[16)]

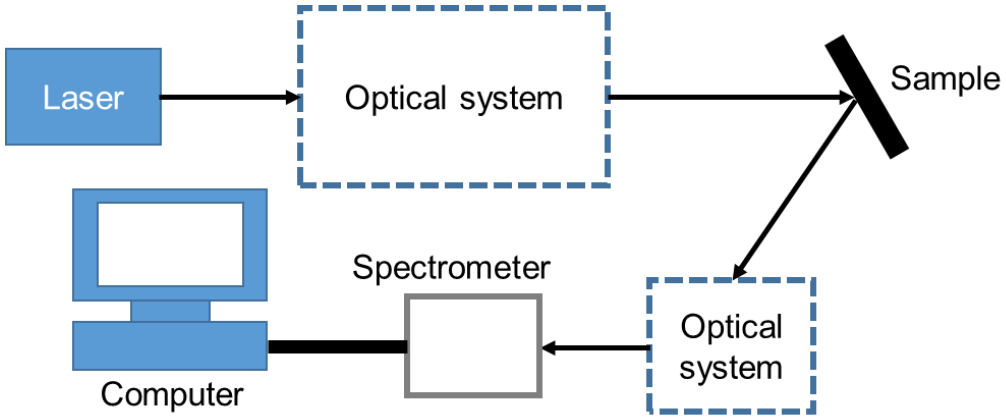

Fig. 2.7 Typical schematic diagram of experimental apparatus.[16)]

2.6.2 PL spectrum of GaN

Firstly, Maruska and Tietjen precisely determined the GaN band gap energy of 3.39 eV.[17] Then, Pankove *et al.* determined the PL spectra of the GaN films at a low temperature of 1.6 K that an intense near-band gap emission at 3.477 eV and a relatively weaker emission at 3.37 eV were observed.[18] Soon after, Dingle *et al.* reported a particular analysis about the PL spectra of the GaN films at a low temperature of 2 K.[19-21] Grieshaber *et al.* reported a typical GaN PL spectrum at RT, as shown in Fig. 2.8.[22] A strong near-band gap luminescence at RT recorded at 3.405 eV (365 nm) was observed, and it was interpreted as several transitions like a free exciton, a donor-bound exciton, or a donor-to-valance-band transition.[22] Moreover, a second yellow luminescence band with an oscillating structure recorded around 2.2 eV (560 nm) identified as an optically active deep-level transition was observed, attributing to the Ga vacancy-containing defects.[23]

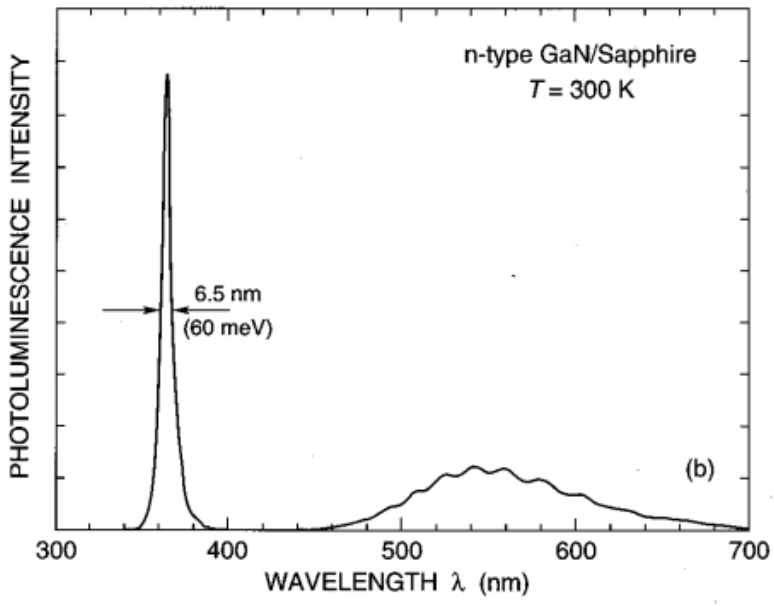

Fig. 2.8 GaN PL spectrum at RT excited by a He-Cd laser emitting at 325 nm (3.81 eV) with an output power of 16 mW.[22]

2.6.3 Penetration depth

The definition of penetration depth is how deep a light or an electromagnetic wave can penetrate into a certain material. In the PL measurement, if an optical excitation with an initial intensity I_0 is injected into a material with an absorption coefficient α, then its intensity after travelling a certain distance d will be exponentially attenuated to I, which can be calculated based on Beer-Lambert law, as formulated in (2.6.0),

$$I = I_0(1 - R)e^{-\alpha d} \tag{2.6.0}$$

where R is the reflectivity of the material. Here, the author notes that penetration depth d_{pe} is determined as the depth where the emission intensity inside the material reduces to 1/e (about 37%) of the primitive value. Hence, d_{pe} can be described as

$$d_{pe} = \frac{1}{\alpha} \tag{2.6.1}$$

Typically, the absorption coefficient of GaN strongly depends on the photon energy of the incident light. Therefore, α can be experimentally obtained to be 1.19×10^5 cm^{-1} from Fig. 2.9[24] for the He-Cd laser (3.81 eV) applied in this dissertation, suggesting that d_{pe} is nearly 84 nm. Here, the author notes that an exciton peak is clearly observed in the absorption spectrum for GaN at RT, showing the excitonic absorption that corresponds to the exciton binding energy.[24]

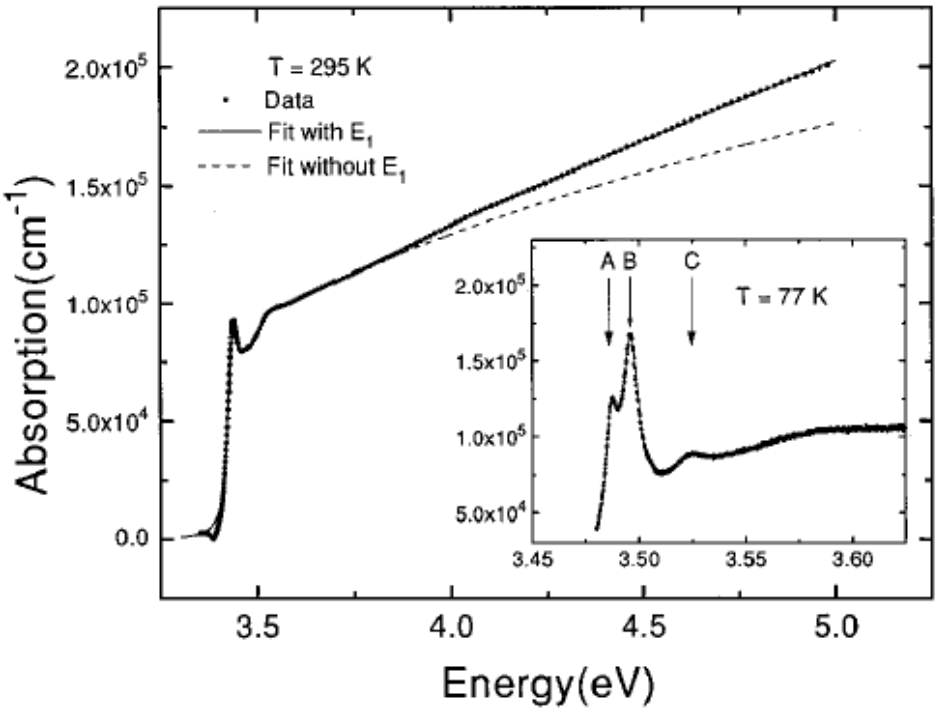

Fig. 2.9 Absorption spectrum for GaN at RT.[24)]

2.6.4 Photoluminescence peak position: Energy levels

The perturbation in the band structure of a certain material that attributes to the broken crystal periodicity by defects or impurities can be identified through analyzing a discrete energy level in the bandgap. The energy level usually behaves as a donor or acceptor state that depends on the species of the defect or impurity. Then, these states should trap carriers for an adequately low temperature in the PL measurement. For a radiative recombination center, the energy level of the defect or impurity could be ascertained based on the emitted light energy. Typically, the states located in shallow levels near the conduction or valence band edge usually act as radiative recombination centers, which should be measured in a sufficiently low temperature to suppress the thermal activation on trapped carriers. On the other hand, the states located in deep levels are more likely to act as nonradiative centers, emitting phonons due to the transitions of carriers from the intermediate level to the valence and conduction bands. Figure 2.10 shows a detailed illustration of both radiative and nonraidative recombination transitions.[16)]

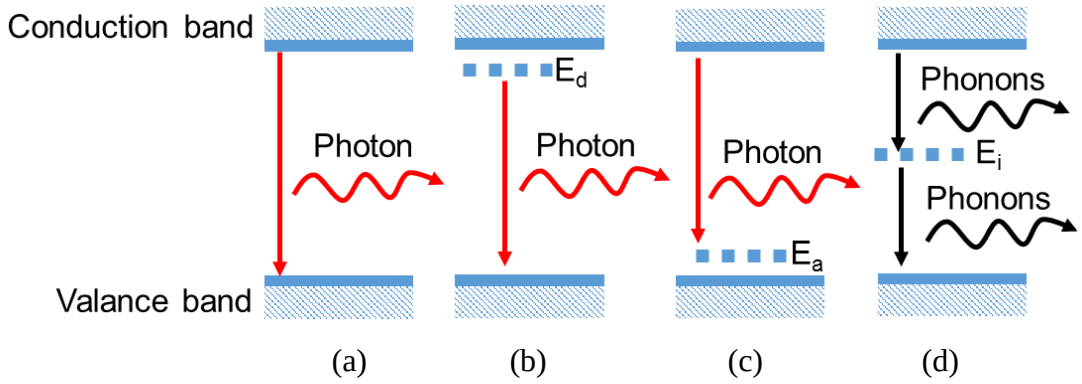

Fig. 2.10 Illustrations of both radiative and nonradiative recombination transiations: (a) a radiative path from conduction to valance band, (b) a radiative path from donor state to a valence band, (c) a radiative path from conduction band to an acceptor state, (d) a nonradiative recombination by an intermediate state.[16)]

2.7 References

1) R. Payling and P. Larkins, *Optical Emission Lines of the Elements* (Wiley, Chichester, U. K., 2004).

2) J. W. Corburn and M. Chen, J. Appl. Phys. **51,** 3134 (1980).

3) Y. Kawai, K. Sasaki, and K. Kadota, Jpn. J. Appl. Phys. **36,** L1261 (1997).

4) R. E. Walkup, K. L. Saenger, and G. S. Sewyn, J. Chem. Phys. **84,** 2668 (1986).

5) H. M Katsch, A. Tewes, E. Quandt, A. Goehlich, T. Kawetzki, and H. F. Dobele, J. Appl. Phys. **88,** 6232 (2000).

6) S. F. Durrant and M. A. B. Moraes, J. Vac. Sci. Technol. A **13,** 2513 (1995).

7) K. Siegbahn, C. Nordling, A. Fahlman, R. Nordberg, K. Hamrin, J. Hedman, G. Johansson, T. Bergmark, S.-E. Karlsson, I. Lindgren, and B. Lindberg, *ESCA: Atomic, Molecular, and Solid Sate Structure Studied by Means of Electron Spectroscopy* (Almqvist and Wiksells, Uppsala, Sweden, 1967).

8) S. Oswald, in *Encyclopedia of Analytical Chemistry*, ed. R. A. Meyers (Wiley, Chichester, U. K., 2013).

9) S. Tanuma, C. J. Powell, and D. R. Penn, Surf. Interface Anal. **11,** 57 (1988).

10) V. Bellitto, *Atomic Force Microscopy – Imaging, Measuring and Manipulating Surfaces at the Atomic Scale* (InTech, Rijeka, Croatia, 2012).

11) T. L. Alford, L. C. Feldman, and J. W. Mayer, *Fundamentals of Nanoscale Film Analysis* (Springer, New York, U. S. A., 2007).

12) Q. Zhong, D. Inniss, K. Kjoller, and V. B. Elings, Surf. Sci. **290,** L688 (1993).

13) The Surface Science Society of Japan, *Scanning Electron Microscope for Nano-technology* (Maruzen, Tokyo, Japan, 2004).

14) P. Sigmund, Phys. Rev., **184,** 383 (1969).

15) D. K. Schroder, *Semiconductor Materials and Device Characterization* (Wiley, New York,

U. S. A., 2006).

16) T. H. Gfroerer, in *Encyclopedia of Analytical Chemistry*, ed. R. A. Meyers (Wiley, Chichester, U. K., 2000).

17) H. P. Maruska and J. J. Tietjen, Appl. Phys. Lett. **15,** 327 (1969).

18) J. I. Pankove, J. E. Berkeyheiser, H. P. Maruska, and J. Wittke, Solid State Commun. **8,** 1051 (1970).

19) R. Dingle and M. Ilegems, Solid State Commun. **9,** 175 (1971).

20) R. Dingle, D. D. Sell, S. E. Stokowski, and M. Ilegems, Phys. Rev. B **4,** 1211 (1971).

21) R. Dingle, D. D. Sell, S. E. Stokowski, P. J. Dean, and M. Ilegems, Phys. Rev. B **3,** 497 (1971).

22) W. Grieshaber, E. F. Schubert, I. D. Goepfert, R. F. Karlicek, Jr., M. J. Schurman, and C. Tran, J. Appl. Phys. **80,** 4615 (1996).

23) M. A. Reshchikov and H. Morkoç, J. Appl. Phys. **97,** 061301 (2005).

24) J. F. Muth, J. H. Lee, I. K. Shmagin, R. M. Kolbas, H. C. Casey, Jr., B. P. Keller, U. K. Mishra, and S. P. DenBaars, Appl. Phys. Lett. **71,** 2572 (1997).

Chapter 3: Suppression of damage formation on GaN by the control of stage temperature

3.1 Introduction

In the fabrication of GaN-based devices, plasma etching technology provides advantageously anisotropic etch profiles, high etch rates, smooth side walls, and clean bottom surfaces.[1,2] GaN is usually etched by applying a Cl_2 plasma at RT. However, a Ga-enriched surface causes preferential loss of N atoms because of the formation of etch products such as NCl_3 or N_2 with vapor pressures higher than that of $GaCl_x$.[3] The resultant nonstoichiometric surface caused a degradation in electrical and optical properties.[4-6] Consequently, a stoichiometric surface should be maintained in the fabrication of GaN-based devices.

As the temperature increased, crystallinity was facilitated by the recombination of dissociated Ga atoms and N atoms in the N_2 plasma on the sputtering surface.[7] At the same time, the N_2 plasma processes at 600 ^oC depressed the preferential N loss and provided a smooth surface.[7] Nevertheless, the high-temperature N_2 plasma failed to provide the desired PL properties.[8] PID is crucial in the degradation of performance and the reliability of the devices (e.g., breakdown at low voltages and the leakage current of diodes).[9,10]

Various reactive species such as ions, radicals, and photons in plasmas are used to irradiate the etching surface. Unfortunately, these species formed damages in the GaN films with their respective mechanisms.[4,11,12] Thus, the effect of each species must be separately investigated.

For the realization of low-damage processing, the author has studied PID in the high-temperature plasma etching. Previously, capacitively coupled Cl_2 plasma etching with stage temperatures ranging between 200 and 600 ^oC was reported to enhance the vaporization of $GaCl_x$ and thereby maintained the stoichiometry at the initial value.[13]

In this chapter, the author extensively studied the mechanism of damage formation in the high-temperature plasma etching. In order to achieve low damage in GaN etching, the author analyzed the PID-degraded PL properties in bulk GaN. Furthermore, the author investigated the effects of ions, radicals, and photons separately from that of plasma using the PAPE method.[14)]

3.2 Experimental details

Samples were 5-μm-thick n-GaN films doped with Si (10^{18} cm^{-3}) and grown by hydride vapor phase epitaxy (HVPE) on a sapphire substrate. Prior to etching, the samples were cleaned by dipping into 2% hydrofluoric acid for 1 min to remove native oxides and then into 17.5% hydrochloric acid for 5 min to remove metallic contaminants.

The experimental setup is shown schematically in Fig. 3.1(a). An inductively coupled plasma (ICP) etcher with a low inductance antenna was developed in house. A showerhead was included to introduce Cl_2 gas at a flow rate of 50 sccm, and the pressure was maintained at 20 Pa using an automatic pressure controller (VAT PM-4). Plasma was generated by 13.56 MHz radio frequency (RF) power (400 W) supplied to the ICP antenna. Negative DC bias voltage as self-bias voltage was measured to be close to 90 V. Both plasma and negative ion density could be estimated from the literature values with a scale of 10^{11} cm^{-3}.[15,16)] A detailed measurement of these plasma parameters should be concerned in the future scope.

The samples were set on the SiC stage, to which was applied 3.2 MHz medium-frequency (MF) power (peak-to-peak voltage: 220 V). The stage was preliminarily heated by radiation from an infrared lamp system (Thermo Riko GV) in the range from 300 to 600 ^{o}C. The stage temperature was measured using a pyrometer (LEC Infrared Thermometer) and the calibration was performed based on the melting point of aluminum. The author notes that the stage was rapidly heated to 205 ^{o}C by Cl_2 plasma heating when the heater was not used. Moreover, the stage temperature during etching fluctuated during the plasma etching as a result of this plasma

heating with an increase rate of approximate 1 ºC/20 s. Hence, the author slowly reduced the current of the infrared lamp system to maintain the stage temperature. Typical etching time was 2 min.

A metal-covered mask of a stack of films 20 nm-thick Ti, 72 nm-thick Al, 12 nm-thick Ni, and 40 nm-thick Au was deposited on a GaN surface using the electron beam physical vapor deposition method. After plasma etching for 10 min, a cross section of an etched sample was observed by SEM (Hitachi S-5200) to measure etch depth. Then, etch rate was calculated.

The surface stoichiometry was evaluated by XPS measurements (ULVAC-PHI XPS 1600) with a Mg Kα X-ray source (1253.6 eV). The take-off angle of the photoelectron was normal to the surface. Peaks were recorded at 20.0 eV for Ga 3d, 397.1 eV for N 1s, and 531.0 eV for O 1s, and atomic compositions were calculated on the basis of the relative sensitivity factor using the values of 0.31 for Ga 3d, 0.42 for N 1s, and 0.66 for O 1s.[17)]

PL spectra were observed *ex situ* at RT using a PL mapping system with excitation by 325-*nm*-wavelength light from a He−Cd laser. The maximum power of this laser is 200 mW. The beam was focused on a spot with a diameter of approximately 100 μm. The accumulation time for PL measurement was 50 ms.

Surface morphologies of the samples were monitored by AFM (Veeco NanoMan VS-1N) in tapping mode with a SiN cantilever. Rms values were averaged from three different areas for each surface morphology image, where no steps were included.

Individual effects of species generated from plasma were evaluated using the PAPE method. Experimental structures for use of the PAPE method are summarized in Fig. 3.1(b). To evaluate separately the effect of photons from the plasma, the sample was covered by a MgF_2 window, which transmitted light with wavelengths above 115 nm. A Si wafer used to analyze the effect of radicals was set at 0.5 mm above GaN. To evaluate the synergistic effect of photons and radicals, the MgF_2 window was placed at a distance of 0.5 mm above GaN.

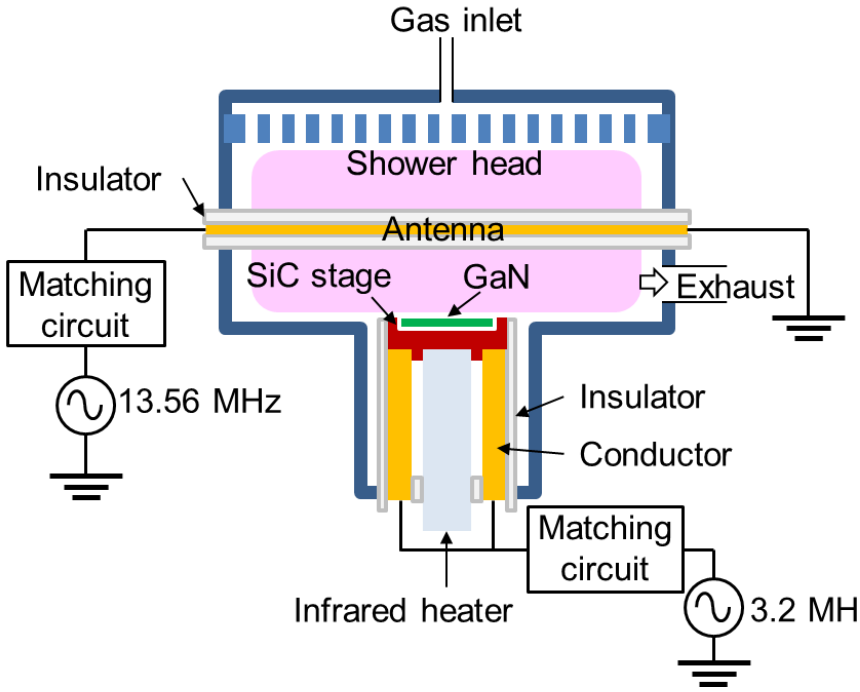

Fig. 3.1. (a) Inductively coupled plasma etching system at high temperatures.

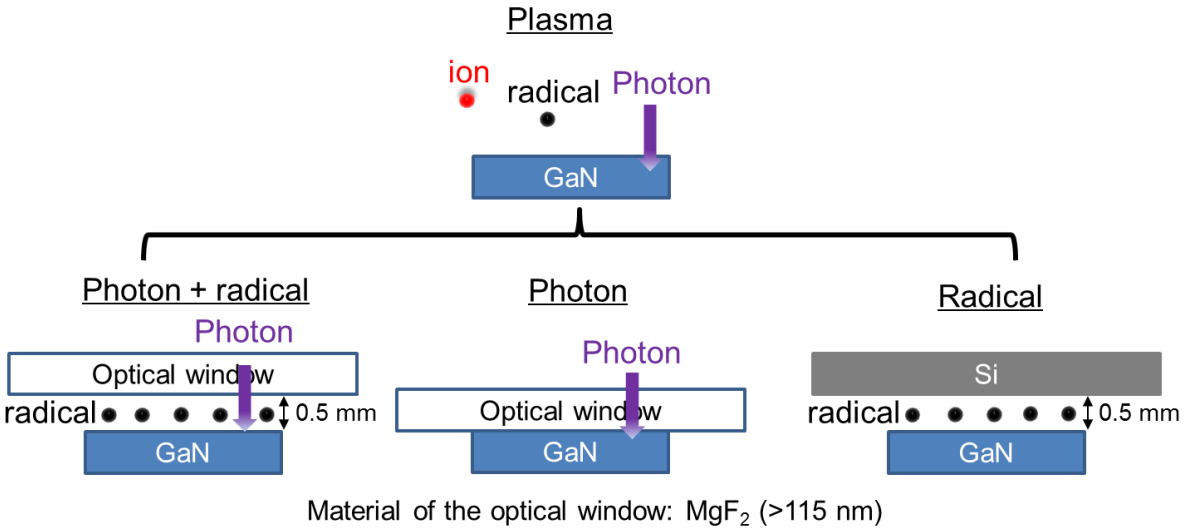

Fig. 3.1. (b) Experimental structure of the PAPE method.

3.3 Results and discussion

3.3.1 Characterization of PID in the Cl_2 high-temperature etching of GaN

Figure 3.2 shows the dependence of stage temperature on etch rate of GaN films ranging from 205 to 600 ^oC for Cl_2 plasma etching. With increasing stage temperature, the etch rates increased monotonically from 5.9 nm/min at 205 ^oC to 25.8 nm/min at 300, then to 33.6 nm/min at 400 ^oC and 70.6 nm/min to 500 ^oC, finally to 199.7 nm/min at 600 ^oC. Under plasma etching, a chlorine etchant forms various chlorine-containing products owing to energetic ion bombardments. Nitrogen was desorbed favorably because the Ga products have low volatilities. The Ga chlorides tended to be favorably desorbed as the stage temperature increased. As a result, the etch depths increased with increasing temperature.

Moreover, the activation energy was calculated approximately to be 290 meV based on Arrhenius plot for temperature-dependent etch rates. Majumdar *et al.* reported an activation energy of 0.9 eV for GaN samples etched by molten KOH.[18] Hence, the estimated low activation energy in this study might be related with the other process such as a surface diffusion besides the chemical etching. Orrman-Rossiter and Armour previously reported a surface diffusion mechanism from the un-bombarded surface area into the bombarded region by Cl ions interacted on the GaAs surface with low energies.[19] According to this idea, the increase of the etch rate with the low activation energy might be a result of the enhanced ion bombardment effect on the diffusion of species that were related to form the volatile products.

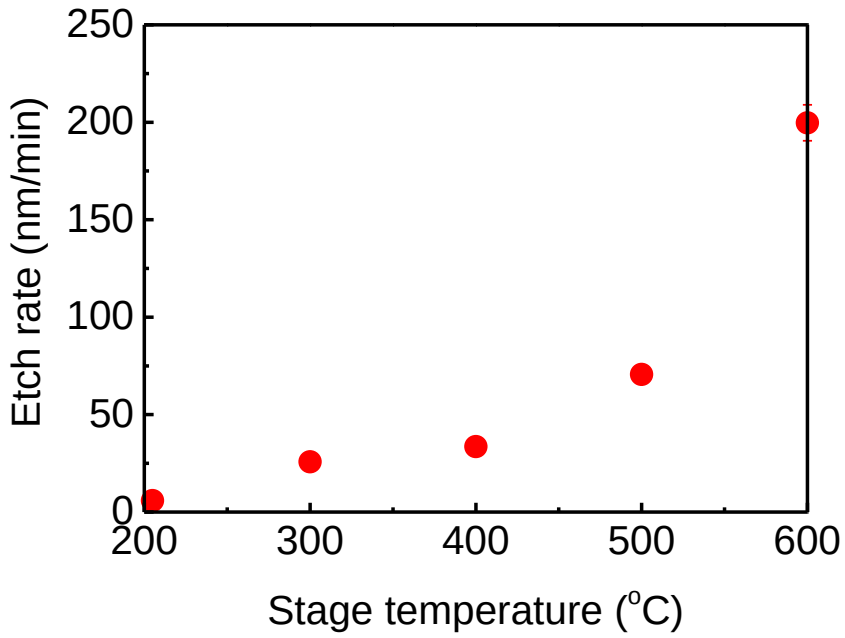

Fig. 3.2. Dependence of stage temperature on etch rate of plasma-etched GaN films.

Figure 3.3(a) shows XPS survey spectra of plasma-etched GaN recorded *ex situ*. The dependence of stage temperature on the stoichiometry of the etched GaN surface was shown in Fig. 3.3(b). The author notes that Cl peaks were hardly observed because most of Cl residuals could react with H_2O in the water vapor ambient. Atomic compositions of Ga and N were estimated by taking into consideration sensitivities. Before the plasma etching, the N/Ga ratio was determined to be almost unity. After the plasma etching at 205 °C, the N/Ga ratio was maintained as initial because of a very low etch rate in GaN, in which the etch depth was approximately 11.8 nm. Even after the plasma etching at temperatures ranging from 300 to 600 °C, the N/Ga ratio remained almost constant. For comparison, in the Ar plasmas at 600 °C, metallic Ga formation tended to degrade the stoichiometry to a N/Ga ratio of 0.10.[7)] In contrast, no metallic Ga could be found in the high-temperature Cl_2 plasma etching because $GaCl_x$ was vaporized as the product of Ga atoms at high temperatures. The desorption of Ga atoms was promoted at high temperatures as a result of the higher vapor pressure of $GaCl_x$, e.g., a vapor pressure approximately equal to that of N atoms.

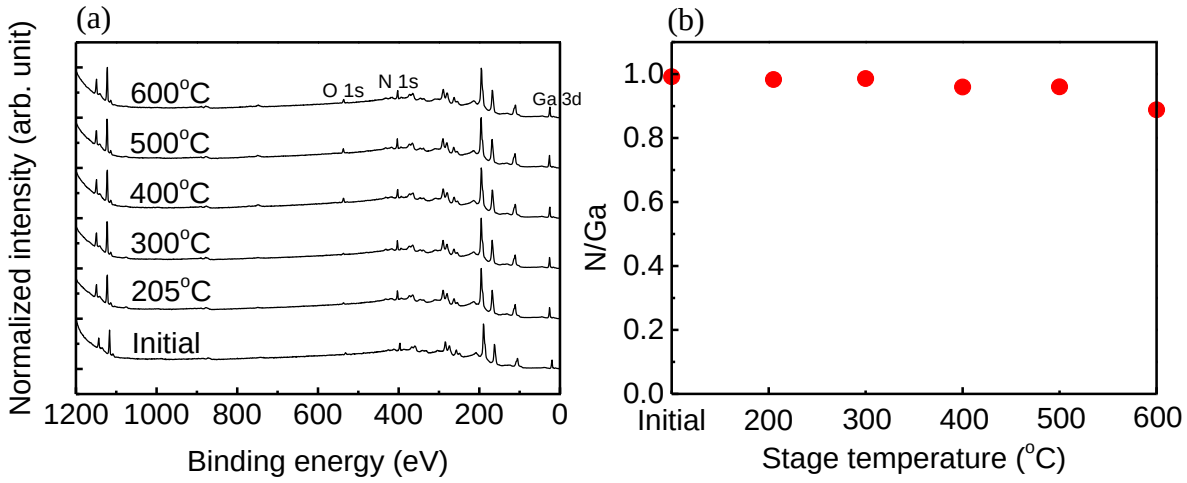

Fig. 3.3 (a) Wide scan XPS spectra of plasma-etched GaN films at different stage temperatures. (b) Dependence of stage temperature on the N/Ga ratios of plasma-etched GaN films.

Next, the dependence of stage temperature on surface roughness was studied. Figure 3.4(a) shows the AFM images of plasma-etched GaN films and typical line profiles of the surface images. A smooth surface was observed for only the samples etched below 400 °C with rms values of 1.20 nm for 205 °C, 1.93 nm for 300 °C, and 2.64 nm for 400 °C, as shown in Fig. 3.4(b).

For etching above 500 °C, a large number of etch pits was observed. Hino *et al.* reported that similar etch pits, corresponding to threading dislocations, were observed on the Si-doped GaN surface, which was etched by a HCl vapor-phase etching technique at 600 °C.[20] These etch pits exposed the {1-102} facet during chemical etching reactions, which caused the selective removal of the {0001} facet. Basically, the density of threading dislocations (1×10^9 cm^{-2}) corresponded to the number of etch pits. Moreover, the author confirmed that a smooth surface was observed even if the sample was annealed at 600 °C in inert ambient. This suggests that the surface was primarily roughened by Cl_2 plasma rather than by high temperature.

The author notes that dislocation density trends to drop with increasing GaN thickness,

indicating that the amount of dislocation of a deeper etched GaN film should be more than that of a shallower etched one. In this study, as the deepest etch depth was nearly 400 nm when the stage temperature was 600 °C and the etch time was 2 min, the dislocation density increased from 1×10^{9} to 1.3×10^{9} cm^{-2}. Namely, the dependence of GaN thickness on dislocation density might be negligible.

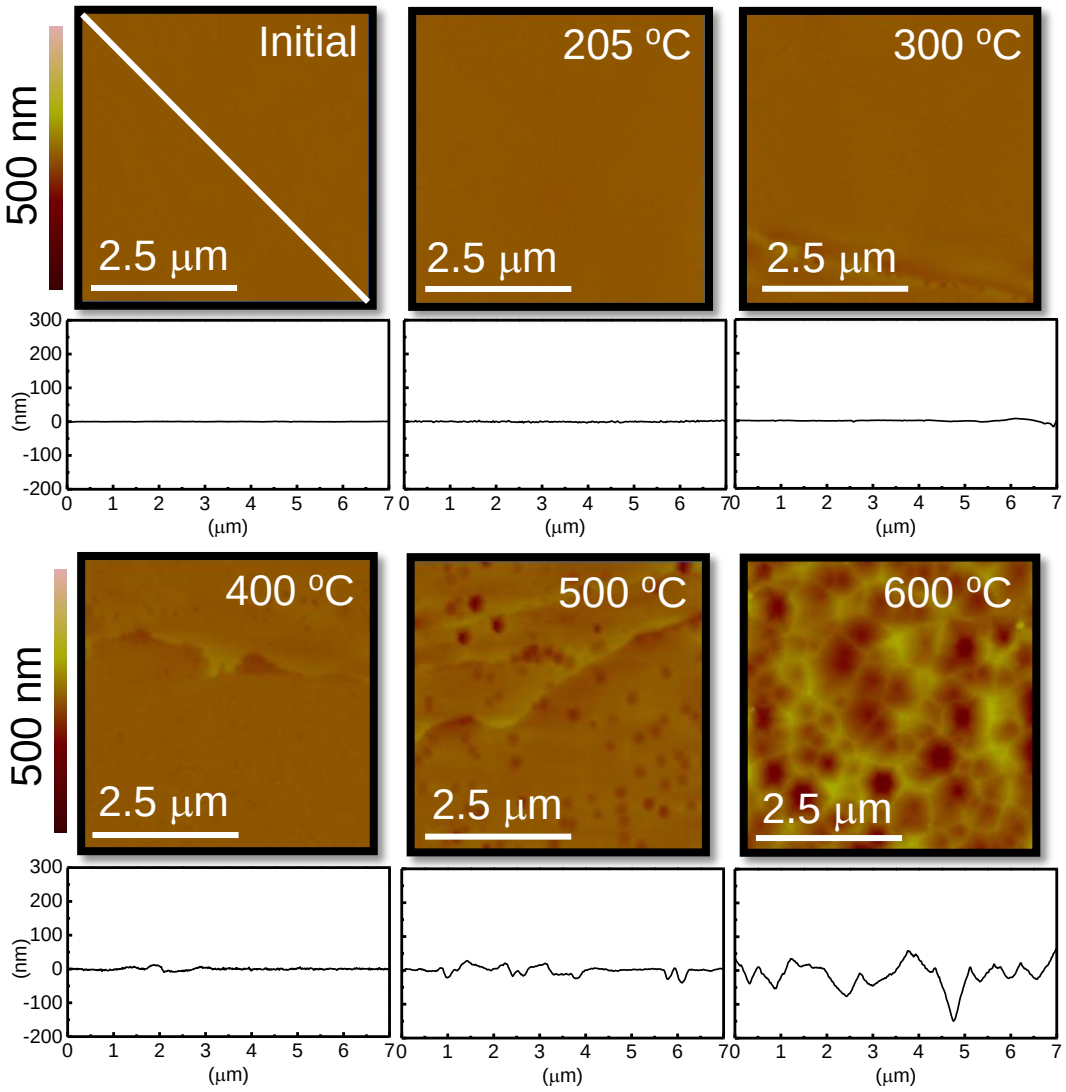

Fig. 3.4. (a) AFM images and line profiles of the surfaces of the plasma-etched GaN films.

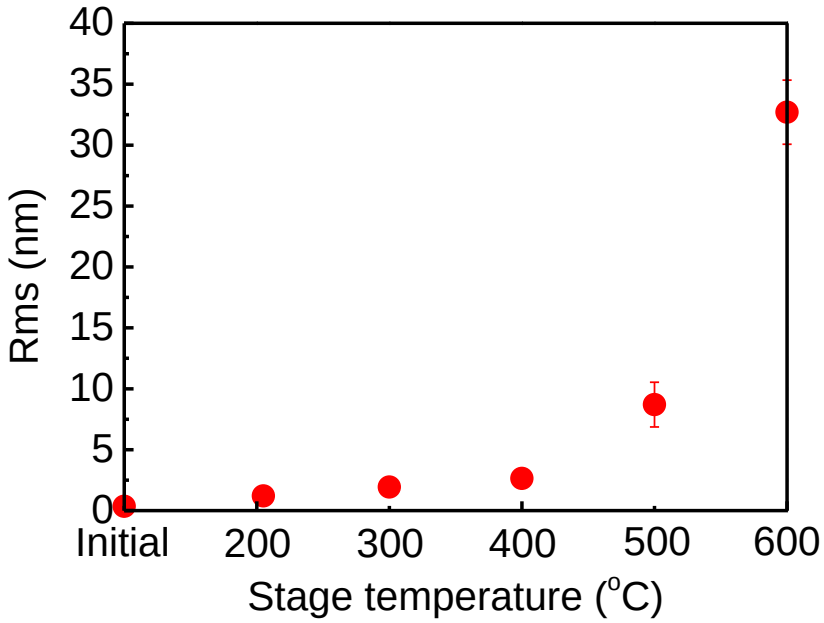

Fig. 3.4. (b) Surface roughness of plasma-etched GaN films.

PL properties were determined to further evaluate the PID in bulk GaN. PL spectra of plasma-etched GaN films are shown in Fig. 3.5 for the samples. Since no obvious variation in yellow luminescence appearing at 2.2–2.3 eV was observed, suggesting that no Ga vacancy-containing defects were formed,[21] the author focused on the variations of near-band-edge emission (NBE) observed at 3.4 eV. The PID in the bulk GaN behaves as nonradiative centers of deep-level states, which trap and recombine carriers. Indeed, the band bending effect might occur after the plasma etching on GaN, which could degrade the NBE intensities.[21] In this study, the author only considered the PID effects on PL properties and remained the discussion of the band bending effect on the NBE intensities in the future scope. The NBE intensities for all GaN films etched at high temperatures were degraded, as shown in Fig. 3.5. Here, the author notes that Cl_2 plasma etching at 500 °C was not recommended because of its severely roughened surface shown in Fig. 3.4, even though it could provide both preferable PL properties and stoichiometry of GaN. As a consequence, the etching process at 400 °C was optimum for suppressing PID, because of its preferable stoichiometry, PL, and smooth surface. No

mechanism describing how the GaN films are damaged has been clarified. However, the author evaluated the key roles of ion, photon, and radical damage formation by employing the PAPE method.

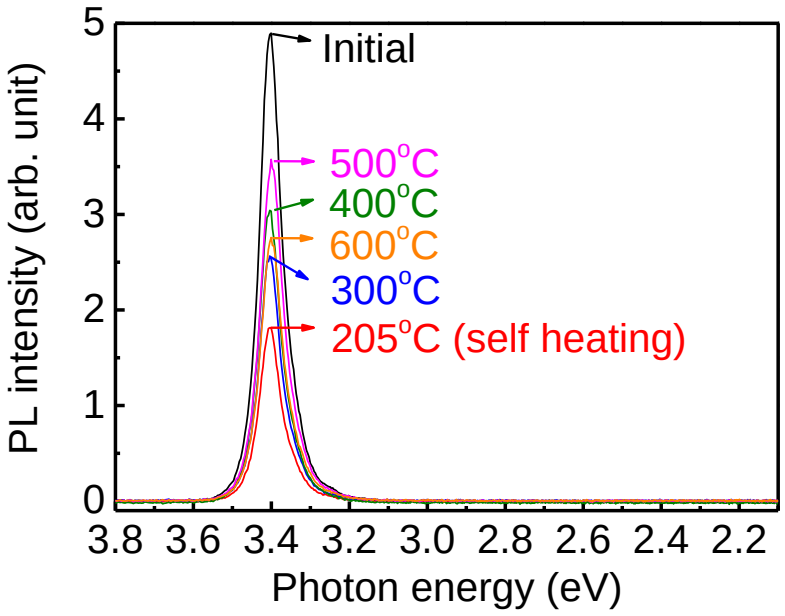

Fig. 3.5. PL spectra of plasma-etched GaN films.

3.3.2 Separation of the effects of ions, radicals and photons on PID

By covering the sample surface with a transparent window, the author discriminated between the effects of ion bombardments and those of photon and radical exposure during etching. The NBE intensities of photon + radical-exposed GaN films are shown in Fig. 3.6. Apparently, photon + radical-induced damage was limited at 205, 300 and 400 ^{o}C but was significant above 500 ^{o}C. The effect of ions on damage formation depended on the stage temperature. Comparison of the degradation in NBE induced by photons and radicals with that induced by plasma showed that the ion-induced damage can be suppressed by increasing the stage temperature. The ion-induced damage dominated PID at 205 ^{o}C, then progressively decreased as the stage temperature increased to 300 and 400 ^{o}C, and finally disappeared at 500 ^{o}C. Namely, the increase in the stage temperature reduced the ion-induced damage.

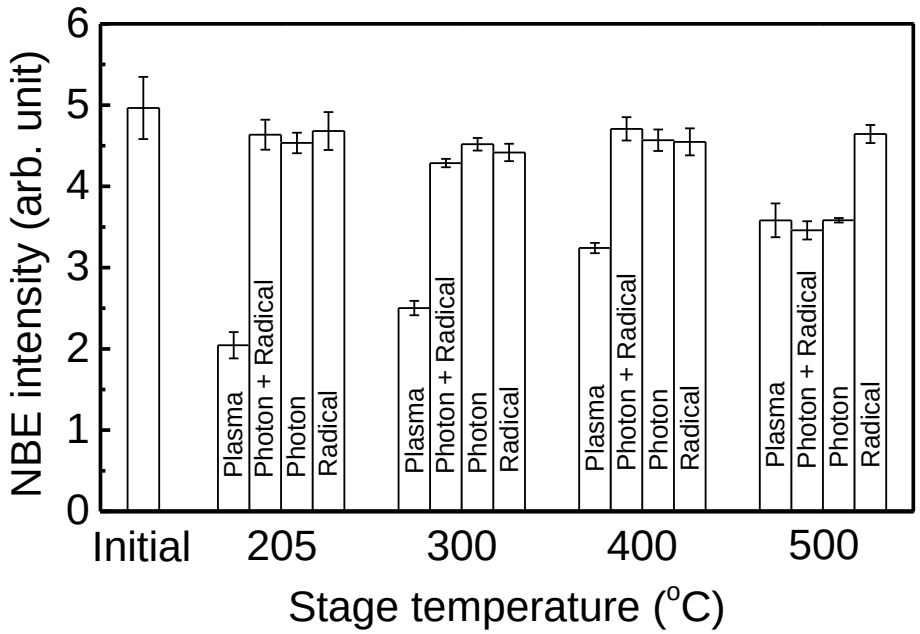

Fig. 3.6. NBE intensities of plasma-etched, photon + radical-exposed, photon-exposed, and radical-exposed GaN films.

Although protrusions of metallic Ga were observed after N_2^+ ion irradiation at RT,[4] N_2 plasma treatments at 600 °C provided stoichiometric and smooth surfaces.[7] As a result, the author considers that a restoration of GaN bonds occurred between Ga and N atoms, which was facilitated at high temperatures.[7] Indeed, Cao *et al.* showed that plasma-induced deteriorations in current-voltage (I-V) properties on Schottky diodes fabricated with the plasma-treated GaN were recovered by thermal annealing at temperatures between 550 and 750 °C after etching.[22] Hence, ion-induced damage was potentially recovered by thermal treatments at temperatures ranging from 400 to 500 °C. On the other hand, etching at temperatures ranging from 205 to 500 °C enhanced chemical reactions, leading to higher etch rates and increasing the removal of ion-damaged layer, which was considered to lower ion-induced damage.

To consider the role of radicals and photons, the author set the Si film and MgF_2 window on the sample surface with or without a gap, as described in the PAPE methods. As shown in Fig. 3.6, radicals-induced damage was insensitive to the stage temperature. Meanwhile, photon-induced damage did not obviously appear in the samples etched at 205, 300 and 400 °C. As the stage temperature increased above 500 °C, PL properties deteriorated because of photon-induced damages. Relative to photon-induced damage, the ion-induced damage was significantly suppressed at 500 °C and thereby the photon-induced damage was predominant. Indeed, the GaN films were penetrated by ions at an energy of 100 eV for approximately 1.5 nm and UV light for 100 nm.[11] Hence, even though ion-induced damage on the GaN surface was suppressed during the plasma etching at 500 °C, photon-induced damage was considered to remain in the bulk GaN film and thereby dominate damage formation. Here, the synergistic work of photon and thermal annealing at 500 °C was suggested to lead to the enhancement in the deterioration of PL, even though such a high temperature of 500 °C also seemed to enhance the effect of annealing on the recovery of the photon-induced damage of GaN. Namely, the amount of damage formation by photon irradiations at 500 °C was more than that of the

recovery by heating. Further detailed analysis of this photon-induced damage will be described in chapter 5.

On the other hand, radicals dominated the development of surface roughness at 500 °C, as shown in Fig. 3.7. The author notes that the etch depth of radical exposure was deeper than that of photon irradiation, indicating a potential effect on the dislocation density for different etch depths. However, as the etch depth of radical exposure was shallower than the deepest one that the GaN film was etched by Cl_2 plasma at 600 °C for 2min. The dependence of GaN thickness on dislocation density might be negligible. Namely, the formation of etch-pits was primarily a result of the chemical reaction between the Cl radicals and the surface GaN at 500 °C.

From the results of depressed ion-induced damage and undeveloped photon-induced damage on a smooth surface at 400 °C, the Cl_2 plasma etching at 400 °C is most appropriate for a low-damage process for GaN-based devices.

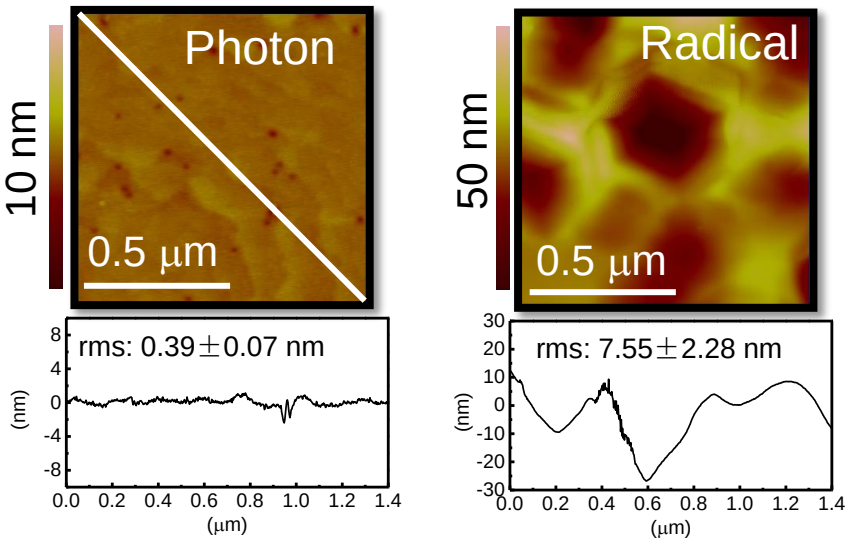

Fig. 3.7. AFM images and line profiles of the surfaces of photon-exposed and radical-exposed GaN films at 500 °C.

3.4 Conclusions

The author investigated etch rates, surface morphology, stoichiometry, and PL of Cl_2-plasma-exposed GaN films. Surface stoichiometry was almost maintained as a result of the enhanced vaporization of Ga chlorides at temperatures ranging from 205 to 600 ^{o}C. The author found that the ion-induced damage could be successfully removed with increasing the stage temperature of plasma etching above 500 ^{o}C. Because photons and radicals respectively degraded PL and formed etch pits above 500 ^{o}C, the author suggests carrying out the high-temperature plasma etching at 400 ^{o}C to fabricate a smooth and stoichiometric GaN surface with less PID. As ion dominated damage formation at 400 ^{o}C, a suppression of these damages could be expected by controlling incident ion energies precisely, which will be concerned in chapter 4. Moreover, the detailed mechanism of photon-induced damage needs to be further studied and will be regarded in chapter 5.

3.5 References

1) M. E. Lin, Z. F. Fan, Z. Ma, L. H. Allen, and H. Morkoç, Appl. Phys. Lett. **64**, 887 (1994).

2) C. B. Vartuli, S. J. Pearton, C. R. Abernathy, R. J. Shul, A. J. Howard, S. P. Kilcoyne, J. E. Parmeter, and M. Hagerott-Crawford, J. Vac. Sci. Technol. A **14**, 1011 (1996).

3) K. Kataoka, Y. Kimoto, K. Horibuchi, T. Nonaka, N. Takahashi, T. Narita, M. Kanechika, and K. Dohmae, Surf. Interface Anal. **44,** 709 (2012).

4) Y. H. Lai, C. T. Yeh, J. M. Hwang, H. L. Hwang, C. T. Chen, and W. H. Hung, J. Phys. Chem. B **105,** 10029 (2001).

5) Y. Han, S. Xue, W. P. Guo, C. Z. Sun, Z. B. Hao, and Y. Luo, Jpn. J. Appl. Phys. **42,** 6409 (2003).

6) J. S. Pan, A. T. S. Wee, C. H. A. Huan, H. S. Tan, and K. L. Tan, J. Appl. Phys. **80,** 6655 (1996).

7) R. Kometani, K. Ishikawa, K. Takeda, H. Kondo, M. Sekine, and M. Hori, Appl. Phys. Express **6,** 056201 (2013).

8) Z. Liu, T. Kako, K. Ishikawa, O. Oda, K. Takeda, H. Kondo, M. Sekine, and M. Hori, Proc. 6th Int. Symp. Advanced Plasma Science and Its Applications for Nitrides and Nanomaterials, 2014, 06aP04.

9) H. Cho, C. B. Vartuli, C. R. Abernathy, S. M. Donovan, S. J. Pearton, R. J. Shul, and J. Han, Solid-State Electron. **42,** 2277 (1998).

10) H. S. Kim, G. Y. Yeom, J. W. Lee, and T. I. Kim, Thin Solid Films **341,** 180 (1999).

11) M. Minami, S. Tomiya, K. Ishikawa, R. Matsumoto, S. Chen, M. Fukasawa, F. Uesawa, M. Sekine, M. Hori, and T. Tatsumi, Jpn. J. Appl. Phys. **50,** 08JE03 (2011).

12) R. Kawakami, T. Inaoka, K. Tominaga, A. Kuwahara, and T. Mukai, Jpn. J. Appl. Phys. **47,** 6863 (2008).

13) R. Kometani, S. Chen, M. Liu, K. Ishikawa, K. Takeda, T. Egawa, H. Kondo, H. Amano,

M. Sekine, and M. Hori, Proc. 5th Int. Symp. Advanced Plasma Science and Its Applications for Nitrides and Nanomaterials, 2013, Tha-A03OA.

14) S. Uchida, S. Takashima, M. Hori, M. Fukasawa, K. Ohshima, K. Nagahata, and T. Tatsumi, J. Appl. Phys. **103,** 073303 (2008).

15) G. A. Hebner, J. Vac. Sci. Technol. A **14,** 2158(1996).

16) S. Samukawa and T. Tsukada, Appl. Phys. Lett. **69,** 1056 (1996).

17) C. D. Wagner, L. E. Davis, M. V. Zeller, J. A. Taylor, R. H. Raymond, and L. H. Gale, Surf. Interface Anal. **3,** 211 (1981).

18) S. Majumdar, S. Shaik, S. Das, R. Kumar, A. Bag, A. Chakraborty, M. M. S. Ghosh, and D. Biswas, Proc. 2nd Int. Conf. on Microwave and Photonics, 2015.

19) K. G. Orrman-Rossiter and D. G. Armour, Nucl. Instrum. Methods B **42,** 334 (1989).

20) T. Hino, S. Tomiya, T. Miyajima, K. Yanashima, S. Hashimoto, and M. Ikeda, Appl. Phys. Lett. **76,** 3421 (2000).

21) M. A. Reshchikov and H. Morkoç, J. Appl. Phys. **97,** 061301 (2005).

22) X. A. Cao, H. Cho, S. J. Pearton, G. T. Dang, A. P. Zhang, F. Ren, R. J. Shul, L. Zhang, R. Hickman, and J. M. Van Hove, Appl. Phys. Lett. **75,** 232 (1999).

Chapter 4: Optimization of plasma conditions for GaN etching in terms of both plasma-induced damage and surface morphology

4.1 Introduction

A gate-recess structure fabricated by plasma etching is an effective approach to realize a normally-off operation for lateral GaN power devices.[1-3] However, PID has remained unsolved and become a critical issue.[4-8]

The author described in chapter 3 that PID in GaN was successfully suppressed by Cl_2 plasma etching at high temperatures.[9] Since the vaporization of Ga-based byproducts was enhanced, the surface stoichiometry was maintained at the initial value. The individual contributions of species (ions, radicals, and photons) onto the *all-inclusive* PID in the GaN films at high temperatures, especially higher than 300 ^{o}C, were separately investigated in chapter 3. The high-temperature Cl_2 plasma etching was suggested to be applied at approximately 400 ^{o}C to suppress PID and obtain a smooth surface. However, the effects of ion energies on PID have not been clarified.

In this chapter, the author focused on the effects of ion energy and studied the mechanisms of PID formation at 400 ^{o}C. The author firstly investigated the dependence of etch time on PL intensity to analyze the temporal damage formation induced by ion irradiation. Furthermore, when the bias power was altered from 0 to 15 W, the V_{pp} was varied from 0 to 220 V, which decreased the ion energy. Then, the author evaluated this ion energy effects on etch rate, roughness, and PL intensity to determine how to obtain minimally damaged GaN films with smooth surfaces etched at high temperatures with Cl_2 plasma.

4.2 Experimental details

The samples were 5-μm-thick n-GaN films doped with Si (10^{18} cm^{-3}) and grown by HVPE on sapphire substrates. Prior to their etching, the samples were cleaned by dipping into 2% hydrofluoric acid for 1 min to remove native oxides and then into 17.5% hydrochloric acid for 5 min to remove metallic contaminants.

The experimental setup was described in chapter 3.[9] The experimental method is described briefly as follows. Cl_2 plasmas were generated in the ICP etcher at an RF power of 400 W. Depending on the applied bias powers at 0, 5, 10, and 15 W, the V_{pp} values were measured as 0, 130, 190, and 220 V, respectively. The half value of bias V_{pp} is regarded approximately as the self-bias voltage that would be the average incident energy of ions on the surface. Since the differences in plasma potential and floating potential on the wafer surface should be less than a few tens of volts (e.g., between 10 and 30 V),[10] these differences can be applied when the bias power was 0 W and relatively smaller than the V_{pp} value at 5 W bias power. The stage temperature was maintained at 400 °C using an infrared lamp heater. The etch times were 0.4, 2.0, and 10 min. Pure Cl_2 gas was introduced into the chamber at a flow rate of 50 sccm. The chamber pressure was maintained at 20 Pa by an automatic pressure controller.

After plasma etching, PL was observed *ex situ* at RT using a PL mapping system with excitation using a 325-nm-wavelength light of a He−Cd laser. The maximum power of this laser is 200 mW. The beam was focused on a spot with a diameter of approximately 100 μm. The accumulation time for PL measurement was 50 ms.

To measure etch depth, a stacked metal film mask consisting of 20 nm-thick Ti, 72 nm-thick Al, 12 nm-thick Ni, and 40 nm-thick Au was firstly prepared on a GaN surface by electron beam physical vapor deposition. After plasma etching for 10 min, a cross section of an etched sample was observed by scanning electron microscopy SEM (Hitachi S-5200) to measure etch depth. Then, etch rate was calculated.

Surface morphologies of the samples were observed by AFM (Veeco NanoMan VS-1N) in the tapping mode with a SiN cantilever. Rms values were averaged from three different areas for each surface morphology image, where no steps were included.

4.3 Results and discussion

4.3.1 Dependence of etch time on damage formation

Etching at an elevated temperature of approximately 400 ^{o}C suppressed PID to a greater extent than that at 300 ^{o}C because of the formation of more highly reactive volatile etched products.[9] However, the detailed mechanisms of damage formation and roughness development in the GaN films have remained unclarified. Here, the author clarified the temporal behavior of damage formation by analyzing PL intensity in relation with etch rate and surface roughness.

The GaN samples were partially etched at a bias power of 15 W for various etch times, e.g., 0.4, 2.0, and 10 min. When the GaN samples were etched at 400 ^{o}C, ion-induced damage was dominant, as reported previously.[9]

Figure 4.1(a) shows the PL spectra of the plasma-etched GaN films for different etch times. The reference spectrum initial was measured using an as-cleaned GaN sample before the plasma etching. Negligible yellow luminescence appearing at approximately 2.2–2.3 eV is observed in the PL spectrum of the initial GaN sample, indicating that no considerable amount of Ga vacancy defects existed.[11] In general, the variations of near-band-edge emission (NBE) observed at 3.4 eV were reasonably evaluated for the analysis of PID, because PID behaved as nonradiative centers of deep-level states, which trapped and recombined photon-generated carriers and resulted in the decrease in NBE intensity.[11] Figure 4.1(b) shows the NBE intensities of the plasma-etched GaN films at 400 ^{o}C with different etch times ranging from 0.4 to 10 min.

It is noticeable that the observed dependence of etch time on NBE intensity appeared characteristically with a saturating behavior in the region at more than 2 min. This means that damage formation in the early period of etching shorter than 2 min could be critical.

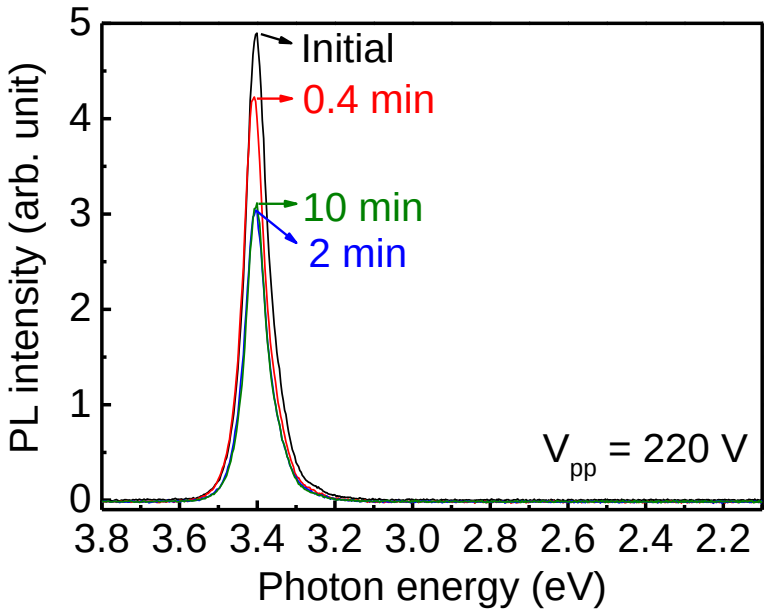

Fig. 4.1 (a) Typical PL spectra of plasma-etched GaN films as a function of etch time (V_{pp} = 220 V).

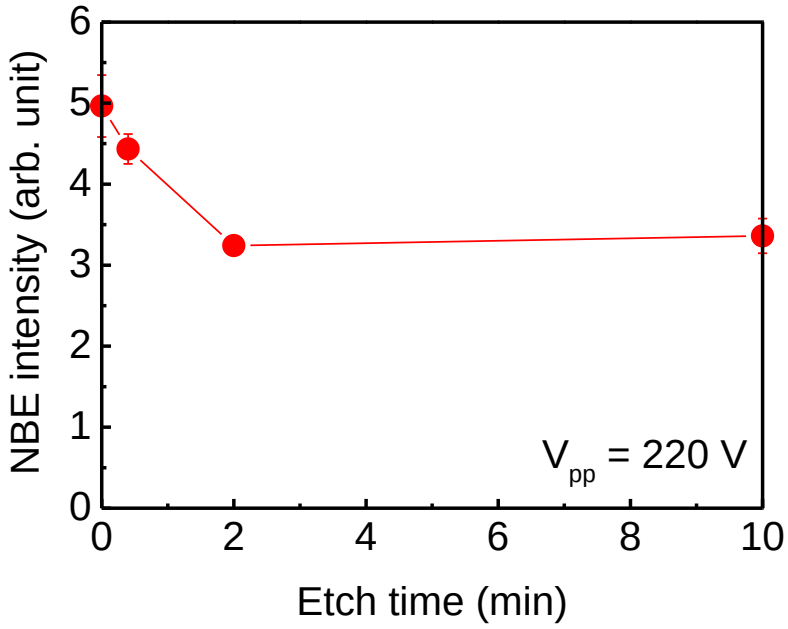

Fig. 4.1 (b) Dependence of etch time on NBE intensity of plasma-etched GaN films.

On the other hand, surface morphology and roughness were observed, as shown in Fig. 4.2(a). Although the PL degradation saturated at an etch time longer than 2 min, the GaN surface etched for 10 min was severely roughened, as compared with the smooth surfaces etched for 0.4 and 2 min. In a previous report, as the stage temperature was elevated to above 500 °C and the etch time was 2 min, a large number of etch pits were observed because of the preferential chemical reactions between Cl radicals and the threading dislocations.[9] The author considers that these chemical reactions at 400 °C were less enhanced than those at 500 °C; however, after a longer etch time, etch pits were formed. Hence, Cl radicals were considered to play a key role in the formation of observed etch pits on the GaN surface etched at 400 °C for 10 min and thereby roughen the surface. Regarding experimental observations, the author showed in Fig. 4.2(b) that the surface roughness with rms values increased linearly from 0.57 nm at 0.4 min of etching to 13.07 nm at 10 min of etching. This result shows that the etch time at 400 °C needs to be carefully controlled to prevent surface roughening, which was predominantly caused by Cl radicals. As described in chapter 3, as the deepest etch depth was nearly 336 nm when the stage temperature was 400 °C and the etch time was 10 min, the increase of dislocation density was negligible in the discussion of the surface morphology.

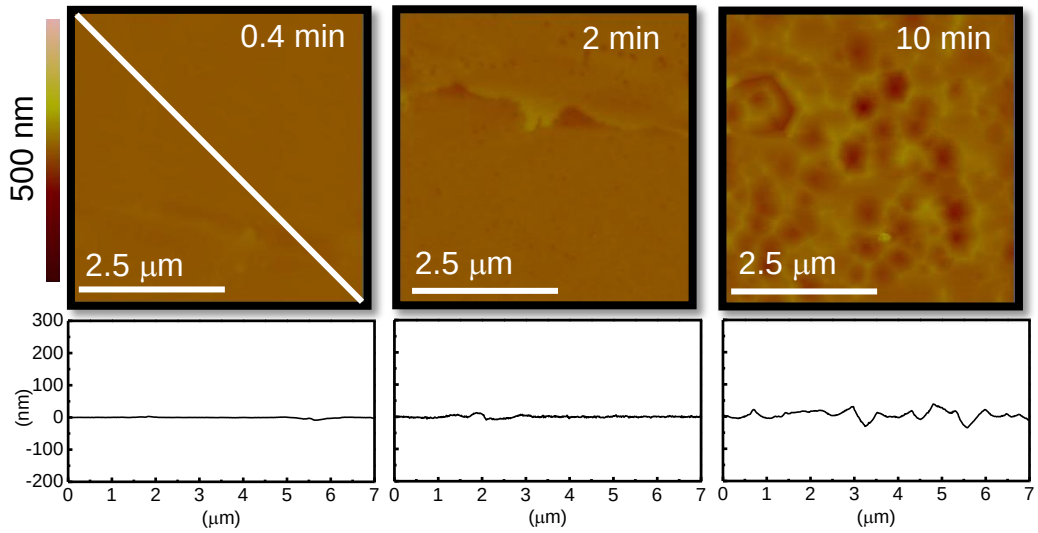

Fig. 4.2 (a) Dependence of etch time on AFM images and line profiles of plasma-etched GaN films (V_{pp} = 220 V).

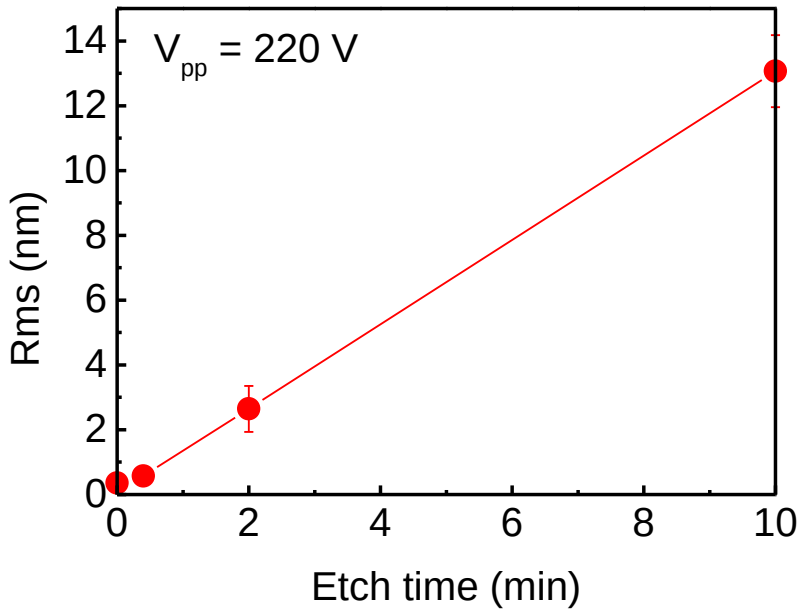

Fig. 4.2 (b) Dependence of etch time on the surface roughness of plasma-etched GaN films.

The etch rate was 33.6 nm/min at 400 °C, an ICP power of 400 W, and V_{pp} of 220 V. Then, the mechanism of this saturated damage formation could be understood as follows. From the beginning of plasma etching, damage began to be formed and then continued to accumulate. Some of the damage would be partially etched off during plasma etching, and then the formation and the etch-removal of damage became balanced. Finally, the amount of damage observed by PL measurements saturated. Namely, damage removal should be taken into account when estimating the damage on an etched GaN film. The penetration depth of Cl ions into the GaN film was considered to be approximately 1.5 nm at an ion energy of 100 eV.[12] In the surface processes, ion-induced damage might be removed immediately within a timescale of nearly 3 s during plasma etching under the above conditions. Then further fresh damage was formed and remained in the bulk region, the removal of which was successful at a high temperature of 400 °C. As a result, the damage that remained in the bulk GaN was completely detected by PL measurement and minimized by decreasing ion energies. The author considers that the net

amount of damage reached an equilibrium between the formation and removal of PID.

Apparently, plasma etching at 400 ºC for less than 2 min was preferable to keep the GaN surfaces smooth with minimal damage. This high-temperature Cl_2 plasma etching technique was expected to be utilized for fabricating a gate-recess structure at a GaN depth of only 7 nm and well-controlled low etch rates,[13] which are highly required in advanced plasma etching. Therefore, the author focused on the first period of etching process to investigate the dependence of incident ion energy on damage formation.

4.3.2 Dependence of incident ion energy on damage formation

Figure 4.3 shows etch rate as a function of V_{pp} of the substrate bias. As the author reported previously, the etch rate increased with increasing temperature because of an enhanced desorption of Ga chlorides.[9] By reducing V_{pp} from 220 to 0 V, the etch rate decreased from 33.6 to 16.9 nm/min. In the chemically assisted chlorine ion etching of GaN, energetic ions removed a chlorination layer of GaN that was formed by Cl radicals with Ga and N atoms.[14] Less of the Ga and N chlorides tended to be removed by ions with low incident energies. This result indicated a solution to achieving a well-controlled low etch rate during the high-temperature plasma etching in GaN, without the need for bias voltage application.

Figure 4.4 shows the dependence of V_{pp} in bias RF power on the NBE intensity of plasma-etched GaN films for an etch time of 2 min. As compared with the reference NBE intensity of initial GaN films, the NBE intensity of plasma-etched samples at a V_{pp} of 220 V decreased to 65%. When V_{pp} was decreased from 220 to 0 V, the NBE intensity increased from 65 to 93% of the initial value. It was apparent that the reduction in ion energies significantly suppressed PID formation. The effects of ion bombardments on damage formation were usually considered to be in the form of lattice disorders in the GaN film, i.e., vacancies, interstitials, and antisite defects.[15] Hashizume and Nakasaki reported that the nitrogen-vacancy-related state near the

conduction-band edge was introduced to the H_2-plasma-treated GaN surface.[16] Aoki *et al.* reported that a high Ga-vacancy density was observed in p-GaN films after CH_2Cl_2 and Cl_2 plasma ICP etching.[17] Hence, NBE at a bias voltage of 0 V resulted from fewer lattice disorders formed by ions. Because Cl ion incident energy determined the penetration depth in the GaN films, the ions with a very low energy at a V_{pp} of 0 V caused PID with a depth of less than 1 nm.[12,18] The ion-dominated damage formation was suppressed by reducing incident ion energy.

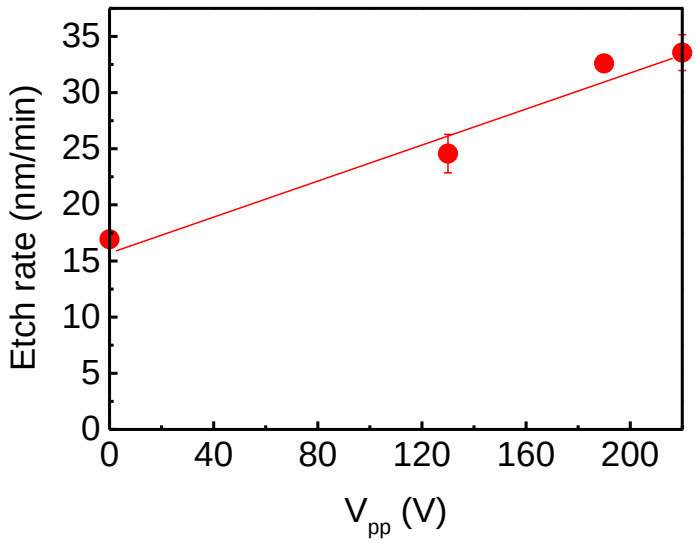

Fig. 4.3 Etch rate as a function of V_{pp} of substrate bias.

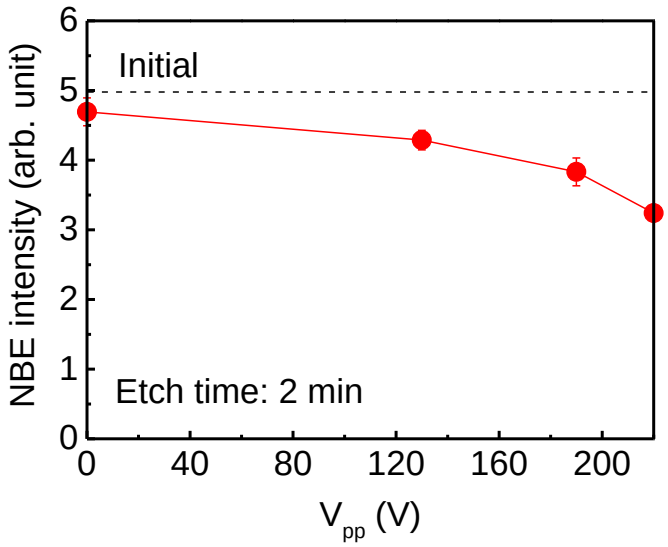

Fig. 4.4 Dependence of V_{pp} of substrate bias on NBE intensity of plasma-etched GaN films (etch time: 2 min).

Surface morphology and roughness are shown in Fig. 4.5. At various V_{pp} values, surface morphologies appeared similar and the roughness values remained almost unchanged. The variation of Cl ion bombardment energy barely affected surface roughness. Here, neutral Cl radicals were hardly affected by bias voltage; thereby, the surface morphology and roughness were maintained. Regarding the mechanism of the increase in roughness at 400 °C from an initial value of 0.36 nm, the author considers that the etch pits that intrinsically exist in the GaN film, which correspond to threading dislocations, were enlarged as a result of the chemical reactions between the surface and the Cl radicals. Hence, even when a clean surface forms after Cl_2 plasma etching at 400 °C, these enlarged etch pits will increase surface roughness.

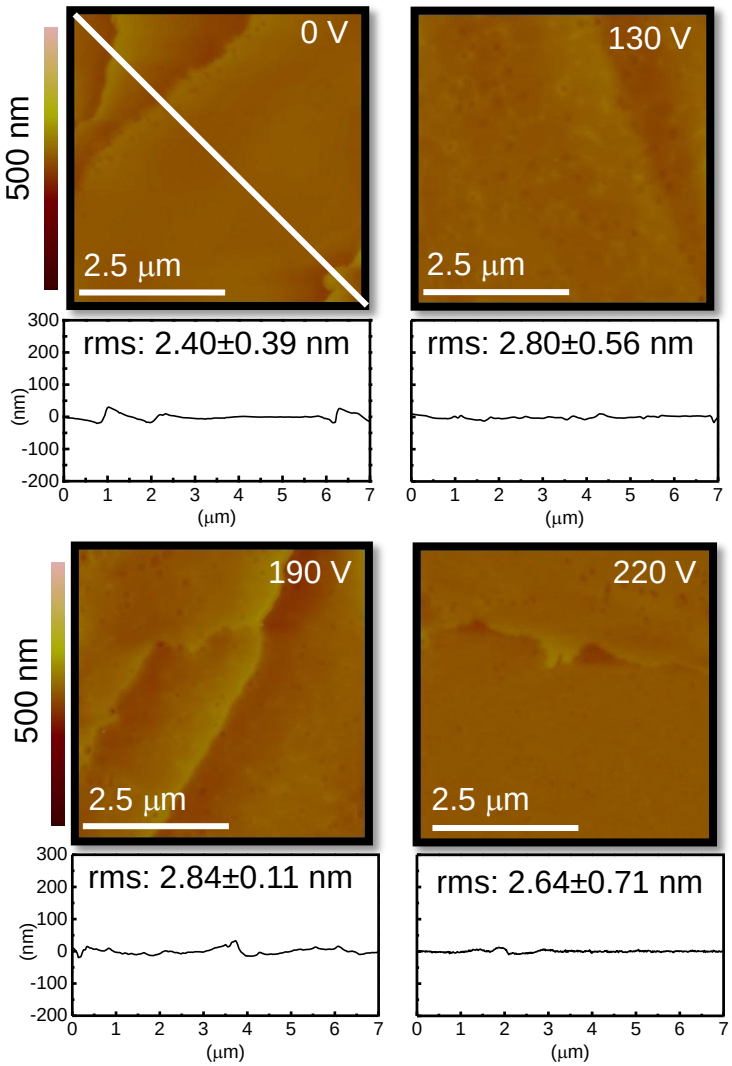

Fig. 4.5 Dependence of V_{pp} of substrate bias on AFM images and line profiles of plasma-etched GaN films (etch time: 2 min).

4.3.3 Optimization of the etching process

To fabricate highly reliable normally-off GaN HEMTs with an etch depth less than 10 nm,[13] the suppression of PID and a smooth surface need to be simultaneously realized. For Cl_2 plasma etching at 400 ^oC, ion-dominated damage is still formed, which could be reduced by optimizing incident ion energy. On the other hand, Cl radicals predominantly increased surface roughness and strongly depended on etch time. Hence, the optimization of the etching process should be focused on incident ion energy and etch time.

Figure 4.6 shows the experimental results of the NBE intensity of plasma-etched GaN films as a function of etch time without applying bias voltage. Similarly to the tendency of PL properties at a high bias voltage of 220 V, NBE intensity finally saturated at etch times longer than 2 min, which means that damage formation and removal were balanced. Indeed, GaN films etched at 400 ^oC without bias voltage for 0.4 min achieved an etch depth of 6.8 nm and kept the NBE intensity to 98.8% of the initial value. Therefore, the author considers that Cl_2 plasma etching at 400 ^oC without applying bias voltage for a short time of 0.4 min could be a promising method of suppressing damage formation in GaN.

Radicals, instead of ions, predominantly increased surface roughness. Namely, no dependence of incident ion energy on surface roughness was observed. This surface roughness increase was intrinsically a result of chemical reactions and strongly depended on etch time. The author investigated surface morphologies and roughness as functions of etch time without bias voltage application, as shown in Fig. 4.7. Here, as the author expected, surface roughness increased from 0.74 nm at 0.4 min of etching to 13.63 nm at 10 min of etching. These values were close to those under a high bias voltage of 220 V, which proved again that incident ion energy hardly affects the surface roughness. For example, in the gate-recess process, the author needs to remove only 7 nm of GaN.[13] This requires GaN to be etched by this optimized method (no bias voltage application at 400 ^oC) for a short time of 0.4 min. Because of the short process,

the surface roughness increase may be negligible. On the other hand, a surface roughness increase of 0.74 nm seemed acceptable and did not have a major impact on the current collapse in AlGaN/GaN gate-recess HEMTs.[19)]

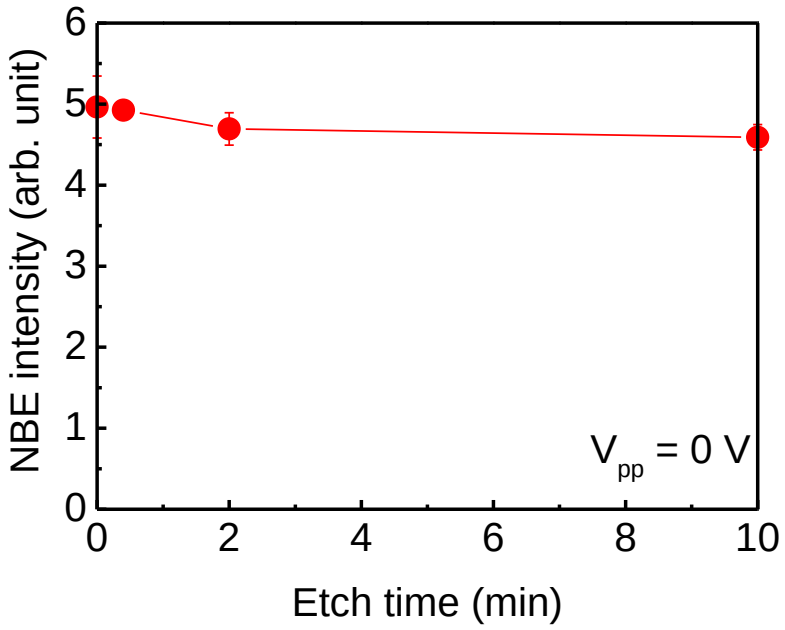

Fig. 4.6 Dependence of etch time on NBE intensity of plasma-etched GaN films (V_{pp} = 0 V).

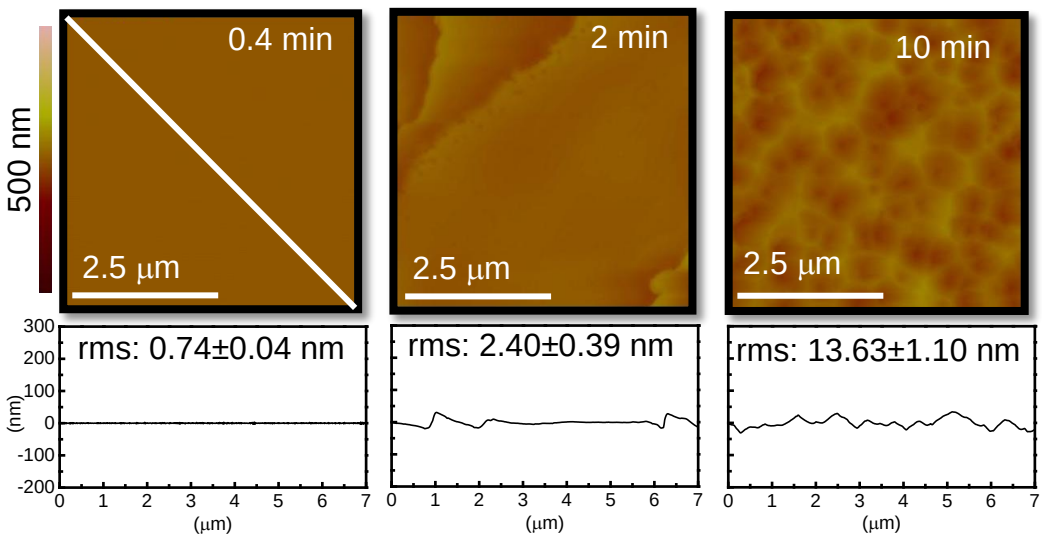

Fig. 4.7 Dependence of etch time on AFM images and line profiles of plasma-etched GaN films (V_{pp} = 0 V).

As a summary of the experimental results, Fig. 4.8 shows a model of the suppression of ion-induced damage by lowering incident ion energy. This suppression could be understood as a competition between damage formation and removal of damage layer by etching. At various incident ion energies for an etch time of 2 min, damage formation by ions was suppressed in the absence of bias voltage application at an etch rate of 16.9 nm/min because of the suppression of the formation of lattice disorders. As byproduct desorption frequently occurred at high incident ion energies when V_{pp} was 220 V, the removal for a nearly 1.5 nm damage layer (d_{ion}) should be enhanced under a high-bias-voltage condition. However, even when less damage was removed in the absence of bias voltage application, the greater suppression of damage formation led to a decrease in the net amount of damage that remained in the bulk region and thereby improved PL properties. For various etch times without bias voltage application, this net amount of damage could be initially ignored for the first 0.4 min and gradually became critical in terms of PL degradation when the etch time was 2 min. Because damage formation and removal became balanced, the net amount of damage formed after 10 min of etching was similar to that formed after 2 min of etching. Figure 4.8 also shows how to achieve a smooth GaN surface by the high-temperature plasma etching. Neutral Cl radicals were predominantly involved in surface development through the formation of etch pits by reactive chemical reactions, and were hardly affected by incident ion energy. Hence, surface morphology and roughness were only affected by etch time, for example, a clean surface with a roughness of less than 1 nm for 0.4 min of etching and a rough surface with a roughness of over 10 nm for 10 min of etching at 400 ^{o}C.

Apparently, this model indicates that ion-induced damage especially that formed in the early period of etching shorter than 2 min was very critical in the degradation of important characteristics of GaN-based power electronic devices. Not only the surface but also the subsurface bulk regions of GaN films showed satisfactory suppression of PID. Consequently,

the author achieved minimal PL degradation and a clean surface of GaN films etched for 0.4 min without bias voltage application at 400 °C.

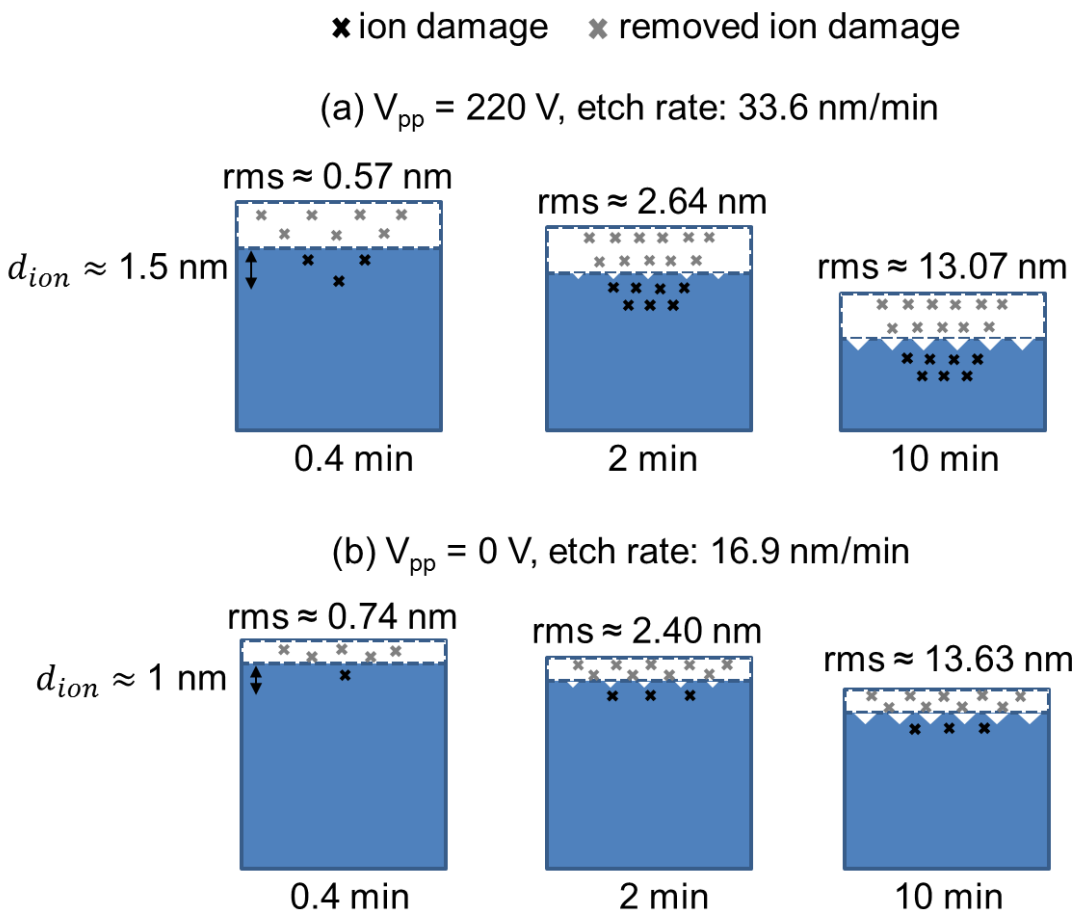

Fig. 4.8 Model of suppression for ion-induced damage and smooth surface in Cl_2 plasma etching of GaN films at 400 °C: (a) V_{pp} = 220 V; (b) V_{pp} = 0 V.

Moreover, the SEM image of the GaN sidewall etched for 10 min without bias voltage application is shown in Fig. 4.9. A promising anisotropic etch profile was observed even at a bias voltage of 0 V. As a result, a preferred pattern transfer was highly achievable in the fabrication of recessed-gate normally-off GaN-based power devices. Considering that the etch profile is not normal, the author assumes that the reasons might be as follows. Etching was performed at a relatively high pressure of 20 Pa with a large amount of Cl radicals, or ions were obliquely accelerated onto the surface owing to a bended sheath structure in the experimental system. Further detailed analysis of this non-normal etch profile will be the focus of another study.

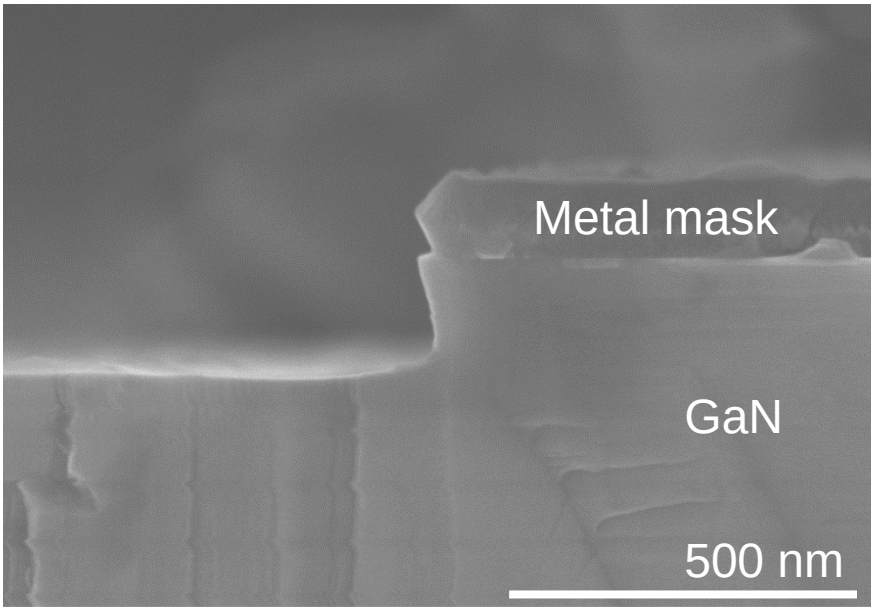

Fig. 4.9 SEM image of GaN sidewall etched at 400 ^{o}C at bias power of 0 W for etch time of 10 min.

4.4 Conclusions

Based on the results in chapter 3, the author further elucidated the mechanism of PID formation of GaN films under the high-temperature Cl_2 plasma etching. The high-temperature etching at 400 ^oC provides smooth surfaces and better PL properties. In this chapter, the author has extensively elucidated ion-induced damage that was predominant in the GaN films by controlling incident ion energy. The temporal evolution of ion-induced damage saturated within the etch time of 2 min because of the balanced net amount between damage formation and the removal of the damage layer. The author emphasizes that the roughening of the surface morphology was inherently caused by chemical reactions between Cl radicals and the GaN surface, suggesting an increase of surface roughness as a function of the etch time and this increase was regardless of Cl ions. Moreover, ion-induced damage strongly depended on incident ion energy, introducing fewer damages detected by PL measurements in the bulk GaN films at a lower incident ion energy within a penetration depth of less than 1 nm. Consequently, Cl_2 plasma etching for a short time of 0.4 min without bias voltage application at a stage temperature of 400 ^oC is recommended to prevent damage formation and provide a clean surface in a gate recess process of GaN.

4.5 References

1) M. Kanamura, T. Ohki, T. Kikkawa, K. Imanishi, T. Imada, A. Yamada, and N. Hara, IEEE Electron Device Lett. **31,** 189 (2010).

2) M. E. Lin, Z. F. Fan, Z. Ma, L. H. Allen, and H. Morkoç, Appl. Phys. Lett. **64**, 887 (1994).

3) C. B. Vartuli, S. J. Pearton, C. R. Abernathy, R. J. Shul, A. J. Howard, S. P. Kilcoyne, J. E. Parmeter, and M. Hagerott-Crawford, J. Vac. Sci. Technol. A **14**, 1011 (1996).

4) H. Cho, C. B. Vartuli, C. R. Abernathy, S. M. Donovan, S. J. Pearton, R. J. Shul, and J. Han, Solid-State Electron. **42,** 2277 (1998).

5) H. S. Kim, G. Y. Yeom, J. W. Lee, and T. I. Kim, Thin Solid Films **341,** 180 (1999).

6) W. V. Schoenfeld, C.-H. Chen, P. M. Petroff, and E. L. Hu, Appl. Phys. Lett. **73,** 2935 (1998).

7) P. Hacke, T. Detchprohm, K. Hiramatsu, and N. Sawaki, Appl. Phys. Lett. **63,** 2676 (1993).

8) J. D. Guo, M. S. Feng, R. J. Guo, F. M. Pan, and C. Y. Chang, Appl. Phys. Lett. **67,** 2657 (1995).

9) Z. Liu, J. Pan, T. Kako, K. Ishikawa, K. Takeda, H. Kondo, O. Oda, M. Sekine, and M. Hori, Jpn. J. Appl. Phys. **54,** 06GB04 (2015).

10) M. A. Lieberman and A. J. Lichtenberg, *Principles of plasma discharges and materials processing* (Wiley, Hoboken, U. S. A., 2005) 2nd ed., p. 482.

11) M. A. Reshchikov and H. Morkoç, J. Appl. Phys. **97,** 061301 (2005).

12) M. Minami, S. Tomiya, K. Ishikawa, R. Matsumoto, S. Chen, M. Fukasawa, F. Uesawa, M. Sekine, M. Hori, and T. Tatsumi, Jpn. J. Appl. Phys. **50,** 08JE03 (2011).

13) J. J. Freedsman, T. Egawa, Y. Yamaoka, Y. Yano, A. Ubukata, T. Tabuchi, and K. Matsumoto, Appl. Phys. Express **7,** 041003 (2014).

14) Y. H. Lai, C. T. Yeh, J. M. Hwang, H. L. Hwang, C. T. Chen, and W. H. Hung, J. Phys. Chem. B **105,** 10029 (2001).

15) C. G. Van de Walle, Phys. Rev. B **56,** R10020 (1997).

16) T. Hashizume and R. Nakasaki, Appl. Phys. Lett. **80,** 4564 (2002).

17) T. Aoki, H. Wakayama, N. Kaneda, T. Mishima, K. Nomoto, and K. Shiojima, Jpn. J. Appl. Phys. **52,** 11NH03 (2013).

18) M. E. Barone and D. B. Graves, J. Appl. Phys. **78,** 6604 (1995).

19) S. Tirelli, Dr. Thesis, Department of Information Technology and Electrical Engineering, ETH Zurich, Zurich (2014).

Chapter 5: Thermally enhanced formation of photon-induced damage on GaN

5.1 Introduction

Radiations in UV and VUV regions are considered to form photon-induced dissociations of Ga-N bonds by irradiations of higher photon energy than 3.4 eV for the GaN band gap energy.[1-3] Hence, the radiation damage in plasma etching of GaN needs to be studied in detail and carefully controlled to obtain a reliable performance for GaN-based devices.

In chapter 3, the author reported that the plasma-emitted photons predominantly degraded PL properties of GaN films at 500 ^{o}C.[4] In the processes at RT, the photon-induced damages were not a predominant cause of PID.[1,2] However, unlike the RT process, thermal annealing enhanced the formation of photon-induced damage at temperatures above 500 ^{o}C. This suggested that synergy of photon and heat could lead to the enhancement in the deterioration of PL.[4] Therefore, the author focused on the clarification of a mechanism of photon-induced damage of GaN films in the high-temperature Cl_2 plasma etching especially above 500 ^{o}C.

In this chapter, the author investigated thermal enhancement of the formation of photon-induced damage. A dependence of irradiation times on PL intensities of photon-irradiated GaN films was analyzed to discuss the temporal damage formation induced by photons. Then, depth profiles of the surface stoichiometry of the photon-irradiated GaN films were compared between 400 and 500 ^{o}C using angle-resolved XPS. Furthermore, the author discussed how UV irradiations degraded both PL properties and surface stoichiometry of the GaN films in terms of photon energy and photon flux.

5.2 Experimental details

5.2.1 Sample preparations

Samples were 5-μm-thick n-GaN films doped with Si (10^{18} cm^{-3}) and grown by HVPE on sapphire substrates. Before the plasma etching process, the samples were cleaned by dipping into 2% hydrofluoric acid for 1 min to remove native oxides and then into 17.5% hydrochloric acid for 5 min to remove metallic contaminants.

Figure 5.1(a) shows the experimental setup of the ICP etcher, which was described in chapter 3.[4] Cl_2 gas was introduced into the chamber with a flow rate of 50 sccm. The chamber pressure was maintained at 20 Pa by an automatic pressure controller. Cl_2 plasmas were generated at an ICP power of 400 W and a bias power of 15 W. Stage temperatures were maintained at 400 and 500 ^oC using an infrared lamp heater. The irradiation times were 0.4, 2.0 and 10 min.

5.2.2 Measurements and calibrations of emission spectra with different optical windows

A dependence of light wavelength on damage formation was evaluated. Optical emissions from Cl_2 plasma separately irradiated the GaN film. The GaN film was covered by an optical window, made from different materials of MgF_2, SiO_2, and BK7. The window surfaces were finely polished. Dimensions for all the windows were 13 mm diameter and 2 mm thickness. All windows were purchased from a vendor named Pier Optics Co., Ltd. Cut-off wavelengths were 115 nm for MgF_2, 170 nm for SiO_2, and 300 nm for BK7. Figure 5.1(b) shows the transmittances with the wavelengths of each optical windows that were measured by a UV-visible (VIS)-near infrared (NIR) spectrophotometer (Jasco V-670) with a wavelength range from 200 to 1000 nm. For the cut-off wavelength of 350 nm, the author used an amorphous carbon (a-C) film deposited on a quartz substrate. The a-C film with a thickness of 280 nm was deposited by a

radical-injection plasma-enhanced chemical vapor deposition (RI-PECVD) using a CH_4/H_2 plasma at 550 ^oC, as described in details elesewhere.[5)]

OES as a plasma diagnostic method was performed to identify active species in the plasmas. Plasma emissions with a wavelength range from 200 to 1100 nm were detected by a spectrometer (Ocean optics HR2000+). Emission spectra (ES) from the Cl_2 plasma were measured through a quartz window, which was equipped at the chamber wall. To measure the respective ES when GaN films were covered by BK7 and a-C. The optical windows of BK7 and the a-C film were respectively placed onto the quartz window, as shown in Fig. 5.1(a). All measured spectral emission intensities were calibrated using a standard light source of a deuterium (D_2) lamp (StellarNet SL3-CAL) for continuous UV emissions in a range from 190 to 450 nm. Then a wavelength-dependent sensitivity for the OES monitoring system was estimated. The calibration setup is schematically shown in Fig. 5.1(c). The optical path was purged with Ar gases to eliminate the air absorption. The quartz window and the optical fiber were identical for the OES measurements of the Cl_2 plasma emissions. On the other hand, a laser power meter (OPHIR ORION-TH) connected with a thermal sensor (OPHIR 30A-P-DIF-V1) was utilized to measure the power of this D_2 lamp through the quartz window and the optical fiber, which allowed the author to calculate the photon flux of Cl_2 plasma emissions according to the calibrated ES.

5.2.3 Approaches of damage diagnoses

The surface stoichiometry was analyzed by XPS (ULVAC-PHI XPS 1600) with a Mg Kα X-ray source (1253.6 eV). Take-off angles of photoelectrons were 15, 30, and 90^o. Peaks were recorded at 20.0 eV for Ga *3d*, 397.1 eV for N *1s*, and 531.0 eV for O *1s*, and atomic compositions were calculated on the basis of relative sensitivity factors using the values of 0.31 for Ga *3d*, 0.42 for N *1s*, and 0.66 for O *1s*.[6)] Depth profiles of the surface stoichiometry were

performed by analyses of the angle dependence of the photoelectron intensities. The thickness of the photon-damaged GaN layer was estimated by assuming a three layer model of the surface gallium oxide layer, the GaN_xO_y layer (x<1) and the substrate GaN layer. The photoelectron intensities I_N and I_{Ga} of the take-off angle θ (normal to the surface takes 90°) are given by

$$I_N = \sigma_N n_N \int_0^{\infty} e^{\frac{-x}{\lambda_N \sin\theta}} dx e^{-\frac{d+d_0}{\lambda_N \sin\theta}} + \sigma_N n'_N \int_0^{d} e^{\frac{-x}{\lambda_N \sin\theta}} dx e^{-\frac{d_0}{\lambda_N \sin\theta}}$$

$$= \sigma_N \lambda_N \sin\theta \left[(n_N - n'_N) e^{-\frac{d+d_0}{\lambda_N \sin\theta}} + n'_N e^{-\frac{d_0}{\lambda_N \sin\theta}}\right]$$

$$I_{Ga} = \sigma_{Ga} n_{Ga} \int_0^{\infty} e^{\frac{-x}{\lambda_{Ga} \sin\theta}} dx e^{-\frac{d+d_0}{\lambda_{Ga} \sin\theta}} + \sigma_{Ga} n_{Ga} \int_0^{d} e^{\frac{-x}{\lambda_{Ga} \sin\theta}} dx e^{-\frac{d_0}{\lambda_{Ga} \sin\theta}}$$

$$+ \sigma_{Ga} n_{Ga} \int_0^{d_0} e^{\frac{-x}{\lambda_{Ga} \sin\theta}} dx = \sigma_{Ga} \lambda_{Ga} n_{Ga} \sin\theta$$

where n is the atomic density, λ the attenuation length of photoelectrons, σ the ionization cross section,[7] d the thickness of the GaN_xO_y layer, and d_0 the thickness of the surface gallium oxide layer. Subscripts stand for N *1s* and Ga *3d*. Here, n'_N and n_N are the N atomic densities in the GaN_xO_y layer and the substrate GaN layer, respectively. The λ values of N *1s* and Ga *3d* were referred from the literature values of 1.8 and 2.4 nm.[8] The σ values of N *1s*, and Ga *3d* were referred from the literature values of 1.77 and 1.19.[9]

PL was observed *ex situ* at RT using a PL mapping system with excitation using a 325-nm-wavelength light from a He−Cd laser. The maximum power of this laser is 200 mW. The beam was focused on a spot with a diameter of approximately 100 μm. The accumulation time for PL measurement was 50 ms.

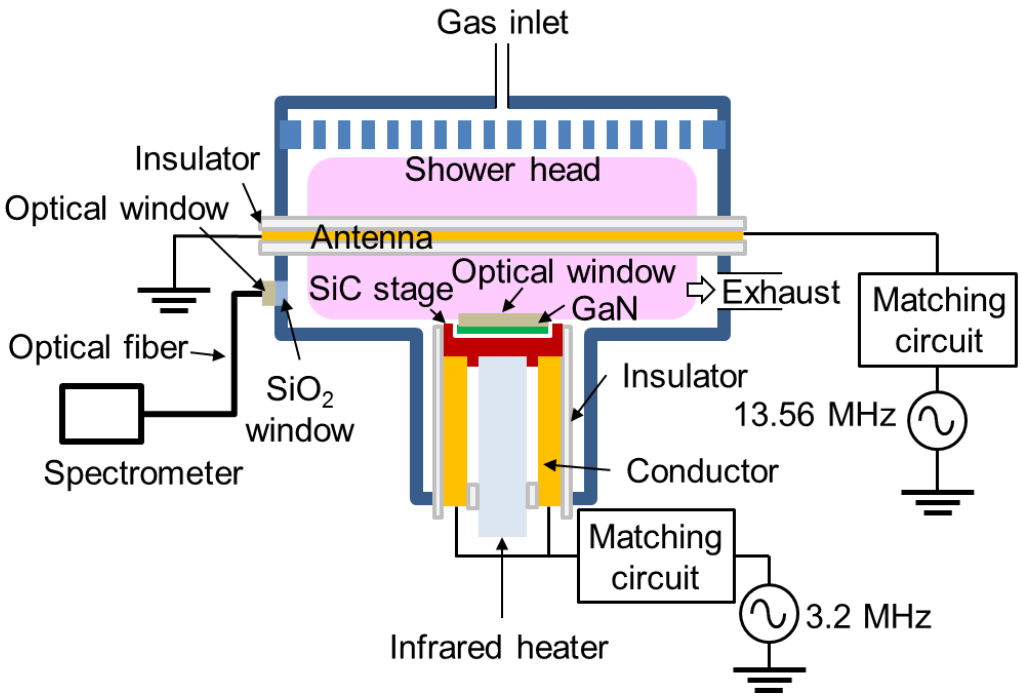

Fig. 5. 1 (a) Experimental setup for ICP etcher at high temperatures with the OES monitoring system.

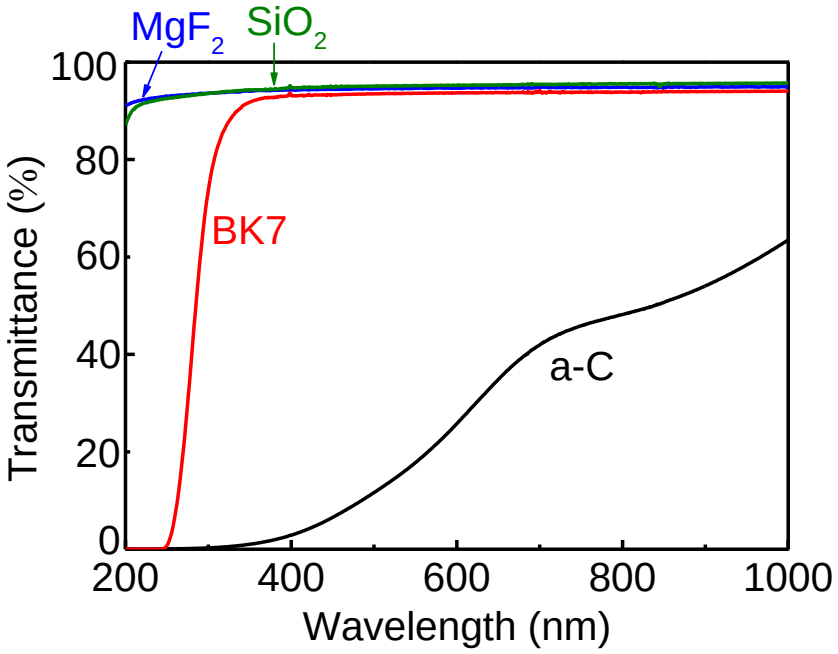

Fig. 5.1 (b) Dependence of wavelength on transmittance for each optical windows of MgF_2, SiO_2, and BK7 and the a-C film.

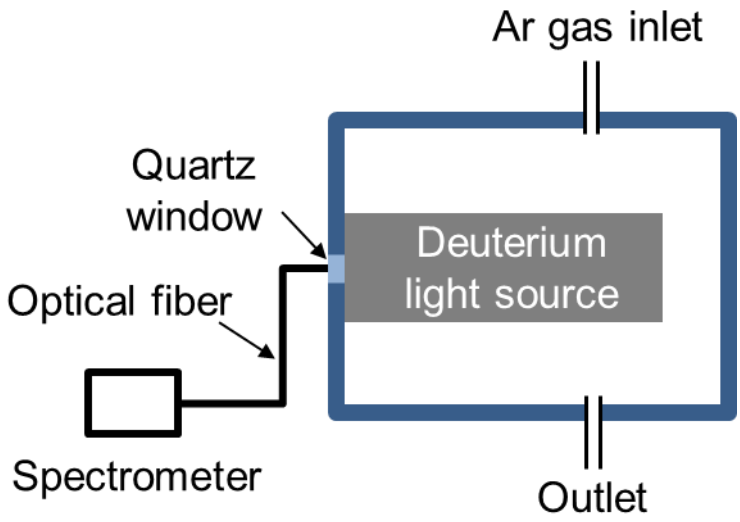

Fig. 5.1 (c) Experimental setup for the OES calibration using a D_2 lamp.

5.3 Results and discussion

5.3.1 Photon-induced PL degradation at early process at 500 °C

The temporal behavior of photon-induced damages at 500 °C was analyzed. By using the optical window made from MgF_2, the GaN film was irradiated by photons from Cl_2 plasma at 500 °C for various irradiation times of 0.4, 2.0, and 10 min. Figure 5.2(a) shows their PL spectra. The author also measured an as-cleaned GaN film before the photon irradiation as a reference spectrum. All the spectra show low intensities for yellow luminescence centered at 2.2 eV. This means a negligible amount of Ga vacancies in the bulk GaN films.[10] In general, the variations of NBE intensities observed at 3.4 eV were evaluated for the analyses of PID,[10] as shown in Fig. 5.2(b). The NBE intensity decreased with increasing the irradiation time until 2 min and then saturated. Namely, the damage formation induced by photons at 500 °C occurred at only the early period of the photon irradiation shorter than 2 min.

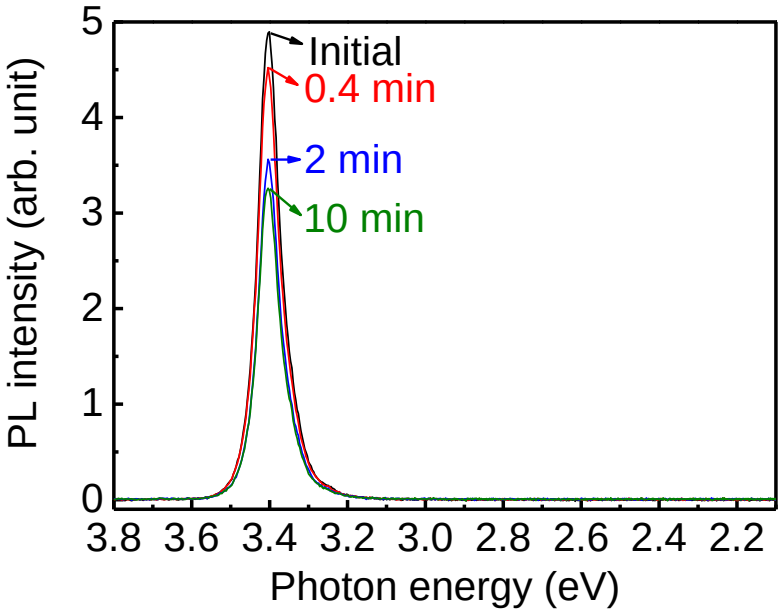

Fig. 5.2 (a) Dependence of irradiation time on PL spectra of photon-irradiated GaN films covered by the MgF_2 window at 500 °C (optical window: MgF_2).

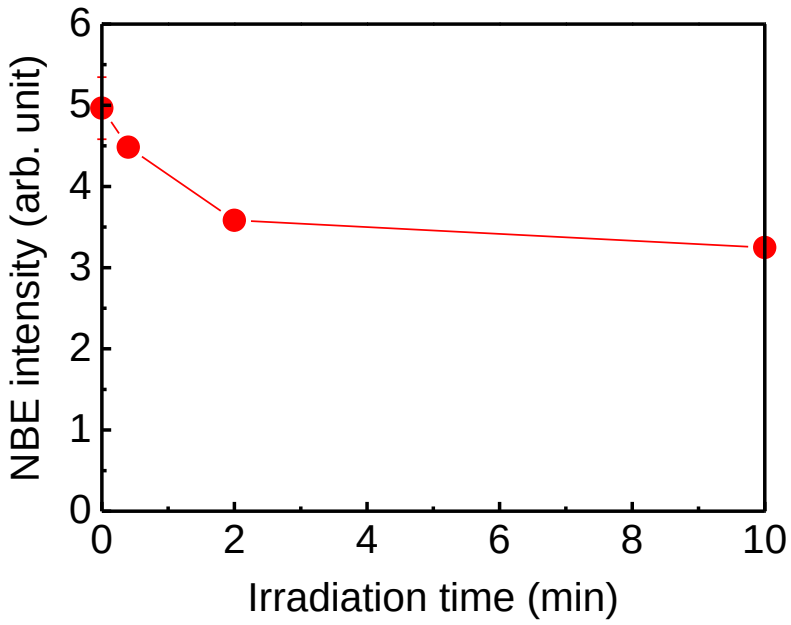

Fig. 5.2 (b) Dependence of irradiation time on the NBE intensity at 500 ºC (optical window: MgF_2).

The temporal behavior of photon-induced damage seemed to be similar with that of ion-induced damage in chapter 4.[11)] The net amount of ion damage also saturated at etch times more than 2 min, reaching the balance between damage formation and etch removal.[11)] Since no etch of the GaN films was observed in the photon irradiation of GaN films, the author considers that photon damage should obey other saturation mechanisms.

Many studies reported about thermal annealing for recovering PID in the GaN films. The protrusions of metallic Ga were observed after N_2^+ ion irradiation at RT.[12)] However, N_2 plasma treatments at 600 ºC provided stoichiometric and smooth surfaces.[13)] A restoration of GaN bonds occurred between Ga and N atoms, which was facilitated at high temperatures.[13)] The plasma-induced deteriorations in I-V properties of GaN Schottky diodes were recovered by thermal annealing at temperatures between 550 and 750 ºC as a post-etching method.[14)] Therefore, the author considers that this saturation of photon damage was restored by thermal annealing at 500 ºC.

A mechanism of this temporal behavior of photon damage is described as follows. At the beginning of photon irradiation shorter than 2 min, plasma emissions with photon energies above GaN band gap energy penetrated into the GaN films with a depth of approximately 100 nm.[1)] Then, Ga-N bonds were partly dissociated by photons with the thermal assistance at 500 ^{o}C. As plasma emission intensities would be attenuated with the penetration depth in the GaN films, a majority of photon damage remained on the surface and a close region beneath the surface. Namely, the nitrogen vacancy (V_N) and dangling bonds were potentially formed in the GaN films, leading to a preferably desorption of N atoms and thereby a Ga-rich subsurface was formed. For the irradiation time longer than 2 min, the net amount of photon damage was determined by a balance between damage formation and damage restoration. This suggests that thermal annealing also assisted the lattice reformation to passivate V_N and dangling bonds in the bulk GaN films and thereby the net amount of photon damage was maintained. In this thermal restoration, photon-dissociated Ga-N bonds were restored and V_N were finally excluded from the GaN films when V_N moved to the top surface.

Namely, photon damage was critical at the early period of the photon irradiation. Therefore, the author focused on a comparison of depth profiles of the surface stoichiometry of the photon-damaged GaN films for an irradiation time of 2 min between 400 and 500 ^{o}C to investigate the detailed mechanisms about this thermally enhanced photon-induced damage.

5.3.2 Photon-induced degradation in the surface stoichiometry

Photon-induced damage became predominantly in the degradative PL properties at a stage temperature above 500 °C.[4] Here, the author investigated the surface stoichiometry of the GaN films, which were irradiated by plasma emissions through the MgF_2 window for 2 min at 400 and 500 °C. Figure 5.3(a) shows angle-resolved XPS spectra for photon-irradiated GaN films at 400 and 500 °C. Peaks of Ga *3d*, N *1s*, and O *1s* for take-off angles of 15, 30 and 90° were normalized based on the areas of Ga *3d*. Because Ga auger spectrum would be included in C *1s* spectrum for a Mg Kα XPS measurement,[15] the author could not calibrate the chemical shifts of Ga *3d*, N *1s* and O *1s* spectra using the C *1s* peak position. Hence, the author performed the calibration of the chemical shifts in N *1s* and O *1s* spectra based on Ga *3d* peak at 20.0 eV. When the take-off angle was fixed at 15°, with an increase of stage temperature from 400 to 500 °C, no obvious variations in binding energies could be found for Ga *3d* spectra, which contained a main peak of GaN at 20.0 eV and a component of gallium oxide at 20.8 eV.[16] As compared with the N *1s* spectrum of the initial GaN films, no obvious changes in binding energies of N *1s* spectra at 397.1 eV could be found for the photon-irradiated samples processed at 400 and 500 °C. However, a decrease in N *1s* intensity could be found for the photon-irradiated samples processed at 400 °C compared with that of the initial one, and a greater degradation in N *1s* intensity was observed for the sample processed at 500 °C. Regarding O *1s* spectra, the author notes that a decrease in O *1s* intensity for the photon-irradiated GaN films compared with that for the initial one was considered as a result of scissions of C-O bonds at 533.0 eV and C=O bonds at 531.5 eV by high-energy photons from Cl_2 plasma emissions ranging around 286-357 nm,[17,18] and these C-related bonds in O *1s* spectra were attributed to organic contaminations attached on the top surface. Moreover, the decrease in O *1s* intensity of the photon-irradiated sample at 500 °C was more than that of the one at 400 °C, indicating that the scissions of C-O and C=O bonds were enhanced as the increase of temperature. With an

increase of take-off angle to 30°, N *1s* intensities increased as expected in the angle-resolved XPS measurement for depth profiling, and the degradations in N *1s* intensities for photon-irradiated GaN films were weaker than those at 15°. At a take-off angle of 90°, no apparent changes for Ga *3d*, N *1s*, and O *1s* spectra could be observed.

Figure 5.3(b) shows a quantitative result of the analyzed N/Ga ratios of the degradative N *1s* spectra of photon-irradiated GaN films. Before the plasma etching, the N/Ga ratio of the initial GaN film was determined to be approximately 0.93. For the initial GaN film, the total thickness of the surface gallium oxide layer and the GaN_xO_y layer was estimated approximately 1 nm. After the photon irradiation at 400 °C, the N/Ga ratio decreased to 0.88 for the sample measured at a take-off angle of 15°. For the photon irradiation at 500 °C, the N/Ga ratio was much decreased to 0.77 for the sample measured at a take-off angle of 15°. Notably, thermal assistance enhanced N atoms loss in the photon irradiation. These results indicate that photon formed V_N and thereby a Ga-rich surface was formed. Based on the three layer model, the thicknesses of the surface gallium oxide layer and the GaN_xO_y layer were estimated to approximately 1.4 and 3.2 nm after the photon irradiation at 400 and 500 °C, respectively. Namely, the thickness of the surface oxides increased with increasing temperature. Hence, the author considers that the component of integrated intensities of O *1s* peak that represented surface gallium oxide layer located at 531.0 eV and the GaN_xO_y layer of photon-irradiated GaN films increased as a function of the stage temperature.

Thermal dissociations of GaN were reported by L'vov with respect to their kinetics and mechanisms.[19] It formed some free N atoms and the free atoms potentially desorbed from the surface. This mechanism of the high-temperature annealing is possible to work for the V_N formations synergistically with the photon irradiation. The author emphasizes that most of photon damage, behaving as V_N on the surface, were formed with a depth of 1.4 nm at 400 °C and 3.2 nm at 500 °C. It is noticeable that this photon-induced damage was enhanced with the

thermal assistance at 500 °C which was greater than that at 400 °C.

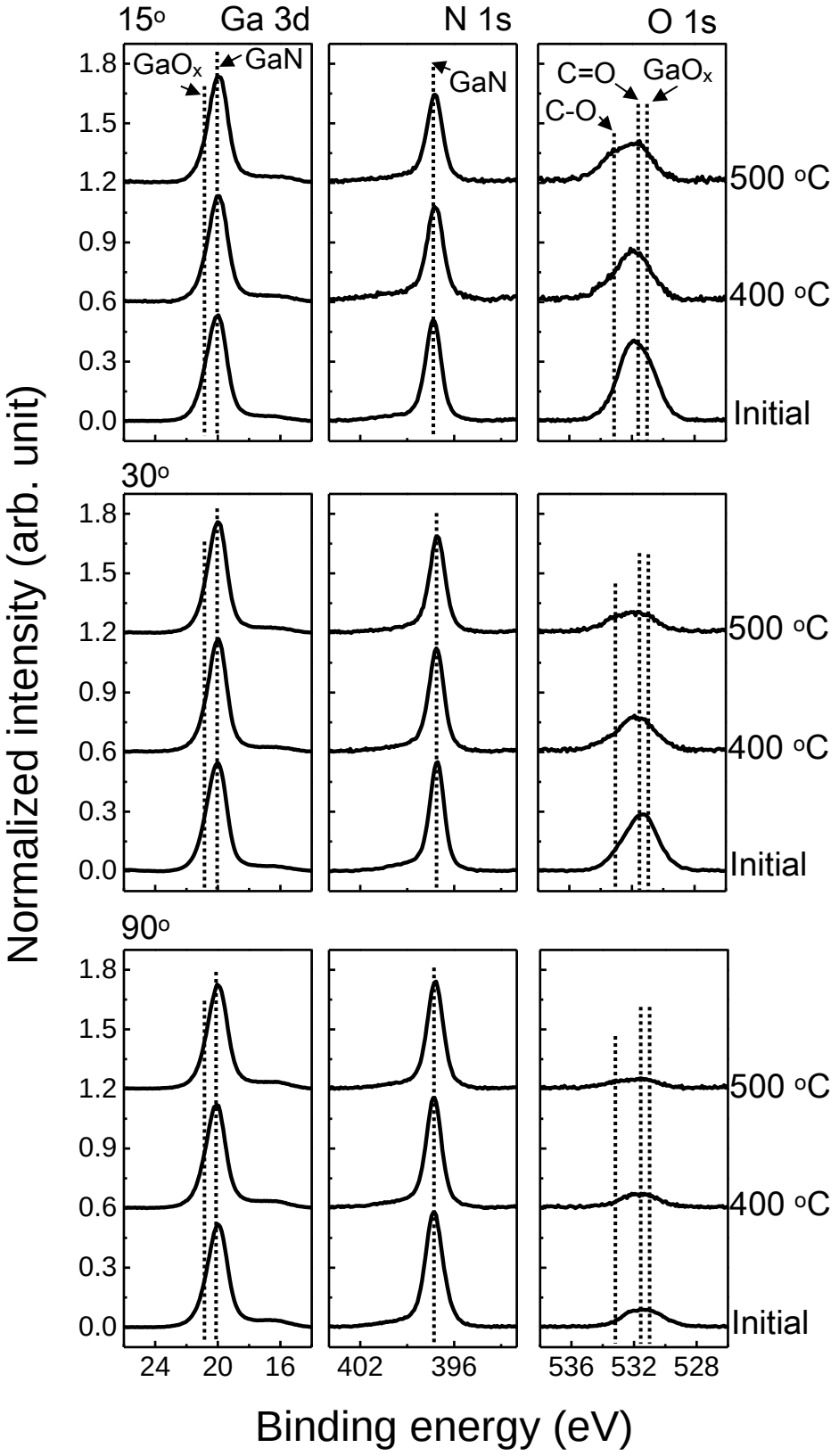

Fig. 5.3 (a) Normalized XPS spectra of Ga *3d*, N *1s* and O *1s* at take-off angles of 15, 30 and 90° for the photon-irradiated GaN films covered by the MgF_2 window at 400 and 500 °C (irradiation time: 2 min).

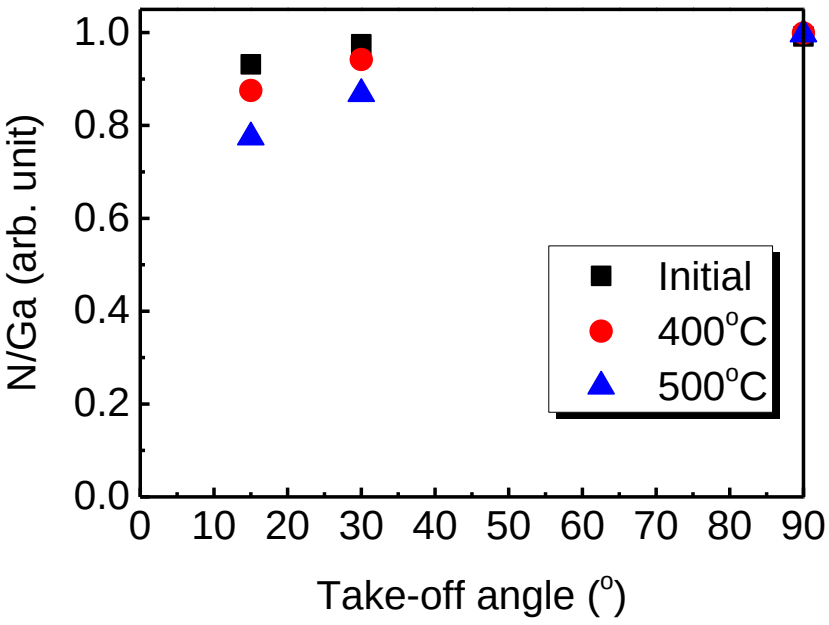

Fig. 5.3 (b) The calculated N/Ga ratios at take-off angles of 15, 30 and 90° for the photon-irradiated GaN films covered by the MgF_2 window at 400 and 500 °C (irradiation time: 2 min).

5.3.3 Wavelength dependence of damage formation induced by the photon irradiation

Figure 5.4(a) shows the ES in Cl_2 plasma measured with various optical windows. The MgF_2 window could transmit photons with energies lower than 10.8 eV, including almost all plasma emissions from Cl_2 plasma. The other optical windows of SiO_2, BK7, and the a-C film were individually used to investigate photons from Cl_2 plasma with the energies lower than 7.3, 4.1, and 3.5 eV, respectively. Because of the limitation of the spectrometer used in this work, the signals in VUV region was unable to be measured. Usually, two emissions in VUV region centered at 134.7 nm (9.2 eV) and 137.9 nm (8.9 eV) with a penetration depth of nearly 15 nm were widely reported in Cl_2 plasmas.[20,21] Donnelly *et al.* reported the assignments of each emission that were referred in this study.[22] Optical emission intensities were recorded at 258 and 306 nm for Cl_2, from 350 to 700 nm for Cl_2, Cl_2^+, Cl, and Cl^+, and from 700 to 900 nm for Cl. Apparently, two Cl_2 emissions at 258 nm (4.8 eV) and 306 nm (4.1 eV) in UV region with penetration depths of approximately 70 and 50 nm were highly considered to form damage in the GaN films because of their higher energies than GaN band gap energy.[20] The integrated intensity from the Cl_2 emission band centered at 306 nm was assigned to the $4s\sigma_g{}^1\Pi_g \rightarrow {}^1\Pi_u$ transition, which is attributed to electron impact of an ion pair state of Cl_2 at 8.4 eV.[23,24] Another emission centered at 258 nm has been widely studied by many groups. Peyerimoff and Buenker assigned the emission at 258 nm to the transition $2({}^3\Pi_g) \rightarrow 2({}^3\Pi_u)$ with an energy threshold of 7.1 eV.[25]

Spectral sensitivity characteristic of the OES monitoring system was carried out using the D_2 lamp, which allows the author to calibrate the measured ES, as shown in Fig. 5.4 (b). Emission intensities at 258 and 306 nm increased strongly after calibration, indicating a weakened sensitivity in the OES monitoring system, especially in UV region. As the power of this D_2 lamp measured in the calibration system was 9 mW, the author calculated the photon flux for Cl_2 plasma emissions with values of 1.04×10^{15} $cm^{-2}s^{-1}$ for the 258 nm-peak and

2.63×10^{15} $cm^{-2}s^{-1}$ for the 306 nm-peak.

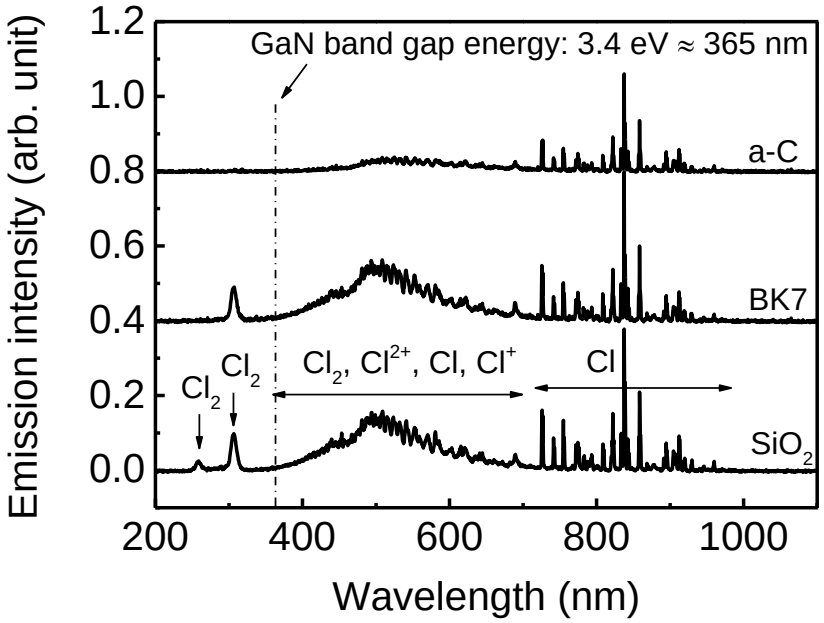

Fig. 5.4 (a) The measured ES for the plasma emissions through various optical windows.

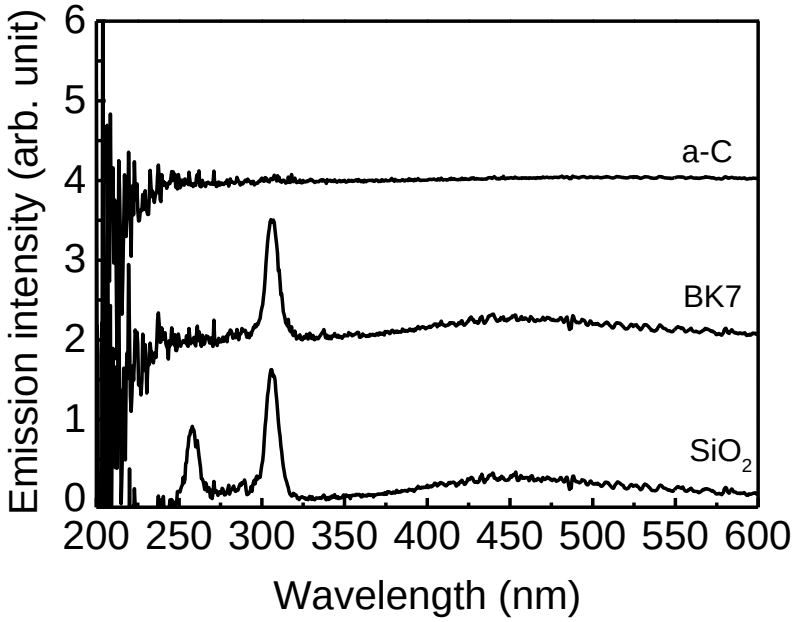

Fig. 5.4 (b) The calibrated ES using the D_2 lamp.

Figure 5.5 shows the NBE intensity of photon-irradiated GaN films covered by different optical windows. The stage temperature was 500 ^{o}C and the irradiation time was 2 min. Photons transmitted through various optical windows resulted in different degradative optical properties. The NBE intensity of photon-irradiated GaN film covered by the SiO_2 window was similar with that covered by the MgF_2 window, indicating a negligible effect of photons in VUV region on damage formation. The NBE intensity was found to be degraded in the photon-irradiated GaN film covered by the BK7 window, suggesting the individual effect of 306 nm-peak on damage formation. The GaN film covered by the a-C film represented the maintained initial NBE intensities after photon irradiations, indicating that Cl_2 plasma emissions with photon energies lower than 3.5 eV hardly induced damage in the GaN films.

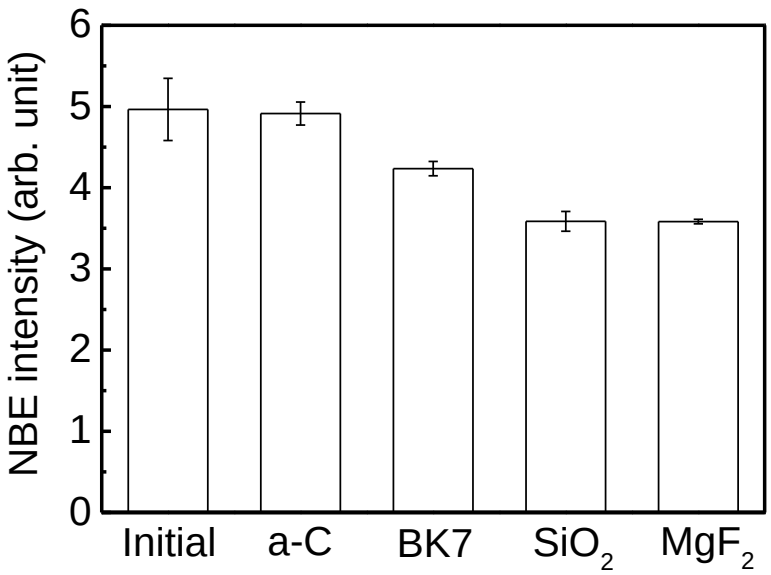

Fig. 5.5 NBE intensities of photon-irradiated GaN films covered by various optical windows at 500 ^{o}C (irradiation time: 2 min).

Figure 5.6(a) shows normalized XPS spectra of these photon-irradiated GaN films with take-off angles of 15, 30 and 90^{o} at 500 ^{o}C. The calibrations of chemical shifts in N *1s* and O *1s* spectra were performed based on Ga *3d* peak position at 20.0 eV. For the GaN surface covered by the a-C film, both intensities and binding energies of N *1s* spectra were hardly affected by the photon irradiation of Cl_2 plasma. Moreover, the N/Ga ratios represented similarly with the initial values regardless of the take-off angles, as shown in Fig. 5.6(b). On the other hand, for the GaN surfaces covered by the SiO_2 window, the degradations in the loss of N atoms that were induced by Cl_2 plasma emissions at 258 and 306 nm exhibited similarly with the one covered by the MgF_2 window, and the binding energies were also maintained. For the GaN film covered by the BK7 window, the degradations in both N *1s* intensity and the N/Ga ratio were fewer than those of the photon-irradiated GaN film covered by the MgF_2 or SiO_2 windows. Here, the thickness of the surface gallium oxide layer and the GaN_xO_y layer formed by 306 nm-peak of the Cl_2 plasma emission was estimated to nearly 2.1 nm based on the depth profile of the N/Ga ratio. The degradations in the NBE intensities and the surface stoichiometry were related. As a result, Cl_2 plasma emissions at 258 and 306 nm were predominant in the formation of photon-induced damage at 500 ^{o}C.

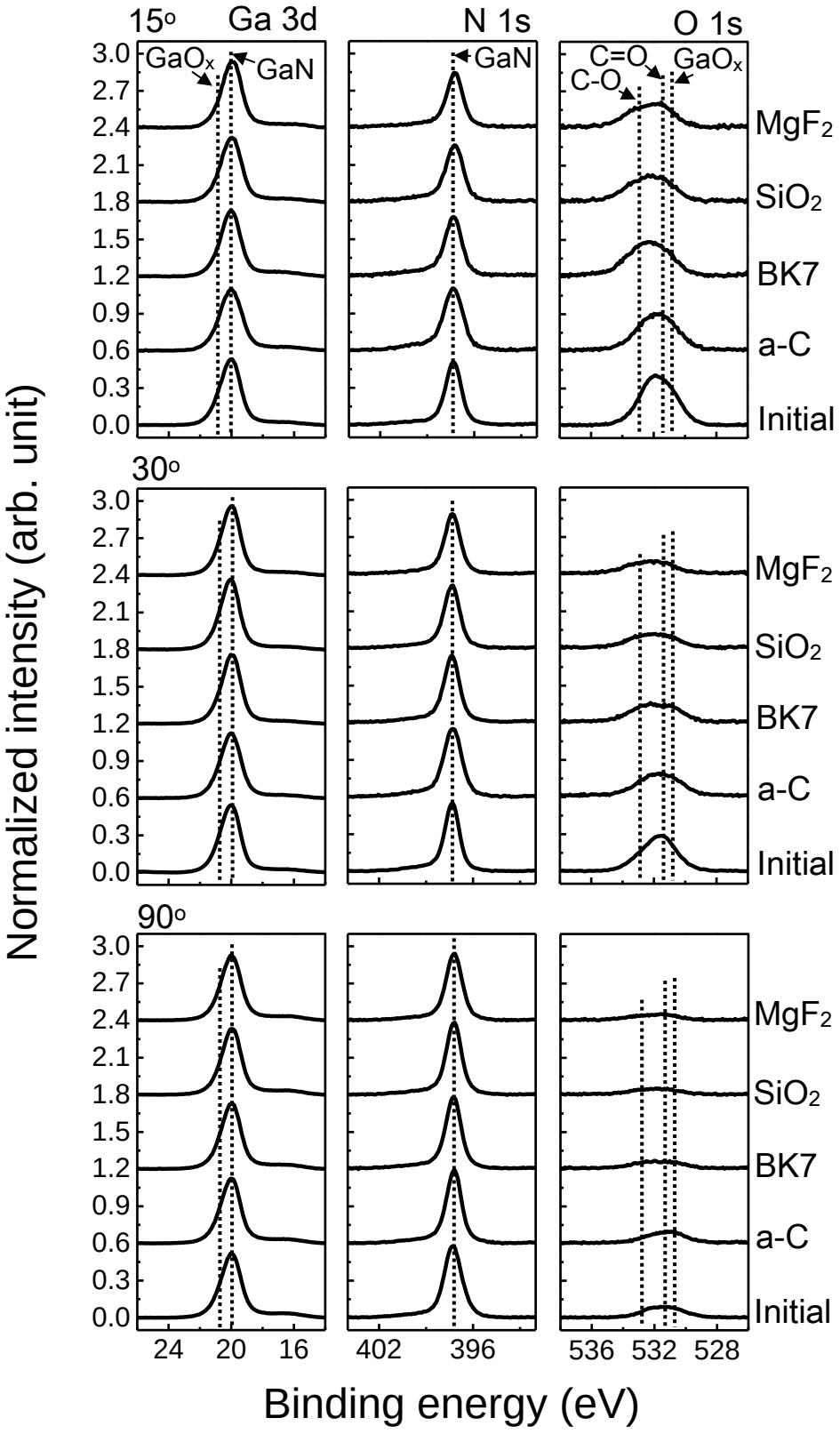

Fig. 5.6 (a) Normalized XPS spectra of Ga *3d*, N *1s* and O *1s* at take-off angles of 15, 30 and 90° for the photon-irradiated GaN films covered by various optical windows at 500 °C (irradiation time: 2 min).

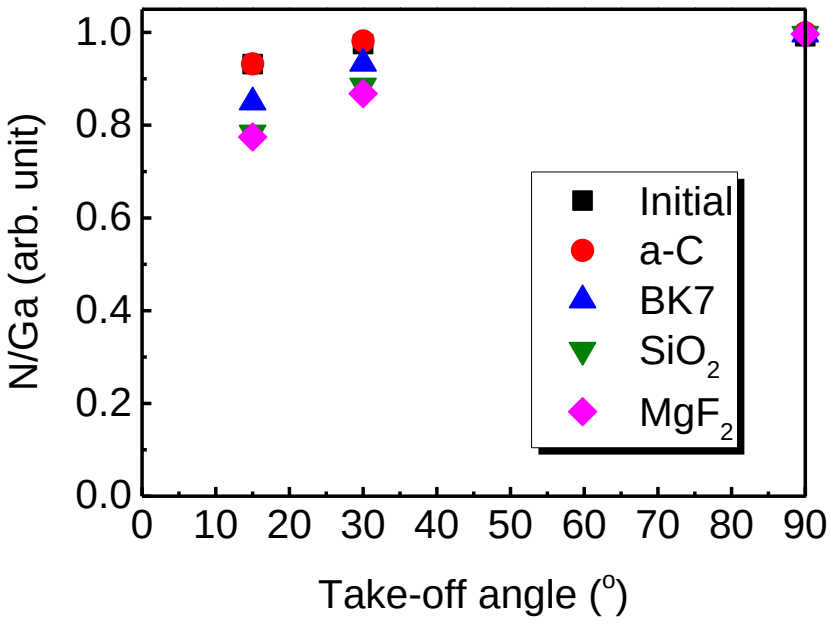

Fig. 5.6 (b) The calculated N/Ga ratios at take-off angles of 15, 30 and 90° for the photon-irradiated GaN films covered by various optical windows at 500 °C (irradiation time: 2 min).

Based on above results, the author focused on the clarification of detailed mechanisms for these two emissions in UV region. The author formulated photon damage in the degradative PL, $\Delta PL/PL_{initial}$ at 500 °C for 2 min irradiation, as described below,

$$\Delta PL/PL_{initial} = \beta_1\lambda_1\Gamma_1 + \beta_2\lambda_2\Gamma_2 ,$$

where λ stands for the wavelength, Γ represents the photon flux, and β is the coefficient of the degradations in PL properties. Subscripts 1 and 2 stand for 258 and 306 nm-peak, respectively. Hence, the values of Γ_1 and Γ_2 are 1.04×10^{15} and 2.63×10^{15} $cm^{-2}s^{-1}$, respectively. Here, the coefficients β took the factor for the effect of thermal recovery into account and were estimated to 4.89×10^{-12} cm·s for β_1 and 1.82×10^{-12} cm·s for β_2. The coefficients β_1 and β_2 were obviously different, which represented a wavelength dependence characteristically. The photon flux of Cl_2 plasma emission at 306 nm was roughly twice larger than that of the emission at 258 nm. Hence, the nearly similar degradations in PL properties between these two emissions, as shown in Fig. 5.5, resulted from the larger coefficient β for

the 258 nm-peak.

Similarly, the author formulated photon damage in the degradative N/Ga ratio at 500 ºC for 2 min irradiation, as described below,

$$\Delta(N/Ga)/(N/Ga)_{initial} = \gamma_1\lambda_1\Gamma_1 + \gamma_2\lambda_2\Gamma_2 ,$$

where γ_1 and γ_2 are the coefficients of the degradations in the surface stoichiometry by Cl_2 plasma emission for 258 and 306 nm, respectively. The coefficients of γ_1 and γ_2 for 500 ºC were estimated to 2.99×10^{-12} cm·s and 1.09×10^{-12} cm·s, respectively. Both γ_1 and γ_2 were wavelength-dependent that increased with shortening the wavelength. Although the photon fluxes of Cl_2 plasma emission at 258 and 306 nm were different, the degradation in the surface stoichiometry represented nearly similar, as shown in Fig. 5.6(b), resulting in the different coefficient γ. Namely, a greater degraded surface stoichiometry of the GaN films could be expected under the photon irradiation with a higher photon energy. Indeed, the optical absorption coefficients of the GaN films increased as a function of the photon energies. Therefore, regarding these wavelength dependences, it is expected that the PL degradation could be caused by nonradiative exciton recombination under the photon irradiation with a higher photon energy. However, further investigations are needed in the future.

According to the above results, the photon-induced degradation in both PL and the surface stoichiometry were related and wavelength-dependent. UV photons with wavelengths of 258 and 306 nm in Cl_2 plasma emissions were predominant in these degradations because photon energies were higher than GaN band gap energy. Moreover, the 258 nm-peak was highly degradative than 306 nm-peak, suggesting a greater extent of photon damage both in the deteriorated PL intensities and the N/Ga ratios. These degradative properties were formulated with the photon energy dependent coefficients β and γ.

5.4 Conclusions

The author elucidated the mechanisms of photon-induced damage of GaN films under the high-temperature Cl_2 plasma etching. Photons with energies higher than GaN band gap energy preferred to degrade PL properties of GaN films at 500 ^oC as a result of the thermally enhanced photon-dissociated Ga-N bonds. Photon-induced damage saturated within the irradiation time of 2 min as a result of the equilibrium between damage formation and thermal recovery. Moreover, Cl_2 plasma emissions at 258 nm degraded both PL properties and N/Ga ratios easier than those degraded by 306 nm-peak because of its higher photon energy. In order to fabricate highly reliable GaN-based devices, UV light during plasma etching processes should be precisely controlled.

5.5 References

1) M. Minami, S. Tomiya, K. Ishikawa, R. Matsumoto, S. Chen, M. Fukasawa, F. Uesawa, M. Sekine, M. Hori, and T. Tatsumi, Jpn. J. Appl. Phys. **50,** 08JE03 (2011).

2) R. Kawakami, T. Inaoka, K. Tominaga, A. Kuwahara, and T. Mukai, Jpn. J. Appl. Phys. **47,** 6863 (2008).

3) Y. Tamura, J. Ohta, H. Fujioka, and S. Samukawa, Ext. Abstr. 2012 Int. Conf. Solid State Devices and Materials, 2012, p.925.

4) Z. Liu, J. Pan, T. Kako, K. Ishikawa, K. Takeda, H. Kondo, O. Oda, M. Sekine, and M. Hori, Jpn. J. Appl. Phys. **54,** 06GB04 (2015).

5) H. Sugiura, L. Jia, H. Kondo, K. Ishikawa, K. Takeda, M. Sekine, and M. Hori, ICRP-9 2015, IW2.00002 (2015).

6) C. D. Wagner, L. E. Davis, M. V. Zeller, J. A. Taylor, R. H. Raymond, and L. H. Gale, Surf. Interface Anal. **3,** 211 (1981).

7) M. P. Seah and I. S. Gilmore, Surf. Interface Anal. **31,** 835 (2001).

8) S. Gangopadhyay, T. Schmidt, C. Kruse, S. Figge, D. Hommel, and J. Falta, J. Vac. Sci. Technol. A **32,** 051401 (2014).

9) J. H. Scofield, J. Electron Spectrosc. Relat. Phenom. **8,** 129 (1976)

10) M. A. Reshchikov and H. Morkoç, J. Appl. Phys. **97,** 061301 (2005).

11) Z. Liu, J. Pan, A. Asano, K. Ishikawa, K. Takeda, H. Kondo, O. Oda, M. Sekine, and M. Hori, Jpn. J. Appl. Phys. (2016) in press.

12) Y. H. Lai, C. T. Yeh, J. M. Hwang, H. L. Hwang, C. T. Chen, and W. H. Hung, J. Phys. Chem. B **105,** 10029 (2001).

13) R. Kometani, K. Ishikawa, K. Takeda, H. Kondo, M. Sekine, and M. Hori, Appl. Phys. Express **6,** 056201 (2013).

14) X. A. Cao, H. Cho, S. J. Pearton, G. T. Dang, A. P. Zhang, F. Ren, R. J. Shul, L. Zhang, R.

Hickman, and J. M. Van Hove, Appl. Phys. Lett. **75,** 232 (1999).

15) R. Kometani, S. Chen, M. Liu, K. Ishikawa, K. Takeda, T. Egawa, H. Kondo, H. Amano, M. Sekine, and M. Hori, Proc. 5th Int. Symp. Advanced Plasma Science and Its Applications for Nitrides and Nanomaterials, 2013, Tha-A03OA.

16) R. Carli and C.L. Bianchi, Appl. Surf. Sci. **74,** 99 (1994).

17) G. Yan, X. Li, , Z. Wang, H. Guo, J. Wang, W. Peng, and Q. Hu, Electrochim. Acta **166,** 190 (2015).

18) F. Weilnboeck, R. L. Bruce, S. Engelmann, G. S. Oehrlein, D. Nest, T.-Y. Chung, D. Graves, M. Li, D. Wang, C. Andes, and E. A. Hudson, J. Vac. Sci. Technol. B **28,** 993 (2010).

19) B. V. L'vov, Thermochimica Acta **360,** 85 (2000).

20) J. F. Muth, J. H. Lee, I. K. Shmagin, R. M. Kolbas, H. C. Casey, Jr., B. P. Keller, U. K. Mishra, and S. P. DenBaars, Appl. Phys. Lett. **71,** 2572 (1997).

21) W. Zhu, S. Sridhar, L. Liu, E. Hernandez, V. M. Donnelly, and D. J. Economou, J. Appl. Phys. **115,** 203303 (2014).

22) V. M. Donnelly, M. V. Malyshev, M. Schabel, A. Kornblit, W. Tai, I. P. Herman, and N. C. M. Fuller, Plasma Sources Sci. Technol. **11,** A26 (2002).

23) N. C. M. Fuller, I. P. Herman, and V. M. Donnelly, J. Appl. Phys. **90,** 3182 (2001).

24) V. M. Donnelly, J. Vac. Sci. Technol. A **14,** 1076 (1996).

25) S. D. Peyerimoff and R. J. Buenker, Chem. Phys. **57,** 279 (1981).

Chapter 6: GaN surface roughness reduction with photon irradiation during etching by chlorine radicals

6.1 Introduction

To fabricate GaN devices in a gate recess process without damage formation using Cl_2 plasma, the author has reported in chapter 4 that an advanced plasma etching by elevating the stage temperature to 400 ^oC for a short time plasma exposure of 0.4 min without bias voltage application, enabling the etch depth of approximately 6.8 nm and the reduction of the degradation of PL properties to 98.8% of initial value with smooth and stoichiometric GaN surfaces.[1,2)] Namely, the author has confirmed that both ion and photon induced damages were successfully reduced or prevented.

However, the increase of surface roughness as a function of the etch time in the high-temperature Cl_2 plasma is a crucial issue for the deep etch of vertical GaN-based power devices, in which patterns as high as 1.5 μm in GaN film would be etched.[3)] The author previously considered that Cl radicals predominantly caused the formation of etch pits and thereby roughness increased linearly with the etch time.[1,2)] In chapter 4, the surface roughness with rms values increased from 0.57 nm at 0.4 min of etching 6.8 nm GaN to 13.7 nm at 10 min of etching 170 nm GaN at 400 ^oC.[2)] On the other hand, this development of roughness was enhanced when the stage temperature increased, indicating an enhanced chemical reactions between reactive Cl radicals and the GaN surface.[1)] The author considered that the density of threading dislocations of GaN corresponded to the number of etch pits in the high-temperature Cl_2 plasma etching.[1,2)] Hence, the suppression of the etch pits in GaN surface is highly demanded.

In this chapter, the author investigated simultaneous irradiations of photon and Cl radical to GaN surface at high temperature of 600 ^oC, where a smoother GaN surface was achieved compared with that exposed to only Cl radicals. The effect of simultaneous irradiations of

photon with wavelength above 115 nm and radical on the surface morphology was analyzed. Furthermore, the author used XPS to investigate the surface bonding states for GaN films after Cl radical exposure and after simultaneous irradiations of photon and radical, in which the mechanisms of this suppression of the surface roughening would be interpreted. The author also discussed a dependence of light wavelength of simultaneous irradiations of photon and radical on the suppression of the etch pit formation.

6.2 Experimental details

The samples were 5-μm-thick n-GaN films doped with Si (10^{18} cm^{-3}) and grown by HVPE on sapphire substrates. Before the etching, samples were cleaned by dipping into 2% hydrofluoric acid for 1 min to remove native oxides and then into 17.5% hydrochloric acid for 5 min to remove metallic contaminants.

The experimental setup of the ICP etcher with the optical emission monitoring system was described in chapter 3. The experimental method is described briefly as follows. Cl_2 plasmas were generated at an ICP power of 400 W and a bias power of 15 W. Stage temperatures were maintained at 600 ^oC using an infrared lamp heater. The process times were 2 and 10 min. Cl_2 gas was introduced into the chamber with a flow rate of 50 sccm. The chamber pressure was maintained at 20 Pa by an automatic pressure controller.

A Si wafer placed at 0.5 mm above the GaN film was used to analyze the effect of radicals on surface morphology. To evaluate the synergistic effect of photons and radicals, an optical window made from MgF_2 was placed at a distance of 0.5 mm above the GaN film, which transmitted light with wavelengths above 115 nm. To evaluate a dependence of light wavelength on the suppression of the roughening of the GaN surfaces, other optical windows made from different materials of SiO_2 and BK7 (ϕ13 mm diameter with a thickness of 2 mm; Pier Optics Co., Ltd) were used. These materials can transmit lights with cut-off wavelengths of 170 and

300 nm, respectively. Regarding a cut-off wavelength of 350 nm, the author used a quartz substrate covered by an a-C film, as described in chapter 5.[4)]

Previously, the author reported that the plasma emission with a wavelength region from 200 to 1100 nm was detected using OES with a spectrometer (HR2000+, Ocean optics, Inc.), as introduced in chapter 5.

Surface bonding states were investigated by *ex situ* XPS measurements (ULVAC-PHI XPS 1600) with a Mg Kα X-ray source (1253.6 eV). The take-off angle of photoelectrons was 15^{o} for a detection depth of nearly 1.8 nm. Peaks were recorded at 20.0 eV for Ga *3d*, 397.1 eV for N *1s*, and 531.0 eV for O *1s* and atomic compositions were calculated on the basis of relative sensitivity factors using the values of 0.31 for Ga *3d*, 0.42 for N *1s*, and 0.66 for O *1s*.[5)]

Surface morphologies of the samples were observed by AFM (Veeco NanoMan VS-1N) in the tapping mode with a SiN cantilever. Rms values were averaged from three different areas for each surface morphology image, where no steps were included.

To evaluate the etch profiles, a stacked metal film mask consisting of 20 nm-thick Ti, 72 nm-thick Al, 12 nm-thick Ni, and 40 nm-thick Au was firstly prepared on a GaN surface by electron beam physical vapor deposition. After radical exposure and simultaneous irradiations of photon and radical, cross sectional images of the etch profiles of the GaN films were observed by SEM (Hitachi S-5200) and then etch depths were measured.

6.3 Results and discussion

Figure 6.1 shows AFM images and line profiles of the GaN surfaces for initial, after plasma etching, after radical exposure, and after simultaneous irradiations of photon and radical, in which the plasma emission transmitted through an optical window of MgF_2 with wavelengths above 115 nm. The process times for all experiments were 2 min. The initial GaN film exhibited a flat surface with an rms of 0.36 nm. Here, the initial GaN surface was flat, where only atomic roughness of step and terrace structures existed. Namely, no large crystalline dislocations could be observed.

After plasma etching at 600 ºC for 2 min, the AFM image shows apparently roughened surface morphology with a large number of etch pits.[1)] An rms for this surface was 32.7 nm. Averaged size for the etch pits were roughly 340 nm in wide and 50 nm in depth. The areal density of number of pits was 4.68×10^8 cm^{-2}, corresponding to the dislocation density of approximately 1×10^9 cm^{-2} for this GaN film.

Once the GaN film was exposed to Cl radical at 600 ºC, a severely roughened surface was observed with an rms of 136.0 nm. Cl ions and plasma emissions were almost eliminated using an opaque plate made of Si for radical exposure. As reported previously, a large amount of etch pits were formed after radical exposure due to a chemical reaction between Cl radicals and the GaN surface.[1)] Therefore, these roughening phenomena were in common for the samples treated by Cl radicals at 600 ºC.

When using the MgF_2 window instead of the Si plate, the GaN surface roughness was measured to be 39.5 nm, which was much less than that of Cl radical exposure. Namely, although the GaN surface was roughened by Cl radical exposure, the smooth surface of initial GaN films might be potentially maintained when both photon and radical are simultaneously irradiated at a relatively lower temperature like 400 ºC. Regarding Cl ions, the author previously reported that Cl ions hardly affected the development of surface morphology in chapter 4.[2)]

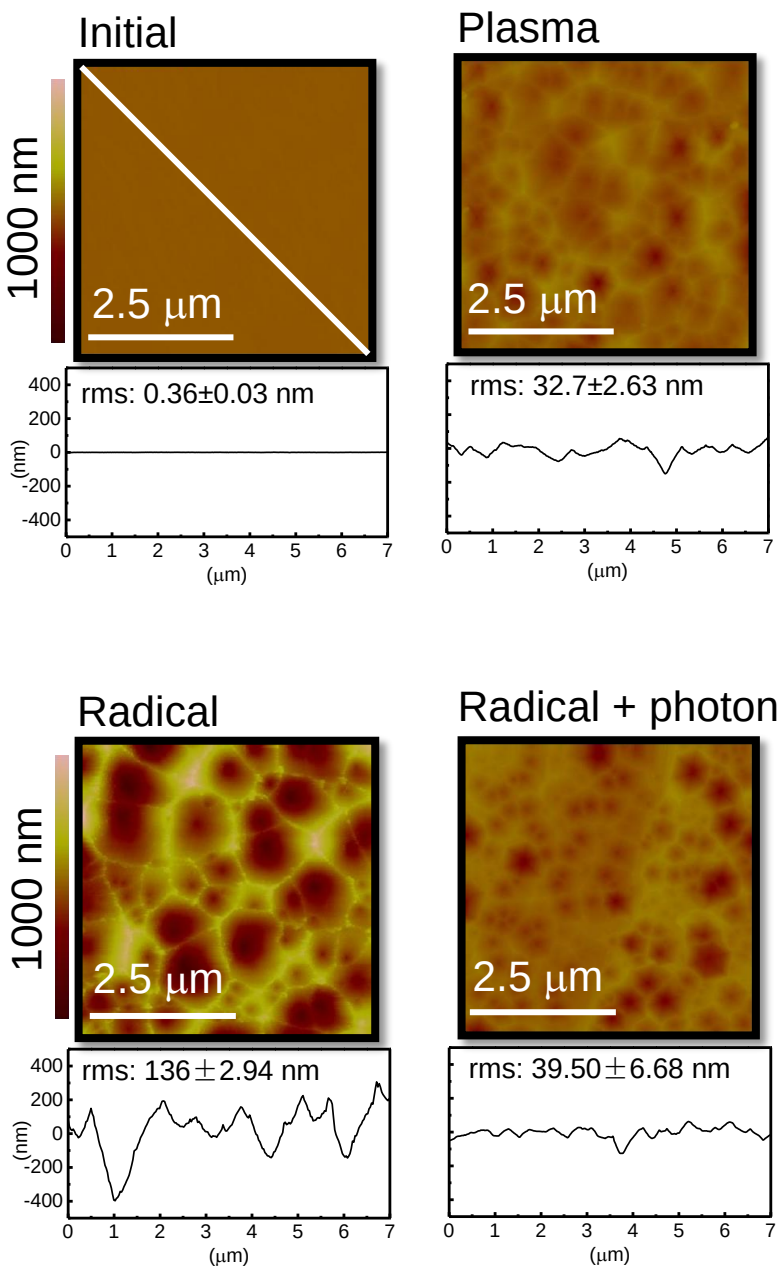

Fig. 6.1 AFM images and line profiles of the GaN surfaces for initial, after plasma etching, after radical exposure, and after simultaneous irradiations of photon and radical (optical window: MgF_2, process time: 2 min).

Cross sectional SEM images of the GaN films after radical exposure and radical + photon exposure were observed, as shown in Fig. 6.2. The etch depth was approximately 500 nm for the radical-etched film, indicating a negligible increase of dislocation density in the discussion of the surface morphology as described in chapter 3. Etch pits were frequently observed with the triangular shapes. The etch pits generally appeared in the roughened GaN surface morphology. Such crystalline-defect-decoration pits were formed by an isotropic etching on the GaN surface. However, a smoother surface was observed after simultaneous irradiations of photon and radical, where the etch depth was approximately 110 nm. Here, etch pits of the triangular shapes were hardly recognized on the etched surface. Namely, deep etch pits were reduced by additional photons. Moreover, the author reported in chapter 3 that the etch depth of plasma etching at 600 ºC for 2 min was nearly 400 nm, in which ions participated in the removal of Ga and N chlorides.[1)] These results indicated that the chemical etching of Cl radicals on the GaN surface was suppressed by additional photon irradiations.

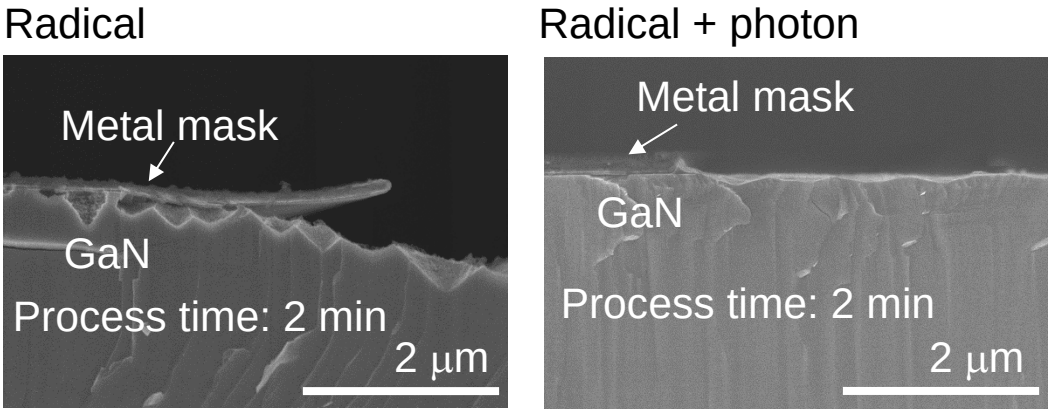

Fig. 6.2 The cross sectional SEM images of the etch profiles of the GaN films after radical exposure and after simultaneous irradiations of photon and radical (optical window: MgF_2, process time: 2 min).

In past, UV irradiation was reported to enhance surface reaction during Si etching process. Samukawa *et al.* reported the dependence of irradiation of photons on etch rates, where a UV lamp was applied during Si etching processes with Cl atom beam.[6] The irradiation of UV photons from 220 to 380 nm generated crystal defects on the Si surface and enhanced chemical reactions between Si and Cl atoms.[6] In the high-temperature Cl_2 plasma etching of GaN, photons from plasma emissions at 258 and 306 nm degraded PL of the GaN films at temperatures above 500 ^{o}C, indicating the formation of point defects on the GaN surface. Therefore, other photochemical reactions should be taken into account to explain why the surface became smoother and the etch depth decreased.

To assess the photochemical reactions in the high-temperature Cl radical etching, the author evaluated the surface stoichiometry of the GaN surfaces. The normalized XPS spectra of Ga *3d*, N *1s*, and O *1s* of the GaN surfaces for initial, after plasma etching, after radical exposure, and after simultaneous irradiations of photon and radical were shown in Fig. 6.3(a), which were determined by the areas of Ga *3d*. The calibrations of chemical shifts in N *1s* and O *1s* spectra were performed based on Ga *3d* peak position at 20.0 eV. As a reference, the spectra of initial GaN film and plasma-etched sample at 600 ^{o}C for 2 min were used. No obvious changes in both intensities and binding energies of Ga *3d*, N *1s*, and O *1s* could be observed before and after plasma etching. For the sample exposed to Cl radicals, besides the main peak of GaN in Ga *3d* spectrum at 20.0 eV and the component of gallium oxide at 20.8 eV,[7] an O *2s* peak recorded at 24.2 eV next to Ga *3d* peak was observed. The peak at 397.1 eV for N *1s*, corresponding to N in GaN and another peak at a higher binding energy at 401. 5 eV related to the component of NO_x was identified. Moreover, the intensity of O *1s* increased significantly compared with that of the initial one that contained the organic contaminations of C=O at 531.5 eV and C-O at 533.0 eV and the gallium oxide at 531.0 eV,[8] which indicates a magnitude of the formation of NO_x on the GaN surface. This increase of oxidation could be considered as the

result of a chemical modification of the chlorination layer (GaCl, $GaCl_3$ and NCl_3) after air exposure. Surface Cl atoms could react with H_2O in the water vapor ambient.

When the GaN film was exposed to simultaneous irradiations of photon and radical at 600 ^oC, the O *2s* peak disappeared and the O *1s* intensity returned to an extent that was close to the initial sample. The author considers that the plasma emission effectively suppressed the formation of thick chlorination layer, and the development of the oxidation was reduced.

The atomic composition of the GaN surfaces for initial, after plasma etching, after radical exposure, and after simultaneous irradiations of photon and radical were shown in Fig. 6.3(b). The process time was 2 min. As a reference, the initial N/Ga ratio was calculated as 93.2%, which meant that native oxides still remained after chemical cleaning. After etching, the N/Ga ratio was degraded to 83.5% because of an ion bombardment or a high-temperature annealing effect on the preferential remove of N atoms.[9)] The N/Ga ratio was not further deteriorated because of the enhanced vaporization of Ga species.[1)] For the GaN exposed to Cl radicals, the O concentration increased to 72.7%, indicating a severe development of the oxidation. The N/Ga ratio increased to 265.8%, behaving as a formation of the N-rich surface. After simultaneous irradiations of photon and radical, the O concentration remained constantly as compared with that for initial and the N/Ga ratio decreased to 73.4%. This degradation of the N/Ga ratio could be considered as a result of the photon-induced damage on the surface stoichiometry, as described in chapter 5.

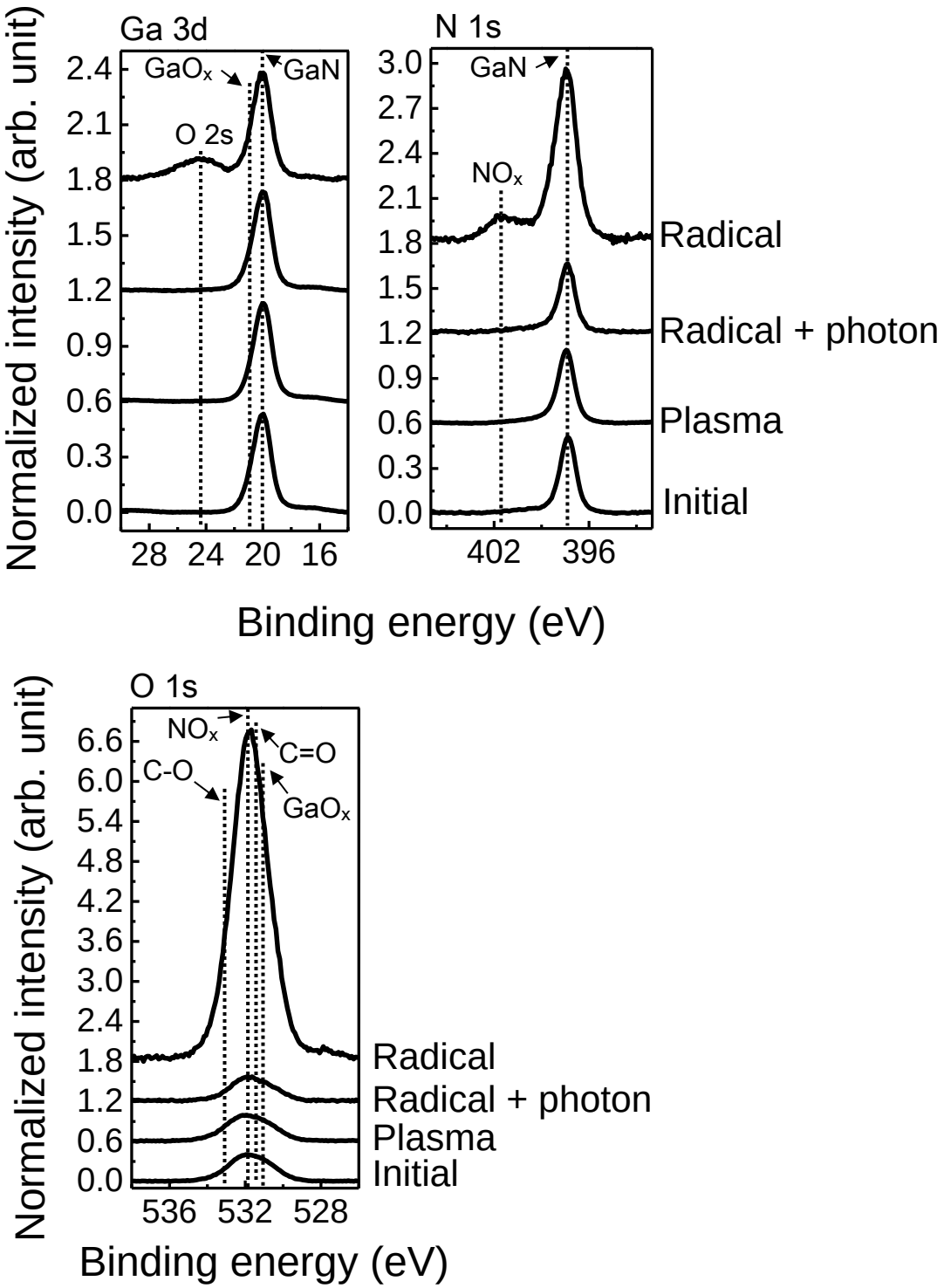

Fig. 6.3 (a) The normalized XPS spectra of Ga *3d*, N *1s*, and O *1s* of the GaN surfaces for initial, after plasma etching, after radical exposure, and after simultaneous irradiations of photon and radical (optical window: MgF_2, process time: 2 min).

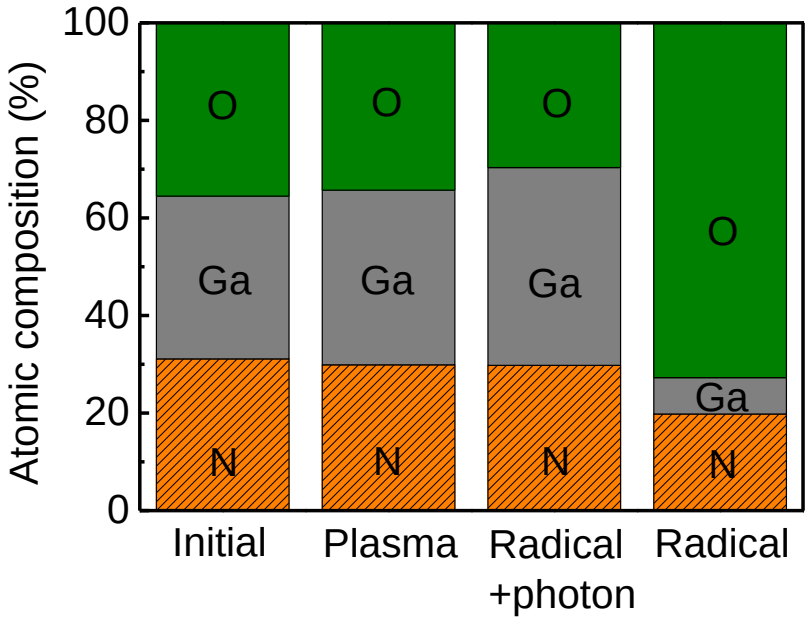

Fig. 6.3 (b) Atomic concentrations of N, Ga and O of the GaN surfaces for initial, after plasma etching, after radical exposure, and after simultaneous irradiations of photon and radical (optical window: MgF_2, process time: 2 min).

Based on the experimental results shown above, a mechanism of the smooth surface fabricated by simultaneous irradiations of photon and radical could be interpreted as follows. When the GaN film was exposed to Cl radicals, chemical reactions between Cl radicals and GaN surface resulted in the formations of Ga chlorides (GaCl and $GaCl_3$) and N chlorides (NCl_3). Without the effects of ion bombardment, the thermal vaporization of Ga species should be more than that of N species because the vapor pressure of $GaCl_3$ is higher than that of NCl_3 at a temperature of 600 ^oC.[10,11] Here, the author notes that the vaporization of GaCl is lower than that of NCl_3 at 600 ^oC,[12] suggesting that $GaCl_3$ might be the main species of the Ga chlorides in the etching process. Hence, a N-rich chlorination layer should remain on the GaN surface even at 600 ^oC. With the simultaneous irradiations of photon and radical, the formation of both Ga chlorides and N chlorides were considered to be suppressed as a result of the photodissociation by plasma emission in VUV or UV region.

The author discusses the effects of additional photon irradiations on the photodissociation of surface chlorides. Clark and Clyne reported the NCl_3 absorption spectrum, exhibiting a strong absorption with a maximum near 220 nm and a long, lower absorbance tail extending into the visible region.[13] Gilbert *et al.* reported the photodissociation of NCl_3 irradiated by either 248 nm-light (KrF) and 308 nm-light (XeCl) from excimer lasers.[14] Coombe *et al.* reported the photodissociation of gaseous NCl_3 irradiated by a pulsed laser at 193 and 249 nm, leading to the formation of doublet fragments (NCl_2 and Cl).[15] Petrikalm and Hochberg reported an absorption region ranging from 320 to 350 nm for GaCl radical.[16] Abdullah reported the calculated dissociation energy of GaCl molecule should be approximately 4.5 eV (276 nm).[17] Because $GaCl_3$ is considered to be formed via the reaction of a GaCl layer and Cl_2.[18] The author notes that the photodissociation of surface binding GaCl should lead to the less formation of volatile $GaCl_3$, resulting in the suppression of the formation of etch byproducts.

The author previously reported two Cl_2 emissions at 258 and 306 nm in the high-

temperature Cl_2 plasma etching that were highly considered to contribute on the photodissociation of both Ga and N chlorides. The thickness of the chlorination layer after simultaneous irradiations of photon and radical was considered to be much thinner than that of radical exposure. Moreover, the photon irradiation inhibited the Cl radical chemical reactions on the surface and suppressed the formation of etch pits and thereby the surface roughness decreased.

The dependence of light wavelength in simultaneous irradiations of photon and radical on the surface morphology was shown in Fig. 6.4. The process time was 2 min. By using the a-C film, only Cl radicals with visible lights from plasma emission could affect the GaN film. Compared with the GaN film exposed to Cl radicals, no obvious variations of the surface morphology could be observed and the surface roughness was nearly maintained. Namely, visible lights from plasma emission can hardly contribute on the photodissociation of Ga and N chlorides. The optical window made from BK7 could transmit a Cl_2 emission for 306 nm and decreased the surface roughness to 106.5 nm. Another Cl_2 emission for 258 nm was then added using the SiO_2 optical window. As the author expected, a further decrease of the surface roughness to 55 nm was found. Interestingly, the GaN surface simultaneously irradiated by photon and radical using the MgF_2 window was smoother than that using SiO_2, indicating the effects of Cl_2 plasma emission in VUV region on the photodissociation of Ga and N chlorides. Because of the limitation of the spectrometer used in this work, the OES in VUV region was unable to be measured. Two peaks centered at 134.7 and 137.9 nm in the emissions of VUV region were widely reported in Cl_2 plasmas.[19,20] The author considers the Cl_2 plasma emission in VUV region should also be considered in the photodissociation of Ga and N chlorides, which requires a future study using VUVOES measurement.

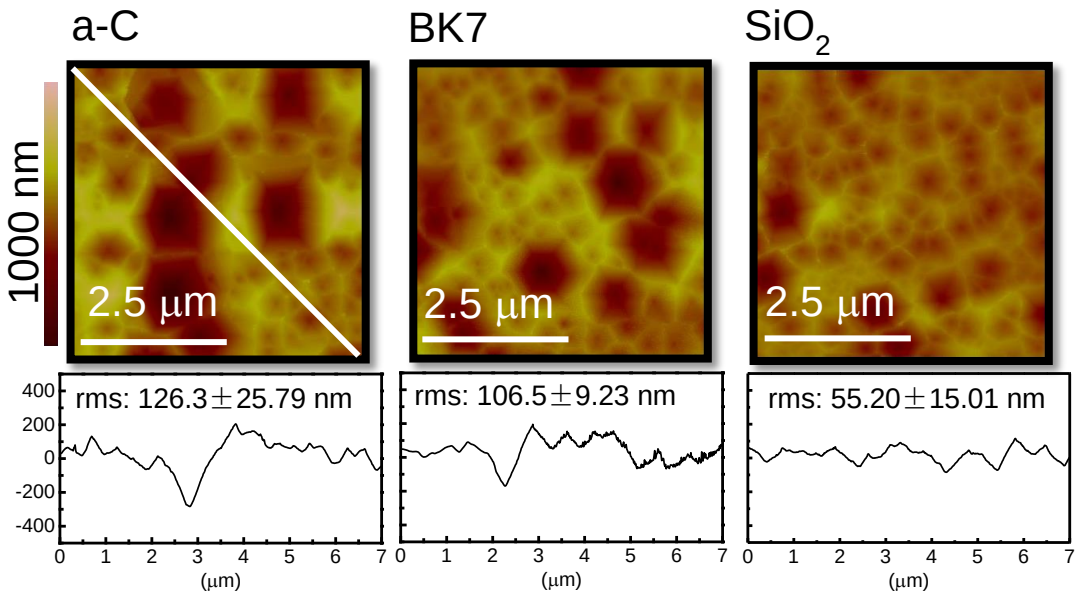

Fig. 6.4 The dependence of optical window materials, a-C film, BK7, and SiO_2 in simultaneous irradiations of photon and radical on surface morphology (process time: 2 min).

Figure 6.5(a) shows an etch profile of GaN fabricated by simultaneous irradiations of photon and radical, in which an optical window of MgF_2 was used and the process time was 10 min. The etch depth was 480 nm, close to that when exposed to Cl radicals for 2 min. Apparently, a smoother surface with fewer etch pits was observed for simultaneous irradiations of photon and radical compared with that for Cl radical exposure. Moreover, surface roughness was 62.33 nm after simultaneous irradiations of photon and radical, as shown in Fig. 6.5(b). Namely, the increase in roughness was lower than that for Cl radical exposure when the etch depth was similar. Hence, the simultaneous irradiations of photon and radical indicates a potential of high-temperature Cl_2 plasma etching in the deep and smooth etching of GaN films when a long process time of a few min (e.g., 5 to 10 min) is needed. Consequently, photons of Cl_2 plasma with wavelength in VUV region and UV region at 258 and 306 nm suppressed the formation of etch pits and thereby decreased the surface roughness. This is considered to be the result of the

photodissociation of both Ga and N chlorides that were formed by Cl radicals on the GaN surface.

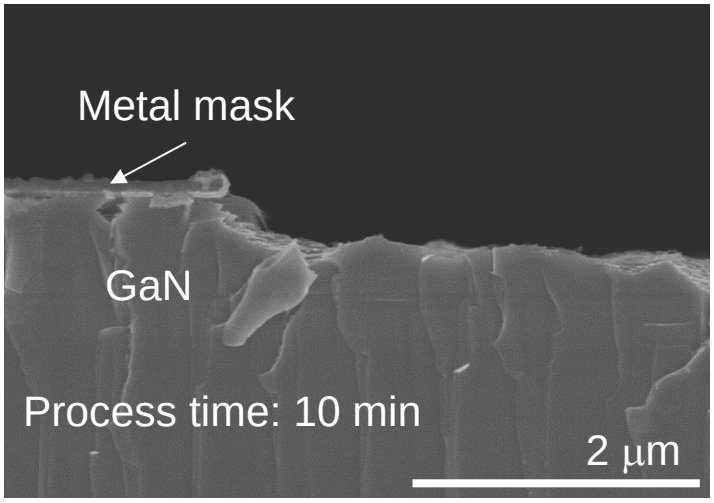

Fig. 6.5 (a) The cross sectional SEM image of the etch profile of the GaN film after simultaneous irradiations of photon and radical (optical window: MgF_2, process time: 10 min).

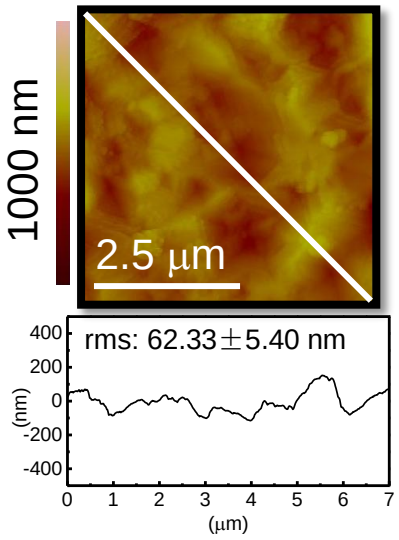

Fig. 6.5 (b) AFM image and line profile of the GaN surface after simultaneous irradiations of photon and radical (optical window: MgF_2, process time: 10 min).

Figure 6.6 shows the model of suppression in the roughening of a GaN surface by simultaneous irradiations of photon and radical. For Cl radical exposure of GaN, because of the preferential chemical reactions of Cl radicals on the dislocations, etch pits were formed and thereby the surface was severely roughened. Namely, GaN surface was chemically modified by Cl radicals into the Ga and N-related chlorination layers that were thermally vaporized at 600 ^{o}C. Apparently, the chemical reactions on the dislocations were greater than those on the flat regions of the GaN surfaces due to a higher etch rate of {1-102} facet compared with {0001} facet, leading to the progressively enlarged dimensions of etch pits. For simultaneous irradiations of photon and radical of GaN, the chemical reactions between Cl radicals and the surface were suppressed as a result of the photodissociation of both Ga and N chlorides by Cl_2 plasma emissions at 258 and 306 nm. Namely, the chemical modification of the Ga and N-related chlorination layers was suppressed, which directly reduced the etch rate. The author notes that the suppression of chemical reactions on the dislocations was greater than that on the flat regions of the GaN surfaces because etch rates on the etch pits might decrease as a result of enlarged dimensions and fewer Cl radical supplements. Namely, Cl radical flux that actually participated in the chemical reactions tended to decrease due to a larger dimension of etch pits and desorption of Cl radicals by photodissociation. As a consequence, even though the etch depths were similar for the GaN films exposed to Cl radicals and simultaneous irradiations of photon and radical, Cl_2 plasma emissions in deep UV region successfully suppressed preferential chemical reactions on the dislocations and thereby limited the development of etch pits.

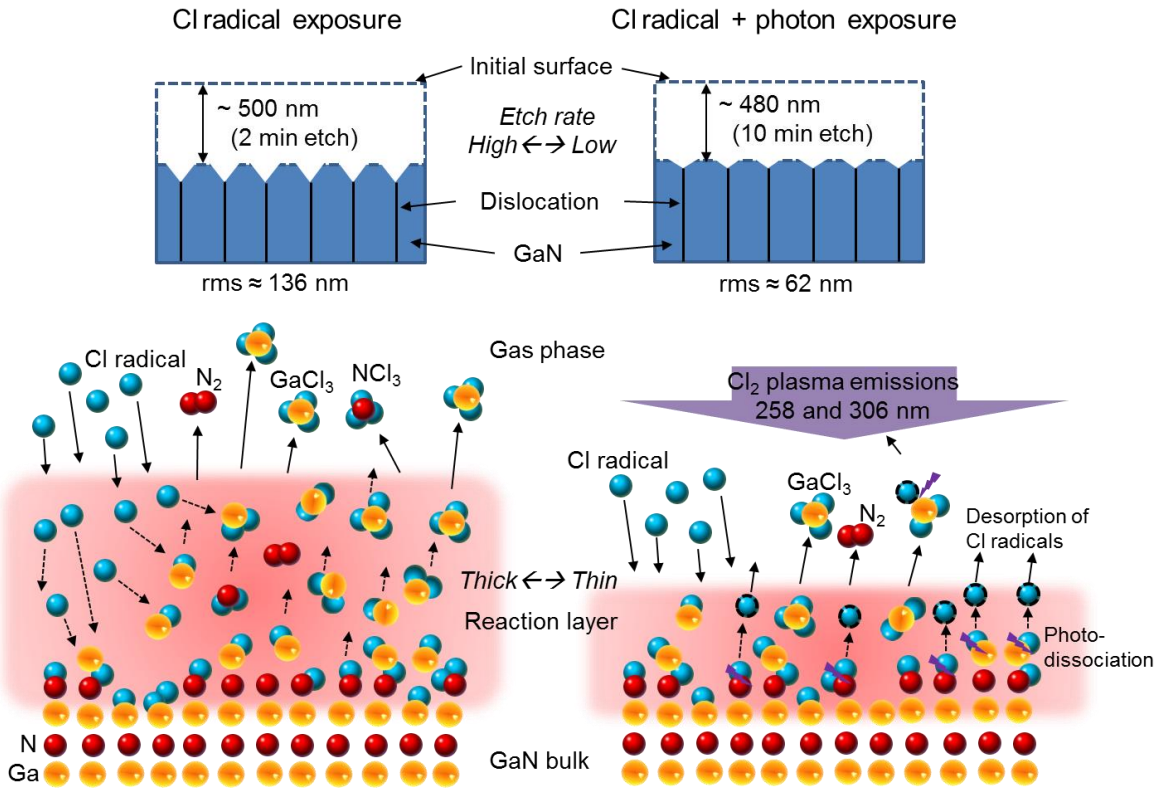

Fig. 6.6 Model of suppression in the roughening of a GaN surface by simultaneous irradiations of photon and radical.

6.4 Conclusions

To be different with chapter 3, 4 and 5 that how to suppress damage formation in a shallow etching of GaN was the focus, the author elucidated how to fabricate a smooth surface instead of discussing damage formation in this chapter, because the rough surface tended to be the critical issue in the deep etching of GaN using the Cl_2 plasma at high temperatures. As the GaN surface was dominantly roughened by Cl radicals with the formation of etch pits, the author elucidated the mechanisms of the suppression of this roughening at 600 ^oC by simultaneous irradiations of photon and radical. A N-rich chlorination layer was formed on the GaN surface after Cl radical exposure, revealing severe chemical reactions and thereby the surface was roughened. However, this chemical reaction was effectively suppressed in simultaneous irradiations of photon and radical as a result of the photodissociation of both Ga and N chlorides by photons in VUV region and UV region at 258 and 306 nm of Cl_2 plasma emission. Namely, photon irradiations like using an additional UV lamp combined in the high-temperature Cl_2 plasma etching of GaN could potentially provide a smooth surface even though the etch depth was very deep. Regarding how to avoid damage formation by photon irradiations, the author suggests that the stage temperature should be controlled around 400 ^oC based on the results shown in chapter 5, which was also the optimum condition for a shallow etching of GaN. Consequently, a smooth and damageless surface would be highly expected for a deep etching of GaN by applying photon irradiations precisely.

6.5 References

1) Z. Liu, J. Pan, T. Kako, K. Ishikawa, K. Takeda, H. Kondo, O. Oda, M. Sekine, and M. Hori, Jpn. J. Appl. Phys. **54,** 06GB04 (2015).

2) Z. Liu, J. Pan, A. Asano, K. Ishikawa, K. Takeda, H. Kondo, O. Oda, M. Sekine, and M. Hori, Jpn. J. Appl. Phys. (2016) in press.

3) S. Chowdhury, B. L. Swenson, and U. K. Mishra, IEEE Electron Device Lett. **29,** 543 (2008).

4) H. Sugiura, L. Jia, H. Kondo, K. Ishikawa, K. Takeda, M. Sekine, and M. Hori, ICRP-9 2015, IW2.00002 (2015).

5) C. D. Wagner, L. E. Davis, M. V. Zeller, J. A. Taylor, R. H. Raymond, and L. H. Gale, Surf. Interface Anal. **3,** 211 (1981).

6) S. Samukawa, B. Jinnai, F. Oda, and Y. Morimoto, Jpn. J. Appl. Phys. **46,** L64 (2007).

7) R. Carli and C.L. Bianchi, Appl. Surf. Sci. **74,** 99 (1994).

8) G. Yan, X. Li, , Z. Wang, H. Guo, J. Wang, W. Peng, and Q. Hu, Electrochim. Acta **166,** 190 (2015).

9) X. A. Cao, H. Cho, S. J. Pearton, G. T. Dang, A. P. Zhang, F. Ren, R. J. Shul, L. Zhang, R. Hickman, and J. M. Van Hove, Appl. Phys. Lett. **75,** 232 (1999).

10) B. Brunetti, V. Piacente, and P. Scardala, J. Chem. Eng. Data **55,** 98 (2010).

11) T. F. O'Brien, T. V. Bommaraju, and F. Hine: in *Handbook of Chlor-Alkali Technology Volume I: Fundamentals* (Springer, New York, U. S. A., 2005) p. 921.

12) C. Bernard, C. Chatillon, A. Ait-Hou, R. Hillel, Y. Monteil, and J. Bouix, J. Chem. Thermodynamics **20,** 129 (1988).

13) T. C. Clark and M. A. A. Clyne, Trans. Faraday Soc. **65,** 2994 (1969).

14) J. V. Gilbert, X. L.Wu, D. H. Stedman, and R. D. Coombe, J. Phys. Chem. **91,** 4265 (1987).

15) R. D. Coombe, J. V. Gilbert, S. S. Beaton, and N. Mateljevic, J. Phys. Chem. A **106,** 8422 (2002).

16) A. Petrikalm and J. Hochberg, Z. Phys. **86,** 214 (1933).

17) H. Y. Abdullah, J. Ovonic Res. **9,** 55 (2013).

18) T. Meguro, M. Ishii, T. Sugano, K. Gamo, and Y. Aoyagi, Appl. Surf. Sci. **82,** 193 (1994).

19) J. F. Muth, J. H. Lee, I. K. Shmagin, R. M. Kolbas, H. C. Casey, Jr., B. P. Keller, U. K. Mishra, and S. P. DenBaars, Appl. Phys. Lett. **71,** 2572 (1997).

20) W. Zhu, S. Sridhar, L. Liu, E. Hernandez, V. M. Donnelly, and D. J. Economou, J. Appl. Phys. **115,** 203303 (2014).

Chapter 7: Conclusions

7.1 Present work

GaN has attracted much attention as a promising candidate for next-generation power devices. To realize normally-off operation in a lateral AlGaN/GaN high electron mobility transistor (HEMT), a precise and damageless etching technology with controllability of several nm-scale in depth is required to fabricate the recess gate structure. These requirements have been achieved by the high-temperature Cl_2 plasma etching process.

The plasma processes remained issues of the PID on degradation of device performances such as a current collapse phenomenon and a high leakage current. In this study, the author focuses on the formation of nonstoichiometric surface of GaN after the conventional Cl_2 plasma etching at RT. The main cause has been widely considered as the higher vapor pressures of nitrogen-containing by-products than those of Ga-containing residues. To solve this problem, the high-temperature Cl_2 plasma etching was proposed.

In chapter 3, the investigation of the optimum stage temperature in the high-temperature Cl_2 plasma etching of GaN to suppress damage formation was presented. Based on comprehensive results of evaluations of PL, stoichiometric composition, and surface roughness, PID was successfully suppressed by the application of Cl_2 plasma etching at 400 ^oC. On the other hand, the individual contributions of ions, photons, and radicals on damage formation were separated from the effects of plasma using the PAPE method. Energetic ion bombardments primarily induced damage at temperatures lower than 400 ^oC and became progressively invalid with the increase of the stage temperature. This reduction of ion damage was considered as the result of the enhanced removal of the damaged layer on the GaN surface when the stage temperature increased. Moreover, irradiations of photons and radicals were enhanced to form damage and to develop surface roughness at 500 ^oC, respectively. Consequently, Cl_2 plasma

etching at 400 ºC resulted optimally in low-damaged, stoichiometric and smooth GaN surface.

In chapter 4, to fabricate gate-recess GaN-based normally-off power electronic devices, the minimization of PID in plasma etching for the precise and smooth removal of a depth of approximately 7 nm of GaN films was investigated. Here, the author focused on how to fabricate a minimal damaged GaN film by reducing ion damage. Then, the PL properties and surface morphologies of GaN films exposed to Cl_2 plasma at 400 ºC have been systematically studied. Although the surface was roughened regardless of the bias voltage, the temporal evolution of ion-induced damage saturated within the etch time of 2 min and depended on incident ion energy. A low ion energy can hardly lead to bulk PID within a penetration depth of less than 1 nm. Consequently, Cl_2 plasma etching for a short time of 0.4 min without bias voltage application at a stage temperature of 400 ºC is recommended to prevent damage formation and provide a clean surface in a gate recess structure.

In chapter 5, the mechanisms of thermally enhanced photon-induced damage of GaN films were presented. The author notes that photons with energies higher than GaN band gap energy degraded PL properties of GaN films at 500 ºC as a result of the thermally enhanced photon-dissociated Ga-N bonds for a depth of approximately 3.2 nm. The equilibrium between damage formation and thermal recovery was reached for photon-induced damage within the irradiation time of 2 min, leading to a saturated temporal behavior. Both PL properties and N/Ga ratios were degraded by Cl_2 plasma emissions at 258 and 306 nm. Moreover, 258 nm-peak was easier to form these damages than 306 nm-peak because of its higher photon energy. In order to fabricate highly reliable GaN-based devices, UV emissions during plasma etching processes should be precisely controlled.

In chapter 6, to fabricate vertical GaN power devices using the high-temperature Cl_2 plasma etching, a suppression of the severely roughened surface in the deep etching of GaN is highly needed. Typically, the chemical reactions between Cl radicals and the GaN surface

dominated the increase in surface roughness. The author described the mechanisms of the suppression of the roughening of a GaN surface etched by Cl_2 plasma etching at 600 ^oC by simultaneous irradiations of photon and radical. After Cl radical exposure, a N-rich chlorination layer was formed on the GaN surface, revealing severe chemical reactions and thereby the surface was roughened. However, this chemical reaction was effectively suppressed in simultaneous irradiations of photon and radical as a result of the photodissociation of both Ga and N chlorides by photons in VUV region and UV region at 258 and 306 nm of Cl_2 plasma emission. Consequently, a smooth and damageless surface would be highly expected for a deep etching of GaN by controlling photon irradiations precisely.

7.2 Perspectives in the future

In this dissertation, the author successfully achieved the prototype of damageless fabrication of GaN using an advanced plasma etching at high temperatures. Based on the clarification of individual effects of ion, photon and radical on damage formation, the author preliminary built up a model of the suppression of PID in the high-temperature Cl_2 plasma etching of GaN films. As the evaluation is mainly focused on the etched characteristics like etch rates, surface morphologies, surface stoichiometry, and PL, the detailed investigations on Cl_2 plasma itself like plasma and negative ion density are important subjects in the near future. Other information about the assignments and absolute quantities of plasma species such as Cl-related ions and radicals would help in the further understanding on mechanisms of the plasma etching of GaN. Hence, the next step is using plasma diagnostics to investigate more precisely the interaction of the plasma species on the GaN surfaces.

The author emphasizes that a decrease in the NBE intensities might be corresponded to an increase in band bending. Indeed, a higher Femi level is easily formed in the etched GaN region and thereby the electrons drift from the etched GaN surface to the bulk region that is not affected by plasma, leading to an occurrence of band bending. Hence, the photo-excitons in PL measurements will transfer along the bended band, which potentially suppress the excitonic recombination and result in the reduction of the NBE intensities. Typically, the core-level energy shifts observed by XPS can be applied to determine the band bending after the plasma etching on GaN.

The optimization of the high-temperature Cl_2 plasma etching of GaN was realized by investigating the effects of ion energies on both PID and surface morphologies. Cl_2 plasma etching for a short time of 0.4 min without bias voltage application at a stage temperature of 400 ^oC was suggested for a shallow remove of approximately 7 nm depth. The author notes that Cl ions were still accelerated by the differences between plasma potential and floating potential

on the wafer surface. As a result, a measurement of this difference is highly needed to provide an applicable guidance in the commercial fabrication of lateral GaN power devices. On the other hand, the anisotropic etch profile for the optimized condition was not perfectly normal and close to a reverse taper shape. Hence, the optimization of the etch profile may need in terms of reducing radical densities by lowering pressure or introducing additional inert gases like N_2 and Ar. Moreover, to totally remove the remained damage on the GaN surface, a post-etching method such as the wet etching for the damaged surface is recommended and may need in the near future.

The damage formation induced by photons from Cl_2 plasma emissions was thermally enhanced above a stage temperature of 500 ^oC. Moreover, the formation of etch pits dominated by Cl radicals was also severely enhanced above 500 ^oC. The author notes that the threshold value of the beginning temperature of this photon-induced damage and radical-dominated formation of etch pits may strongly depend on crystal qualities of the GaN films because of their high densities of both point and dislocation defects. Namely, these issues may be negligible in the future as the growth technology for high-quality GaN films will be matured. However, regarding the recent quality of GaN films, how to precisely control plasma emission without or with less photon-induced damage and how to reduce the preferential chemical etching on GaN surfaces will be essential tasks in the near future.

Additional photon irradiations in the high-temperature Cl_2 plasma etching of GaN seem to be an approach to prevent the increased surface roughness when a deep etch of the GaN films is needed. Even though the author elucidated the effects of simultaneous irradiations of photons and radicals on the suppression of the roughening of a GaN surface by *ex situ* XPS measurements, *in situ* film characterizations such as XPS and spectroscopic ellipsometry and plasma diagnostics such as vacuum ultraviolet absorption spectroscopy (VUVAS) and vacuum ultraviolet optical emission spectroscopy (VUVOES) are expected to help in the further

understanding on the mechanisms.

The evaluations of the electrical properties of the GaN films after the high-temperature Cl_2 plasma is desired to diagnose PID comprehensively. Deep-level transient spectroscopy (DLTS) is needed to identify and quantify deep-level defects in plasma-etched GaN films.

Other subjects in the high-temperature Cl_2 plasma etching of GaN should also be addressed. Suitable masks are now extremely demanded in terms of the high durability in the high-temperature Cl_2 plasma and the negligible effects on the GaN surfaces. Apparently, both photoresists and metal masks are unrecommendable because of their low durability and damages in the physical vapor deposition, respectively. Here, the author recommends an advanced organic mask that can meet these two requirements simultaneously.

Acknowledgements

Studying for a doctoral degree has become the most unforgettable experience in the author's life. The author is very gratitude when thinking of all these wonderful people for their supervising, supporting, and cooperating, which result in an enriching period as a Ph. D. candidate in Hori & Sekine Lab. of Nagoya University.

Words are not adequate to convey the thankfulness to Prof. Dr. Masaru Hori, who is an amazing supervisor and examiner in the author's Ph. D. research and a kind mentor in the author's daily life. He is an eminent scholar and a hardworking educator who inspires his students to pursue thorough scholarship. The author learns a lot through his words, deeds and demeanor. He has enlightened the author on every aspect during the doctoral course. The author acknowledges his supervision and patience and feels sincerely grateful to him from the bottom of the author's heart.

The author shows a special emotion of acknowledgement to Prof. Dr. Makoto Sekine and Prof. Dr. Kenji Ishikawa as co-supervisors. They supervised this work thoroughly and carefully. Without their effective suggestions and guidance, the author is unable to construct the whole theory of the doctoral dissertation.

The author expresses the deepest appreciation to Prof. Dr. Hirotaka Toyoda, Prof. Dr. Seiichi Miyazaki, and Prof. Dr. Yoshio Honda of Nagoya University and Prof. Dr. Keiji Nakamura of Chubu University as co-examiners of the dissertation. They propose constructive comments and suggestions on both basic principles and experimental details that were remarkably valuable to improve up on the Ph. D. dissertation.

The author is very truly grateful to Prof. Dr. Osamu Oda, Prof. Dr. Hiroki Kondo, Prof. Dr. Naohiro Shimizu, and Prof. Dr. Keigo Takeda. Their valuable instructions in the author's daily experiments are extremely important to guarantee the quality of the Ph. D. dissertation.

The author would like to thank Prof. Dr. Hiroshi Amano, Prof. Dr. Maki Kushimoto, and

Dr. Zheng Sun of Nagoya University for technical support in PL measurements and valuable comments.

The author acknowledges the kindness from Prof. Dr. Toshio Hayashi, Prof. Dr. Hitoshi Itoh, Prof. Dr. Satomi Tajima, Prof. Dr. Hiromasa Tanaka, Prof. Dr. Hiroshi Hashizume, Prof. Dr. Fengdong Jia, Prof. Dr. Noboru Ebizuka, Prof. Dr. Jagath Kularatne, Dr. Jerome Jolibois, Dr. Hyung Jun Cho and Dr. Takayoshi Tsutsumi. Their extensive knowledges extended the author's horizons about plasma technologies.

The author expresses a deep sense of gratitude to Prof. Dr. Yutaka and Mr. Toshiya Matsumura of Aichi Institute of Technology for the generous instruction and help in educating how to measure deep-level transient spectroscopy (DLTS) of GaN.

Thanks are due to Prof. Dr. Matthew Goeckner, Prof. Dr. Daisuke Ogawa, Dr. Stephan Thamban, Mr. Robert Bates, Mr. David Urrabazo, Mr. John Poulose, Ms. Caroline Liu, Ms. Yanping Chen, Mr. Cassius Fagioli of University of Texas at Dallas, who gave the author a chance to study the principle of Fourier transform infrared spectroscopy. Their kind supervisions and valuable comments helped the author have a better understanding on gas phase reaction in plasma.

Thanks are also due to Dr. Tetsuya Tatsumi, Dr. Yasufumi Miyoshi, Dr. Masanaga Fukasawa, Dr. Shouichiro Izumi, and Dr. Shigetaka Tomiya of Sony Semiconductor Solutions Corporation, who provided suggestions in the cooperative projects of transient behavior of pulse modulated ICP and photon-induced damage from Cl_2 plasma on InGaN/GaN SQW.

The author is very fortunate to consult with Dr. Hiroyuki Kano (NU Eco Engineering Co., LTD) and Dr. Koji Yamakawa (Katagiri engineering co., ltd.) on the basic principle of vacuum technology and know-how of equipment manufacturing.

The author is particularly grateful to Atsushi Tanide, Shohei Nakamura, Akira Horikoshi, Motohiro Kohno, Shigeru Takatsuji, and Kazuo Kinose of SCREEN Holdings Co., Ltd., and

Masazumi Nishikawa and Akinori Ebe of EMD Corp., who participated in the development and daily maintenance of the ICP etching system at high temperatures.

The author shows a special acknowledgement to members who have strived together in the GaN group of Hori & Sekine Lab., Dr. Shang Chen, Dr. Yi Lu, Dr. Frank Wilson, Mr. Ryosuke Kometani, Mr. Takashi Kako, Mr. Kazuki Iwamoto, Mr. Jialin Pan, Mr. Atsuki Asano, Mr. Shinnosuke Takai, and Mr. Masato Imamura for technical helps in experimental setup and fruitful discussions.

Many acknowledgements are due to the alumni in Hori & Sekine Lab., because of their resultful discussions and precious comments: Dr. Hiroshi Yamamoto, Dr. Arkadiusz Malinowski, Dr. Yusuke Abe, Dr. Yudai Miyawaki, Dr. Takehiro Hiraoka, Dr. Hitoshi Watanabe, Ms. Sachiko Iseki, Dr. Hironao Shimoeda, Dr. Toshiya Suzuki, Mr. Jong Yun Park, Dr. Yusuke Kondo, Mr. Shinpei Amasaki, Mr. Naoya Sumi, Mr. Tatsuya Hagino, Mr. Takayuki Kanda, Mr. Kohei Asano, Mr. Jun Kuki, Mr. Atsushi Fukushima, Mr. Takeyoshi Horibe, Ms. Ya Lu, Mr. Leyong Yu, Mr. Atsushi Ando, Dr. Lingyun Jia, Mr. Tomohiro Takahashi, Mr. Jiadong Cao, Mr. Kuangda Sun, Mr. Haoran Wang, Mr. Tomokazu Ishiyama, Mr. Itsuko Sakai, Mr. Hideshi Miyajima, Mr. Tomoki Amano, Mr. Makoto Isobe, Mr. Ryo Gonda, Mr. Masayuki Nakamura, Mr. Keita Miwa, Ms. Sijie Liang, Mr. Da Xu, Mr. Yan Zhang, Mr. Timothy Ryan Brubaker, Mr. Yohei Takahashi, Mr. Nobuyuki Negishi, Mr. Naoto Kihara, Mr. Hirotsugu Sugiura, Mr. Yusuke Fukunaga, Mr. Kazui Iwamoto, Mr. Naoyuki Kurake, Mr. Shun Imai, Mr. Masakazu Toumatsu, Mr. Borude Ranjit Rohidas, Mr. Islam Md. Anwarul, Mr. Takumi Kumakura, Mr. Takumi Ito, Mr. Kazuaki Kojima, Mr. Shunichi Saito, Mr. Suiki Tanaka, Mr. Takuya Tonami, Mr. Kenichi Naito, Mr. Ryo Furuta, Mr. Naoki Yoshitake, Mr. Toshinari Ueyama, Mr. Daiki Kanno, Mr. Ren Kuramashi, Mr. Yukihiro Kurokawa, Ms. Mika Takahashi, Mr. Tomonori Ichikawa, Ms. Kaede Katsuno, Mr. Naoki Takeda, Mr. Yuugo Hosoi, Mr. Kaishi Murakami, Mr. Soutarou Yamaoka, Mr. Xitong Xie, and Ms. Yan Hao.

Acknowledgements

At the same time, the author is also in acknowledgement of the thoughtful secretarial supports from Ms. Megumi Oshigane, Ms. Rieka Kamiya, Ms. Naoko Kataoka, Ms. Masako Takahashi, Ms. Kotomi Shioya, Ms. Hiroko Miyakawa, Ms. Noriko Ushio, Ms. Yukie Kase, Ms. Mitsuko Era, Ms. Yoko Kuwabara, Ms. Kanae Teshigawara, and Ms. Asako Nishiyama.

The author deeply appreciates his beloved wife and children, Ms. Yuling Yin, Mr. Chengyun Liu, Ms. Xiyao Yin for their excellent care and persistence for cheering the author up by his side and help the author continue the path of research.

Finally, the author warmly appreciate his parents and parents-in-law, Mr. Zheng Liu, Ms. Xin Cheng, Mr. Long Yin, and Ms. Zhuying Yang for their both financial and spiritual supports that help the author finish the doctoral course.

Zecheng Liu

January 2017

Award

2015 Young Research Award, 36th International Symposium on Dry Process

International Research Project

2013 Jan. – Mar.

International Training Program (For training young researchers on plasma nanotechnology materials and device processing, conducted by Japan Society for the Promotion of Science) at Prof. Goeckner's group in University of Texas at Dallas, United States of America.

Journal publications

Title	Journal	Authors
1. Suppression of plasma-induced damage on GaN etched by a Cl_2 plasma at high temperatures	Jpn. J. Appl. Phys. **54,** 06GB04 (2015).	Z. Liu, J. Pan, T. Kako, K. Ishikawa, K. Takeda, H. Kondo, O. Oda, M. Sekine, M. Hori
2. Investigation of effects of ion energies on both plasma-induced damage and surface morphologies and optimization of high-temperature Cl_2 plasma etching of GaN	Jpn. J. Appl. Phys. **56,** 026502 (2017).	Z. Liu, J. Pan, A. Asano, K. Ishikawa, K. Takeda, H. Kondo, O. Oda, M. Sekine, M. Hori
3. Thermally enhanced formation of photon-induced damage on GaN in Cl_2 plasma	J. Appl. Phys. to be submitted.	Z. Liu, A. Asano, M. Imamura, K. Ishikawa, K. Takeda, H. Kondo, O. Oda, M. Sekine, M. Hori
4. GaN surface roughness reduction with photon irradiation during etching by chlorine radicals	Jpn. J. Appl. Phys. to be submitted.	Z. Liu, M. Imamura, A. Asano, K. Ishikawa, K. Takeda, H. Kondo, O. Oda, M. Sekine, M. Hori

International conferences

Title	Conference	Authors
1. Recovery of plasma-damaged GaN by employing exposure of radicals	The 11th APCPST (Asia Pacific Conference on Plasma Science and Technology) and 25th SPSM (Symposium on Plasma Science for Materials), 2-P25, Kyoto, Japan, Oct. 2-5, 2012	Z. Liu, S. Chen, Y. Lu, R. Kometani, K. Ishikawa, H. Kano, K. Takeda, H. Kondo, M. Sekine, T. Egawa, H. Amano, M. Hori
2. An in-situ sequential H and N radical exposure process for recovery of plasma-damaged GaN	34th International Symposium on Dry Process, H-3, Tokyo, Japan, Nov. 15-16, 2012	Z. Liu, S. Chen, Y. Lu, R. Kometani, K. Ishikawa, H. Kano, K. Takeda, H. Kondo, M. Sekine, T. Egawa, H. Amano, M. Hori
3. Sequential exposure of N and H atoms for recovery of plasma-damaged GaN	5th International Symposium on Advanced Plasma Science and its Applications for Nitrides and Nanomaterials, P3-0003A, Nagoya, Japan, Jan. 28-Feb. 1, 2013	Z. Liu, S. Chen, Y. Lu, R. Kometani, K. Ishikawa, H. Kano, K. Takeda, H. Kondo, M. Sekine, T. Egawa, H. Amano, M. Hori
4. GaN etching at high temperature employing N_2 added Cl_2 Plasma	6th International Symposium on Advanced Plasma Science and its Applications for Nitrides and Nanomaterials, 06aP04, Nagoya, Japan, Mar. 2-6, 2014	Z. Liu, T. Kako, K. Ishikawa, O. Oda, K. Takeda, H. Kondo, M. Sekine, M. Hori

5. Damage-formations in GaN processed at high temperatures	36th International Symposium on Dry Process, F-4, Yokohama, Japan, Nov. 27-28, 2014	Z. Liu, J. Pan, T. Kako, K. Ishikawa, K. Takeda, O. Oda, H. Kondo, M. Sekine, M. Hori
6. Optimization of stage temperatures on etch-reactions of GaN films	The 21st Korea-Japan Workshop on Advanced Plasma Processes and Diagnostics & The Workshop for NU-SKKU Joint Institute for Plasma-Nano Materials, 17:00-17:10, Yangyang, Republic of Korea, Oct. 3-4, 2015	Z. Liu, J. Pan, T. Kako, K. Ishikawa, K. Takeda, O. Oda, H. Kondo, M. Sekine, M. Hori
7. Low plasma-induced damage on GaN etched by a Cl_2 plasma at high temperatures	37th International Symposium on Dry Process, P-7, Awaji Island, Japan, Nov. 5-6, 2015	Z. Liu, J. Pan, A. Asano, T. Kako, K. Ishikawa, K. Takeda, H. Kondo, O. Oda, M. Sekine, M. Hori
8. Low damage etching of Gallium Nitride with Cl_2 plasma at high temperature	8th International Symposium on Advanced Plasma Science and its Applications for Nitrides and Nanomaterials, 09P11, Nagoya, Japan, Mar. 6-10, 2016	Z. Liu, J. Pan, A. Asano, K. Ishikawa, K. Takeda, O. Oda, H. Kondo, M. Sekine, M. Hori